The molecular logic of retinal cell types

Inauguraldissertation

zur

Erlangung der Würde eines Doktors der Philosophie

vorgelegt der

Philosophisch-Naturwissenschaftlichen Fakultät

der Universität Basel

von

Sandra Siegert

aus

Deutschland

Basel, 2010

Genehmigt von der Philosophisch-Naturwissenschaftlichen Fakultät auf Antrag von

Prof. Dr. Silvia Arber
Botond Roska, MD, Ph.D
Prof. Dr. Heinz Wässle

Basel, den 21. September 2010

Prof. Dr. Martin Spiess

Table of Contents

Abstract

The mammalian brain is assembled from thousands of neuronal cell types, which are organized in distinct circuits to perform behaviorally relevant computations. Transgenic mouse lines with different cell types selectively marked would facilitate our ability to dissect functional components of complex circuits. We performed a screen for cell type-specific GFP expression in the retina using BAC transgenic mice from the GENSAT project. Among others we identified mouse lines in which the inhibitory cell types of the night vision and directional selective circuit are selectively labeled. We quantified the stratification patterns to predict potential synaptic connectivity between marked cells of different lines and show that some of the lines enable targeted recordings and imaging of cell types from developing or mature retinal circuits. Then, we selected some of those mouse lines and genetically profiled the labeled cell types to reveal if adult cell types have a unique genetic fingerprint. Our data suggests that each cell type has a unique genetic signature that is likely to be a consequence of a unique transcriptional code in each cell type. A hierarchical clustering of the cell types showed that each cell type cluster to their corresponding biological cell class. We found genes exclusively expressed for cell classes and for biologically relevant combinations of cell types.

Introduction

The extensive diversity of neurons in the brain poses significant challenges for the understanding of the structure and function of neuronal circuits [1-3]. Cells that have similar morphology and function, and are marked by the same immunohistochemical marker, are called a *cell type*. Cell types that share broader features like localization of their cell bodies in a distinct stratum, but differ in their morphology and function, are defined as a *cell class*.

Developmental studies [4, 5] have revealed that temporally and spatially restricted expression of genes is responsible for the formation of individual cell types. But little is known about how long after final cell division it is necessary to keep specialized gene expression patterns. Here we ask if adult cell types have a unique genetic fingerprint. Moreover, we were interested in correlating functional relationships with genetic relationships among cell types.

The main bottleneck to addressing such questions is the lack of *in vivo* markers that specifically label cell types or classes and which would allow those cells to be isolated. Since the number of neuronal cell types in the brain is predicted to be very large, it is unlikely that unique promoters can be found for each cell type. In contrast, in restricted brain areas such as the olfactory bulb, cerebellum, local cortical regions or, in particular, the retina such specificity might exist. As an example, the innate promoter for choline acetyltransferase (ChAT) labels different cell types in the whole brain, but in the retina it marks only the starburst amacrine cells [6]. The Gene Expression Nervous System Atlas (GENSAT) project generated hundreds of mouse lines which express green fluorescent protein (GFP) driven by different bacterial artificial chromosomes (BACs) [7]. But a comprehensive mapping of these mouse lines to individual cell types in different brain regions has not yet been performed. In order to approach the scientific questions posed above, my first goal was to identify mouse lines that specifically mark individual cell types, or combinations, in the retina. My second goal was to reveal the genetic identity of 14 cell types or classes labeled in individual mouse lines and compare them.

The retina as a model system

The retina is an ideal brain region to screen for cell type-specific genetic markers [8, 9], since many cell types have already been defined morphologically. The retina is a part of the brain localized at the back-side of the eye. It processes incoming light information and sends the resulting neural activity patterns to higher brain regions (**Fig. 1**).

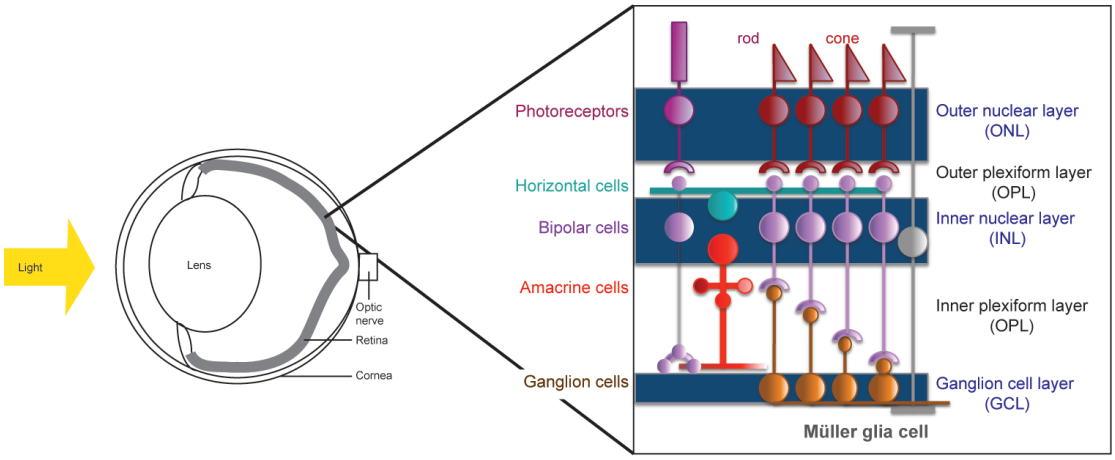

Figure 1. Schematic overview of the mouse eye and the retina.

Mammalian retinas share a common architecture (**Fig. 2a–c**) [10-12]: most of their 50-60 cell types are regularly spaced across the retina, and are neatly laminated in narrow strata. Retinal cells are organized in a number of different circuits that perform parallel computations of the visual scene [13]. Cone photoreceptors, which are the light sensors during daylight, connect to approximately ten types of bipolar cells. Half of the cone bipolar cells are activated by decreases (OFF cells), and the other half by increases (ON cells) in light intensity. Axon terminals of OFF and ON bipolar cells settle at different depths within the inner plexiform layer (IPL) in a stereotyped manner: OFF terminals in the distal part and ON terminals in the proximal. Order exists at an even finer scale; bipolar cell terminals occupy one or only a few of the 10 IPL strata (**Fig. 3a**). Dendrites of more than a dozen types of ganglion cells also arborize in these strata, and receive excitatory input from co-stratified bipolar cell terminals. The response polarity of a ganglion cell is determined by the types of bipolar cells that provide input: ON, OFF or ON-OFF. The excitatory route from photoreceptor to ganglion cell is longer during low light levels when rods are the

active light sensors. Rods connect to rod bipolar cells, which terminate in the most proximal part of the IPL (**Fig. 2b**). Rod bipolar cells excite a set of interneurons, the A2 amacrine cells, that provide inhibitory input to OFF bipolar cells and are electrically coupled to ON cone bipolar cells, which in turn activate the corresponding ganglion cells. Alternative rod pathways have also been described [14, 15].

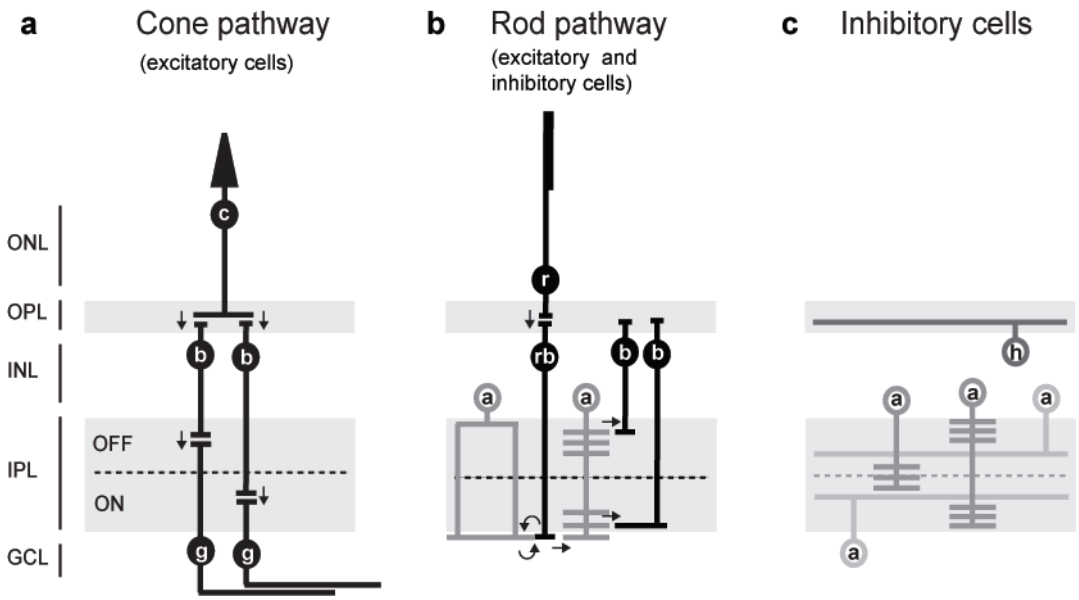

Figure 2. Retinal cell types and their stratification properties. **a**–**b**, Schematic overview of cone (**a**) and rod (**b**) pathways. Black arrows indicate the flow of information. c; cone b; bipolar cell, g; ganglion cell, r; rod, rb; rod bipolar cell, a; amacrine cell. **c**, Inhibitory cell classes in the retina. h; horizontal cell, a; amacrine cell.

The excitatory cone and rod pathways are modified by two classes of inhibitory interneurons (**Fig. 2c**). The photoreceptor-to-bipolar synapse in the outer plexiform layer (OPL) is regulated by horizontal cells, which are of a single type in mice and exist in two types in most other mammals. The excitatory synapse between bipolar and ganglion cells is modulated by amacrine cells. These cells receive excitatory input from bipolar cells, and they feedback and feed-forward to bipolar terminals and ganglion cell dendrites, respectively. Amacrine cells are extremely diverse; more than 30 morphological types have been described [16], giving rise to almost half of all retinal cell types. The function of most of them is unknown. Two broad subclasses of amacrine cells have been differentiated based on coarse morphology [10, 11]. Wide field

cells have larger processes and these processes are confined to thin IPL strata. Two highly studied subtypes of wide field cells are the starburst cells, which were implicated in the circuit of directionally selective ganglion cells, and the A17 cells, which have been suggested to modify the flow of information from rod bipolar cells to A2 amacrine cells [10, 11]. The neural processes of narrow-field cells, like A2 cells, are laterally confined and organized vertically, spanning several strata of the IPL [10, 11]. The retina also contains glia cells called Müller glia.

The defined complex structure of cell types within the retina makes it a very attractive model for studying the genetic identity of individual cell types. In the first part of my thesis, I will focus on the identification of mouse lines with retinal cell type/class-specific labeling. In the second part, I analyzed the gene expression patterns of 14 different cell types/classes isolated from identified mouse lines.

Genetic address book for retinal cell types

Sandra Siegert[1], Brigitte Gross Scherf[1], Karina Del Punta[2], Nick Didkovsky[2], Nathaniel Heintz[2,3] & Botond Roska[1*]

[1]*Neural Circuit Laboratories, Friedrich Miescher Institute for Biomedical Research, Maulbeerstrasse 66, CH-4058 Basel, Switzerland*

[2]*GENSAT project, The Rockefeller University, 1230 York Ave., New York, New York 10065, USA.*

[3]*Laboratory of Molecular Biology, The Rockefeller University, 1230 York Ave., New York, New York 10065, USA.*

Introduction

In order to find mouse lines in which retinal cell types are specifically labeled, we took advantage of the finding that both the cell bodies and the neural processes of most retinal cell types are arranged in different layers. In some cases, specific antibodies are also available to mark individual or combination of cell types. We screened the retinas of 536 mouse lines generated in the GENSAT project. We observed stratum- or cell type-restricted GFP labeling in ~100 mouse lines. Among the labeled cell types, we found the well-known AII, A17 and starburst amacrine cells and also several ganglion cell types projecting to different target regions in higher visual centers. Quantification of cell stratification within the retina allowed us to predict connectivity between different cell types. Our screen provides the means for targeted recordings from identified retinal cells, for developmental studies of axon guidance, neural connectivity, cell type specification and cell type specific gene expression. The different retinal labeling patterns have been organized in a publicly available database (*http://www.gensat.org/retina.jsp*) from which 3D confocal stacks as well as optical sections can be downloaded.

Results

Screening strategy

We analyzed the retinas of 536 GENSAT mouse lines, each created with a different BAC. One retina of each eye pair was processed for wholemount labeling with anti-GFP and anti-ChAT antibodies (**Fig. 3a**–**b**). The anti-ChAT antibody labels a subset of amacrine cells that have processes in two thin strata within the inner plexiform layer (IPL), thereby providing a natural "depth marker"[17] (**Fig. 3a**). To label the nuclear layers, we stained the cell nuclei with diamidino-phenylindole (DAPI). All GFP-positive retinas were scanned in 3D at three wavelengths using a confocal

microscope, allowing for the separate visualization of GFP, ChAT and DAPI. Stratification was quantified relative to the ChAT strata (**Fig. 3a**,**b**, **Supplementary Fig. 15** and Experimental Procedures) [18]. After obtaining information about the stratification pattern from the first retina, we sectioned the second retina and stained with a variety of antibodies. We grouped the different retinas according to the labeled cell classes in the outer and inner retina.

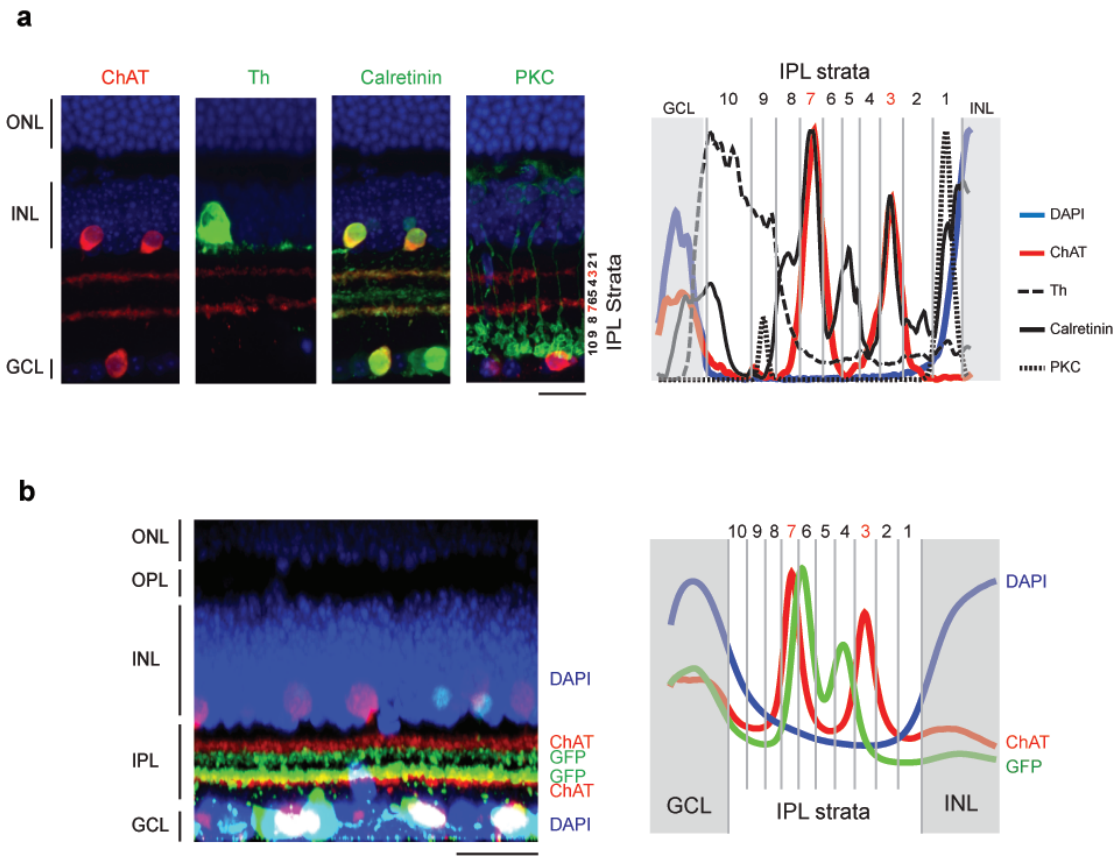

Figure 3. Definition of IPL strata. **a,** Left, confocal images of vertical sections of mouse retinas labeled with a combination of ChAT (red), Th (green), Calretinin (green), and PKC (green) antibodies and DAPI (blue). Right, antibody labeling profiles for Th (dashed line), Calretinin (black line) and PKC (dotted line) in relation to the ChAT strata (red) and the DAPI (blue) labeled nuclear layers. These profiles define 10 strata in the IPL (see Experimental Procedures). **b**, Left, example of a vertical optical section from a GENSAT retina. Right, depth distribution of the GFP (green), ChAT (red) and DAPI (blue) signals (see Experimental Procedures). The GFP labeled processes are located between the ChAT strata in stratum 4 and 6 in the IPL. Scale bars, 20 μm.

Labeled cell types in the outer retina

The outer retina is populated by photoreceptors, horizontal cells and bipolar cells. For all three cell classes, we found transgenic mouse lines that highlighted individual cell types. *Chrnb4* marked cone photoreceptors, indicated by the characteristic position of the cell bodies at the outer margin of the outer nuclear layer (ONL) and co-labeling with the cone marker peanut agglutinin [19] (**Fig. 4a**). *Cbln4* labeled only horizontal cells, which were identified by exhibiting lateral processes exclusively in the outer plexiform layer (OPL) and by calbindin staining[17] (**Fig. 4b**). Additionally, 20 other mouse lines showed horizontal cell labeling in combination with bipolar, amacrine or ganglion cells (**Supplementary Table 1**).

We found several transgenic mouse lines with GFP expression only in bipolar cells. *Dbx1* specifically yet sparsely marked type 5 bipolar cells (**Fig. 4c**). In other transgenic lines dense cell labeling was observed: *Kcng4* labeled mostly type 5, 6 and 7 bipolar cells, *Nr5a1* marked bipolar cells with axon terminals close to the ganglion cell layer (GCL) (**Fig. 4c**), *Lhx4_KN189* highlighted a subset of bipolar cells terminating between the ChAT strata. Furthermore, in several mouse lines specific types of bipolar cells were marked in combination with subtypes of amacrine or ganglion cells (**Supplementary Table 2-3**). One example is *Syt13* that labeled a mixed bipolar and amacrine cell population terminating only in selected OFF strata (**Fig. 4c**). Therefore, our mouse catalogue contains a number of lines that label specific cell types with processes in the OPL.

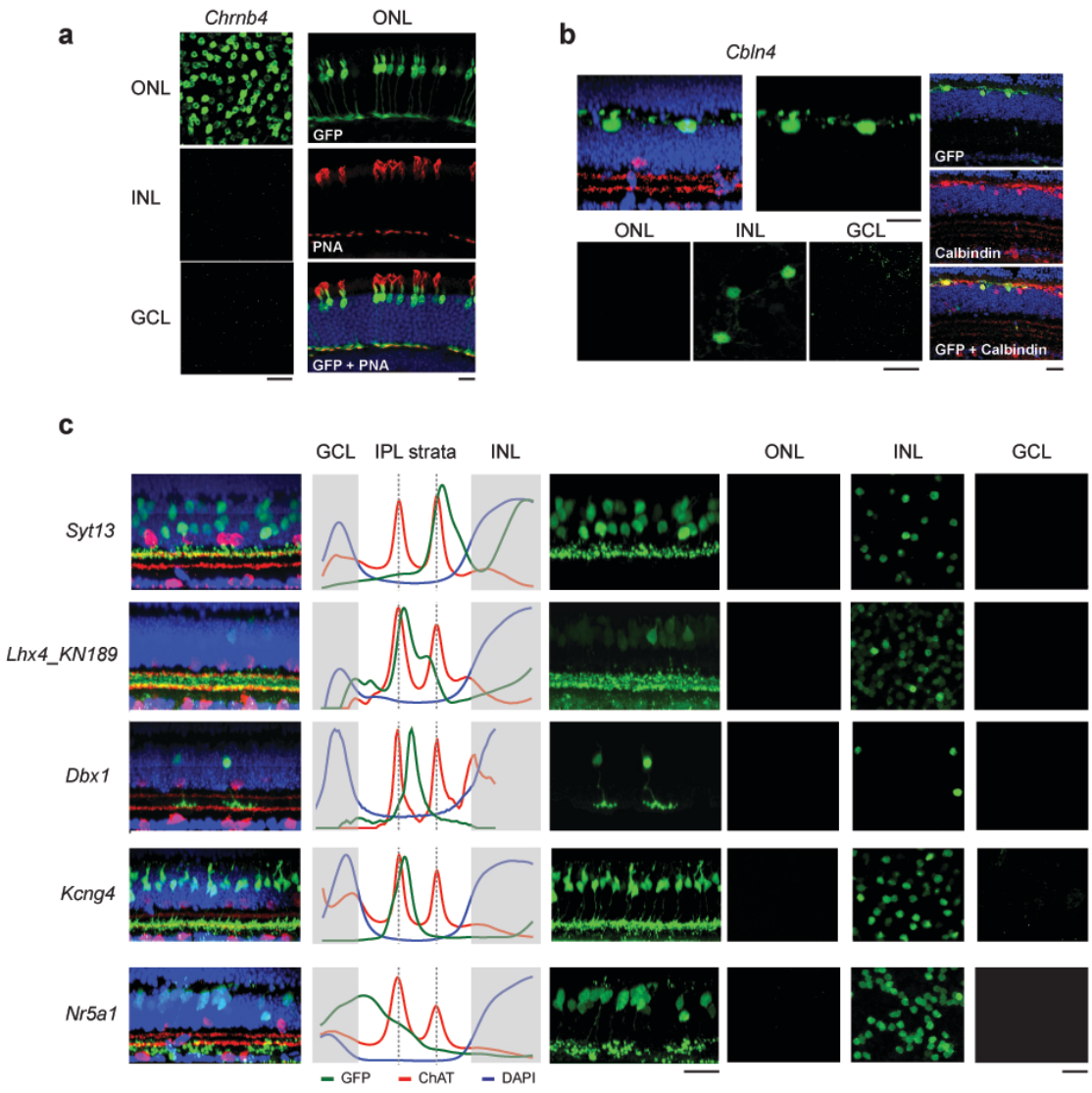

Figure 4. Cell type specific GFP expression in the ONL. GFP is green and DAPI is blue in all panels. **a**, Cones are labeled in *Chrnb4* mice. Left, GFP labeling in the ONL, INL and GCL. Right, GFP (top) and PNA (red, middle) labeling and the merge of the two images (down) in vertical sections showing the ONL and OPL. **b**, Horizontal cells are labeled in *Cbln4* mice. Left-top, GFP, ChAT (red). Left-down, GFP in the ONL, INL and GCL. Right, GFP (top), Calbindin (middle) and merge (down). **c**, First column, optical sections from selected transgenic mouse lines with different bipolar cell types labeled, ChAT is red. Second column, curves represent the fluorescent profiles of GFP, ChAT and DAPI. The dashed line shows the location of the two ChAT maxima (see Experimental Procedures). Third column, same as first column but only GFP is shown. Fourth-sixth columns, GFP labeling in the ONL, INL and GCL. Scale bars, 20 μm.

Labeled cell types in the inner retina

The inner retina consists of the amacrine and ganglion cell classes. The diverse cell types of each class can be distinguished by their processes stratifying in different depths in the IPL. We found more than 60 BAC transgenic lines with one or more commonly several types amacrine and/or ganglion cells were marked in a stratum-specific way (examples are shown in **Fig. 5**–**10**). *Doc2b* labeled an amacrine cell type with processes in the central stratum. *Aldh7a1* (**Fig. 5**), *Fgf15* and *Igfbp5* (**Fig. 10**) marked two mirror symmetric strata between the ChAT strata and the corresponding cell bodies in the inner nuclear layer (INL) and GCL. In *Ier5*, *Igfbp2* and *Tgif1* thicker bands at different depths in the IPL were labeled, yet in other BAC lines like *Pcbd1* and *Cartpt* narrow strata and thicker bands were marked in combination (**Fig. 5**). The large number of stratum-specific expression patterns (**Supplementary Table 4**–**8**) raised the possibility that in several mouse lines individual amacrine or ganglion cell types are selectively labeled.

There are few well studied amacrine cell types [10, 11] with characteristic morphology and defined function for which immunohistochemical markers are available. We tested if those distinct cell types are present and uniquely labeled in our mouse catalogue. One of the cell types are the mirror symmetric starburst amacrine cells with cell bodies in the INL and GCL. These cells are a key component of directional selective circuits [20] and are marked with the anti-ChAT antibody [17]. We found eight mouse lines with GFP and ChAT double positive neurons (**Fig. 6** and **Fig. 8a**): In *Ppm2c*, almost all ChAT-positive cells were GFP-positive, suggesting a one-to-one relation between the GFP-positive amacrine cells and the starburst amacrine cells. In *Klf13*, *Scube2* and *Slc5a7*, a fraction of ChAT-positive cells were GFP-labeled. In *Nrip3* and *Cbln2*, ChAT-positive cells and another amacrine cell type stratifying at the proximal part of the IPL were marked. Interestingly, in *Pcbd1* and *Nrip3*, only the ChAT-positive OFF stratum was labeled together with proximal IPL

strata, suggesting genetic differences in the mirror symmetric ON and OFF starburst amacrine cells.

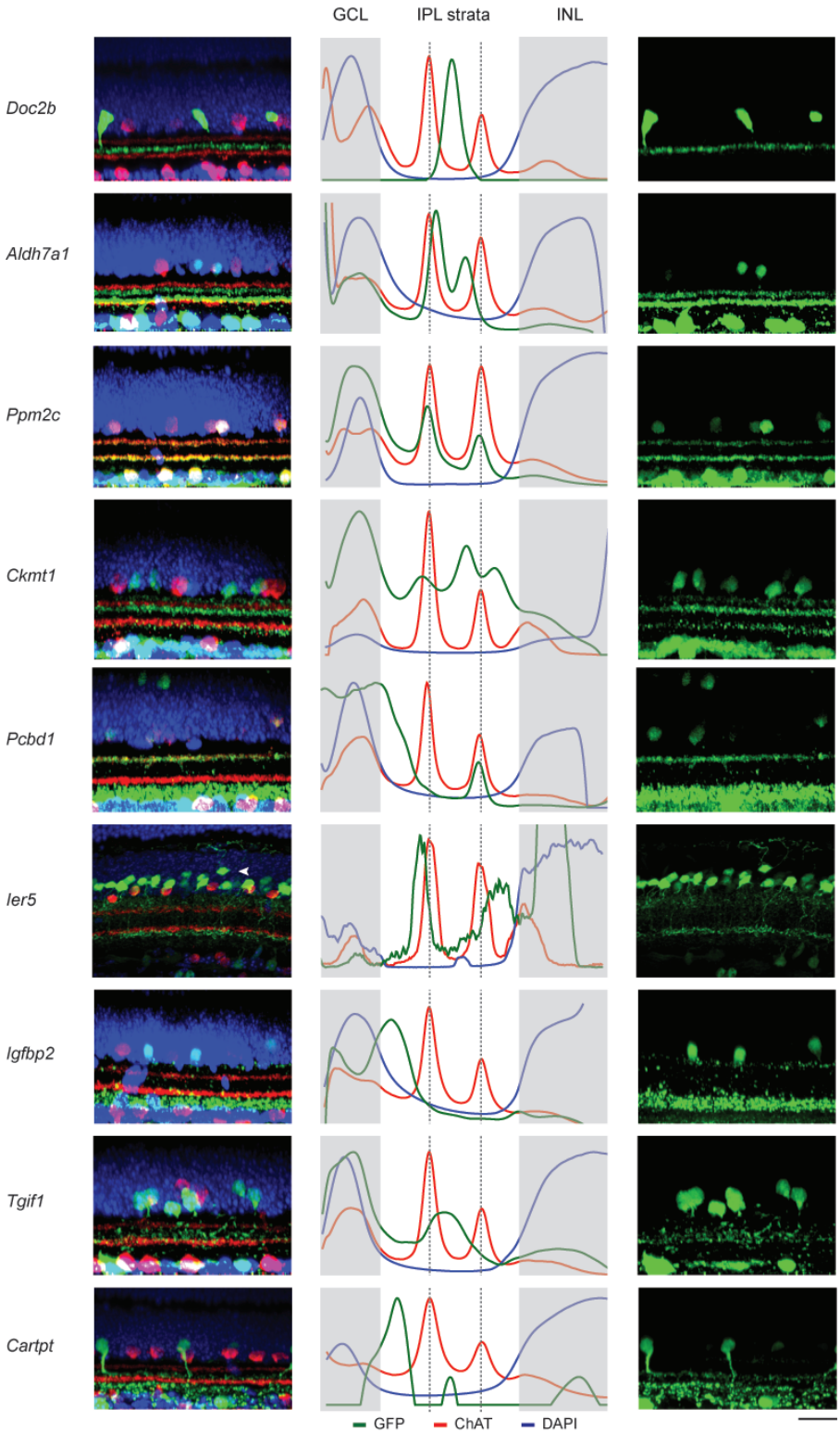

Figure 5. IPL stratum specific GFP expression in the INL in amacrine cell types (some also have ganglion types labeled). GFP is green, ChAT is red and DAPI is blue in all panels. First column, optical sections from selected transgenic mouse lines. Second column, curves represent the fluorescent profiles of GFP, ChAT and DAPI in the IPL. The dashed line shows the location of the two ChAT maxima (see Experimental Procedures). Third column, same as first column but only GFP is shown. Arrow in *Ier5* shows an interplexiform cell. Scale bars, 20 μm.

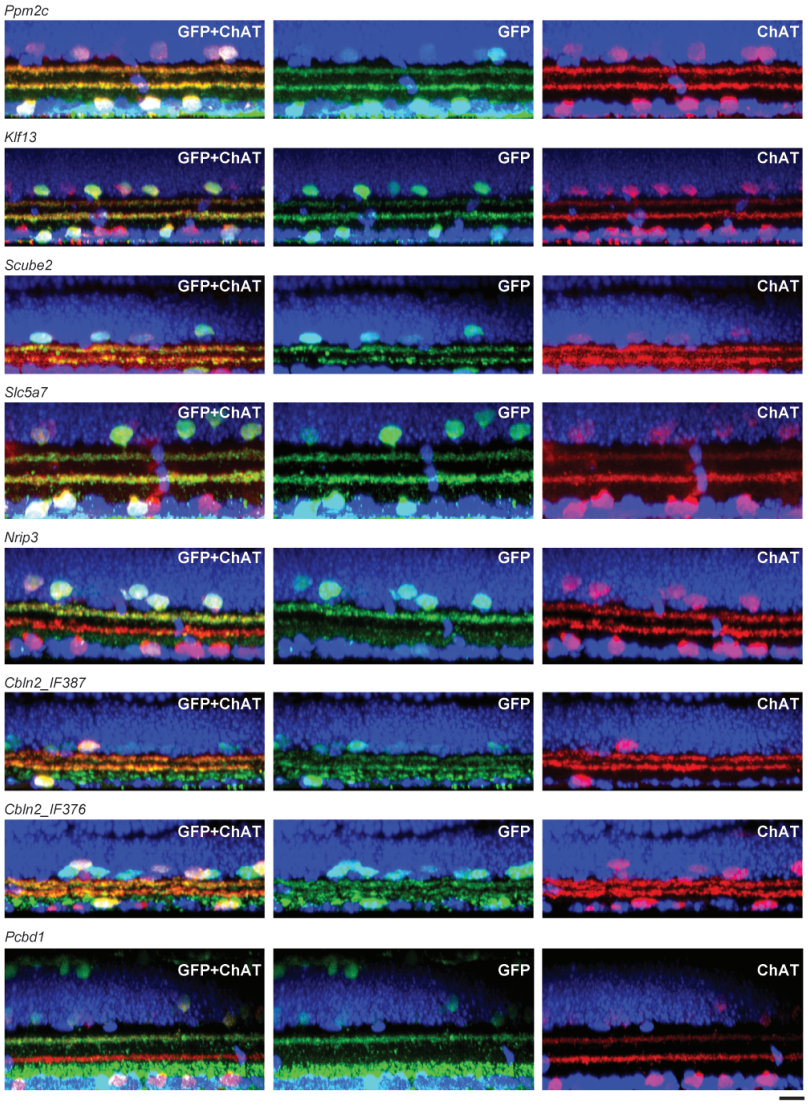

Figure 6. Identification of GENSAT mice with GFP labeled starburst amacrine cell types. GFP is green, ChAT is red and DAPI is blue in all panels. Vertical optical sections from four transgenic mouse lines which show colocalization with the ChAT antibody (red). Arrows indicate GFP and cholinergic positive cell bodies. Scale bar, 10 µm

Other examples of well studied amacrine cells with characteristic morphology are the AII and the A17 cells of the rod pathway. AII cells can be identified with the anti-disabled homolog 1 (Dab1) antibody [21]. In six mouse lines Dab1 labeled GFP-positive cells in the INL (**Fig. 7**, **Fig. 8b**–**c**). These mouse lines can be further distinguished based on the distribution of the GFP labeled cells throughout the retina: In the *Fam81a* line, the GFP-labeled cells almost covered the whole retina whereas in the *Slc18a3* line only a few cells were GFP-labeled.

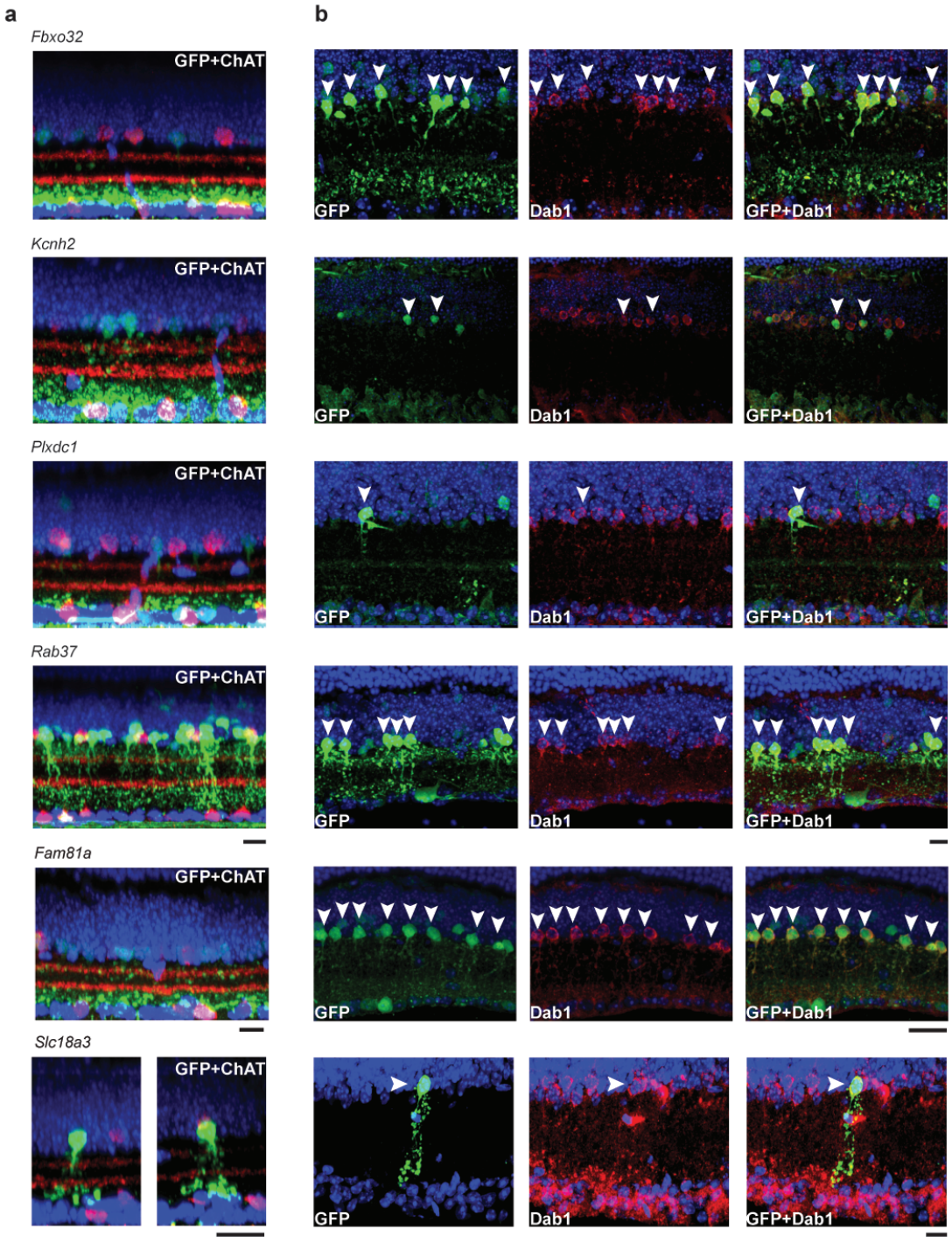

Figure 7. Identification of GENSAT mice with GFP labeled AII amacrine cell types. GFP is green and DAPI is blue in all panels. **a**, Stratification of the GFP labeled cells in the IPL referring to the ChAT antibody labeling in red. **b**, Colocalization of a subclass of GFP labeled cells with the AII amacrine cell marker Dab1 (red). Arrows indicate cell bodies which are Dab1 and GFP positive. Scale bar, 10 μm.

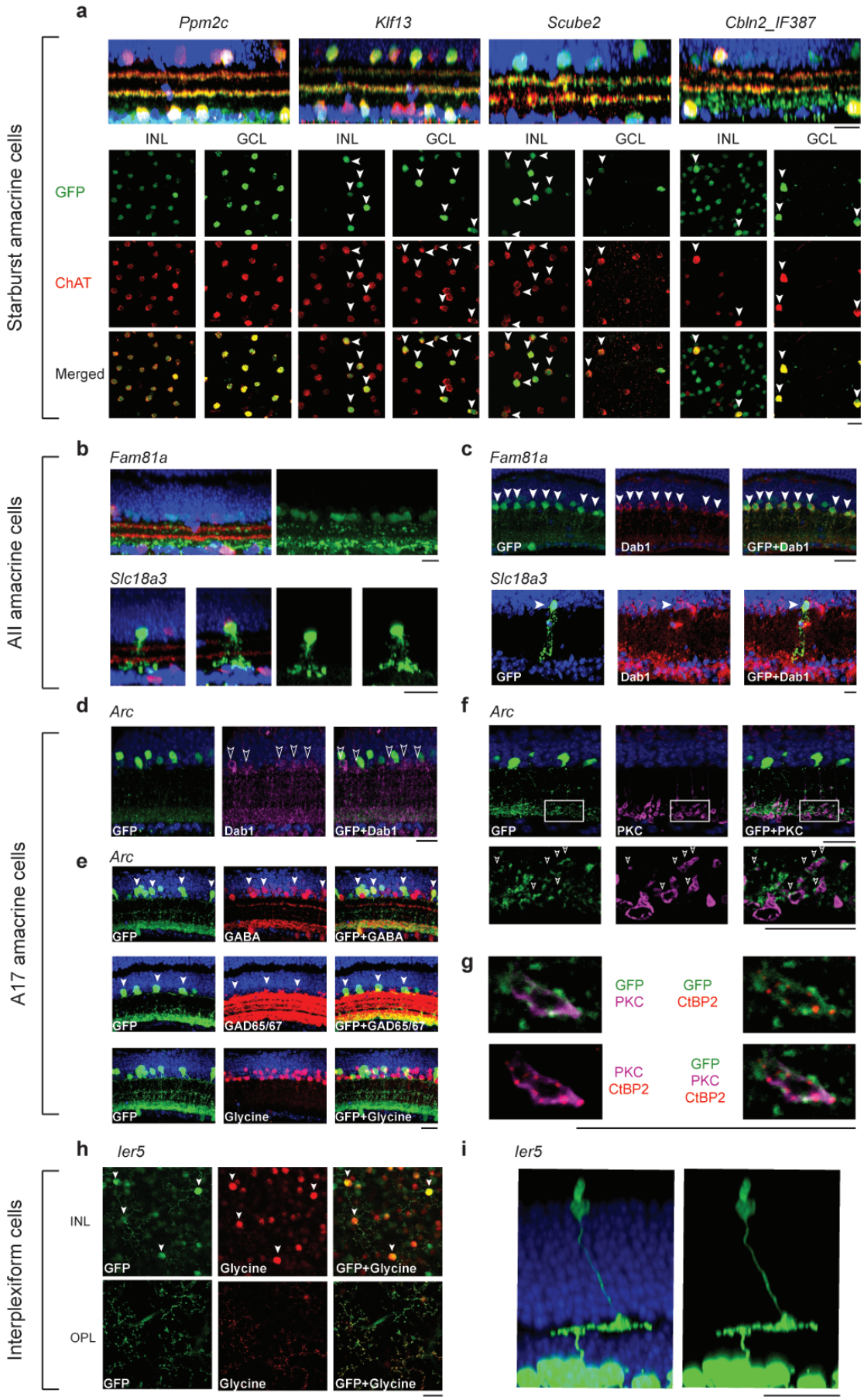
a
Ppm2c
Klf13
Scube2
Cbln2_IF387
INL
GCL
GFP
ChAT
Merged
Starburst amacrine cells
b
Fam81a
Slc18a3
c
Fam81a
Slc18a3
GFP
Dab1
GFP+Dab1
All amacrine cells
d
Arc
e
Arc
f
Arc
GFP
Dab1
GFP+Dab1
GABA
GFP+GABA
GAD65/67
GFP+GAD65/67
Glycine
GFP+Glycine
PKC
GFP+PKC
g
GFP
PKC
GFP
CtBP2
PKC
CtBP2
GFP
PKC
CtBP2
A17 amacrine cells
h
Ier5
i
Ier5
INL
OPL
Interplexiform cells

Figure 8. Identification of GENSAT mice with GFP labeled amacrine cell types. GFP is green and DAPI is blue in all panels. **a**, Starburst amacrine cells. Top, vertical optical sections from four transgenic mouse lines which show colocalization with the ChAT antibody (red). The lower panel shows the labeled cell bodies in the INL and GCL. Arrows indicate GFP and cholinergic positive cell bodies. In *Ppm2c* all cells are double positive (no arrows are shown). **b**–**c**, Two transgenic mouse lines with labeled AII amacrine cells. On **b**, stratification of AII amacrine cells. ChAT is red. **c** shows staining with the AII amacrine cell marker Dab1 (red). Arrows indicate cell bodies which are Dab1 and GFP positive. **d**–**g**, A17 amacrine cell. **d**, Dab1 (purple) labeling. White, open arrows indicate position of Dab1 positive cells. **e**, GABA (red), glutamate dehydroxylase 65/67 (GAD65/67, red) and Glycine (red) staining. Cells colocalizing with GFP and GABA and GAD are indicated by white, filled arrows. **f**, PKC (purple) marked rod bipolar cells are in close contact with the GFP positive processes in the proximal part of the IPL indicated by white arrows. Lower panels are magnified from the top panels (white boxes). **g**, A single rod bipolar terminal stained with PKC (purple) and the ribbon synapse marker CtBP2 (red). **h**, *Ier5* retina stained with Glycine antibody. Arrows indicate interplexiform cell bodies which colocalize with the Glycine antibody. **i**, GFP labeled interplexiform cells of *Ier5* contact GFP labeled photoreceptors. Scale bars, 20 μm.

In several other mouse lines, a broader stratum, co-stratifying with the axon terminals of rod bipolar cells, was uniquely GFP-labeled, raising the possibility that the marked cells are the GABAergic A17 cells (see **Fig. 9**). In the *Arc* line, GFP-labeled cells were Dab1- and glycine-negative but stained positive for anti-GABA and anti-GAD65/67 antibodies (**Fig. 8d**–**e**), suggesting that these amacrine cells are not the AII cells. High resolution confocal imaging of the IPL triple-stained with the rod bipolar marker, PKC, ribbon synapse marker, CtBP2, and GFP (**Fig. 8f**–**g**) indicated that the GFP-positive processes likely receive input from rod bipolar cells. Therefore at least some of the GFP-positive cells are the A17 cells (evidence will be published elsewhere showing that most if not all cells are the A17 cells).

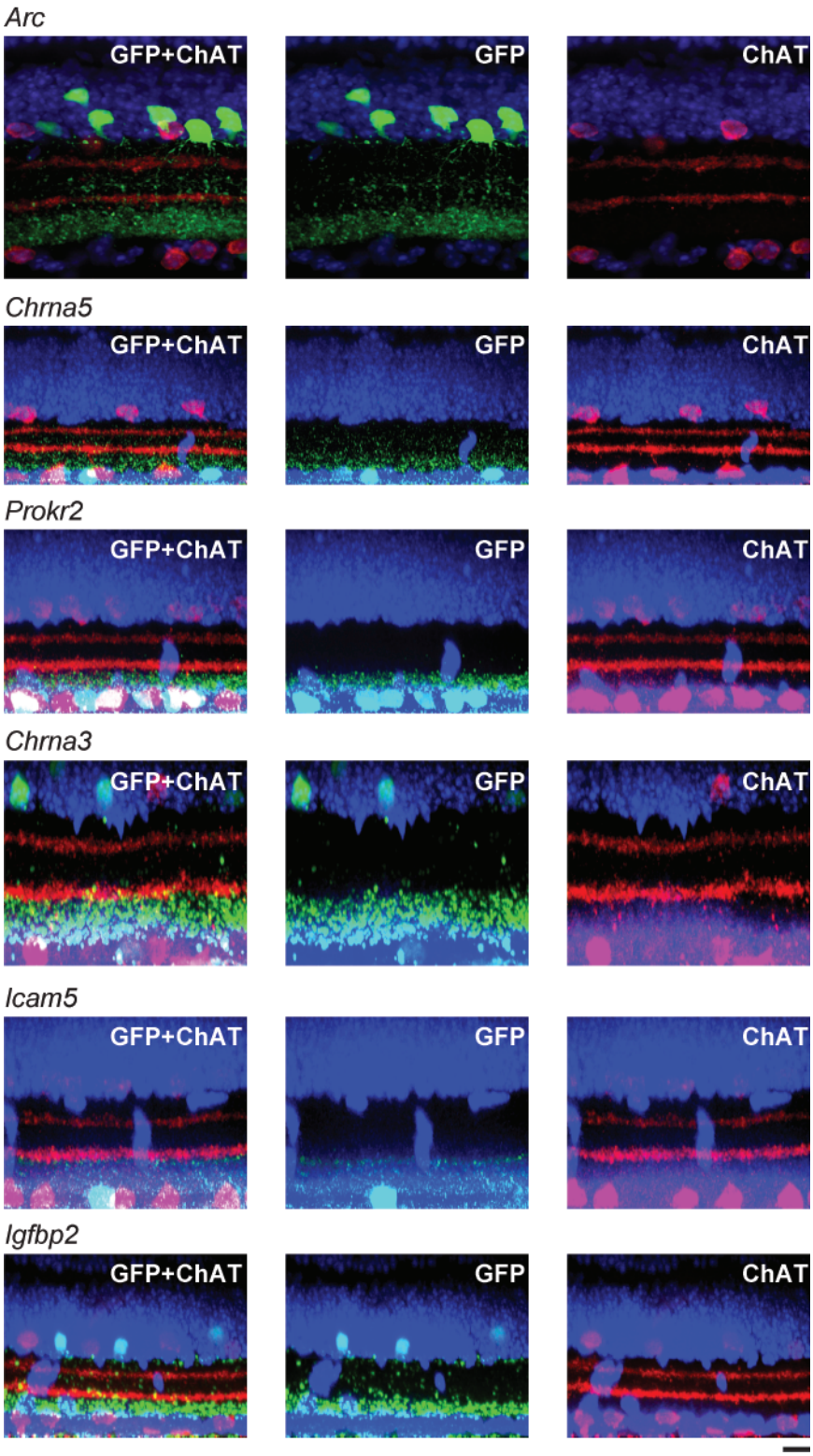

Figure 9. Identification of GENSAT mice with GFP labeled amacrine cell types stratifying in stratum 9 and 10 in the IPL. GFP is green, ChAT is red and DAPI is blue in all panels. Scale bar, 10 µm.

Another example of an identified cell type was found in the *Ier5* line. *Ier5* labeled a subset of amacrine cells that stratified in two bands within the IPL (**Fig. 5**). In the same mouse line a small subset of amacrine cells with processes reaching the

OPL (**Fig. 5**, white arrow) was marked. These OPL-projecting cells were strongly labeled with an anti-glycine antibody (**Fig. 8h**), suggesting that they are the glycinergic interplexiform cells of the mouse retina [17]. Interestingly, a subset of cone photoreceptors were also GFP-positive in this mouse line and many of the cone axon terminals were closely opposed to the processes of the *Ier5* interplexiform cells (**Fig. 8i**). Since glycinergic input to a subset of cone photoreceptors has recently been described [22], the GFP-labeled glycinergic interplexiform cells and the GFP-marked cones might be synaptically connected. The above examples show that our catalogue contains mouse lines with morphologically and immunohistochemically characterized GFP labeled amacrine cell types.

Mouse lines with GFP labeled ganglion cell subsets [23-26] were also present in our mouse library. Retinal ganglion cells are the output cells of the retina with dendrites occupying narrow IPL strata and axons projecting to different target regions in the brain. We screened for mouse lines based on three criteria: The labeled cell bodies are in the GCL, GFP positive axons are detectable and selective IPL strata are marked (**Fig. 10a**). The presence of GFP stained axons are important for identifying ganglion cells since ~60 % of the cells in the GCL of mice are displaced amacrine cells [27]. **Figure 10a** shows that *Fgf15* and *Cartpt* ganglion cells project to the upper strata in the superior colliculus (SC) while the axonal projection of *Coch* cells is complementary, terminating in lower SC strata. A similarly complementary labeling pattern is shown in the optic tract between *Chrna3* and *Fgf15* ganglion cells. In these examples GFP labeling in the brain was sparse (**Fig. 11**) and therefore the axons of ganglion cells could be followed through serial brain sections up to the target regions, this may not be possible if GFP densely labels different brain nuclei. These results suggest that similar to amacrine cells, the ganglion cell types are selectively labeled in different mouse lines.

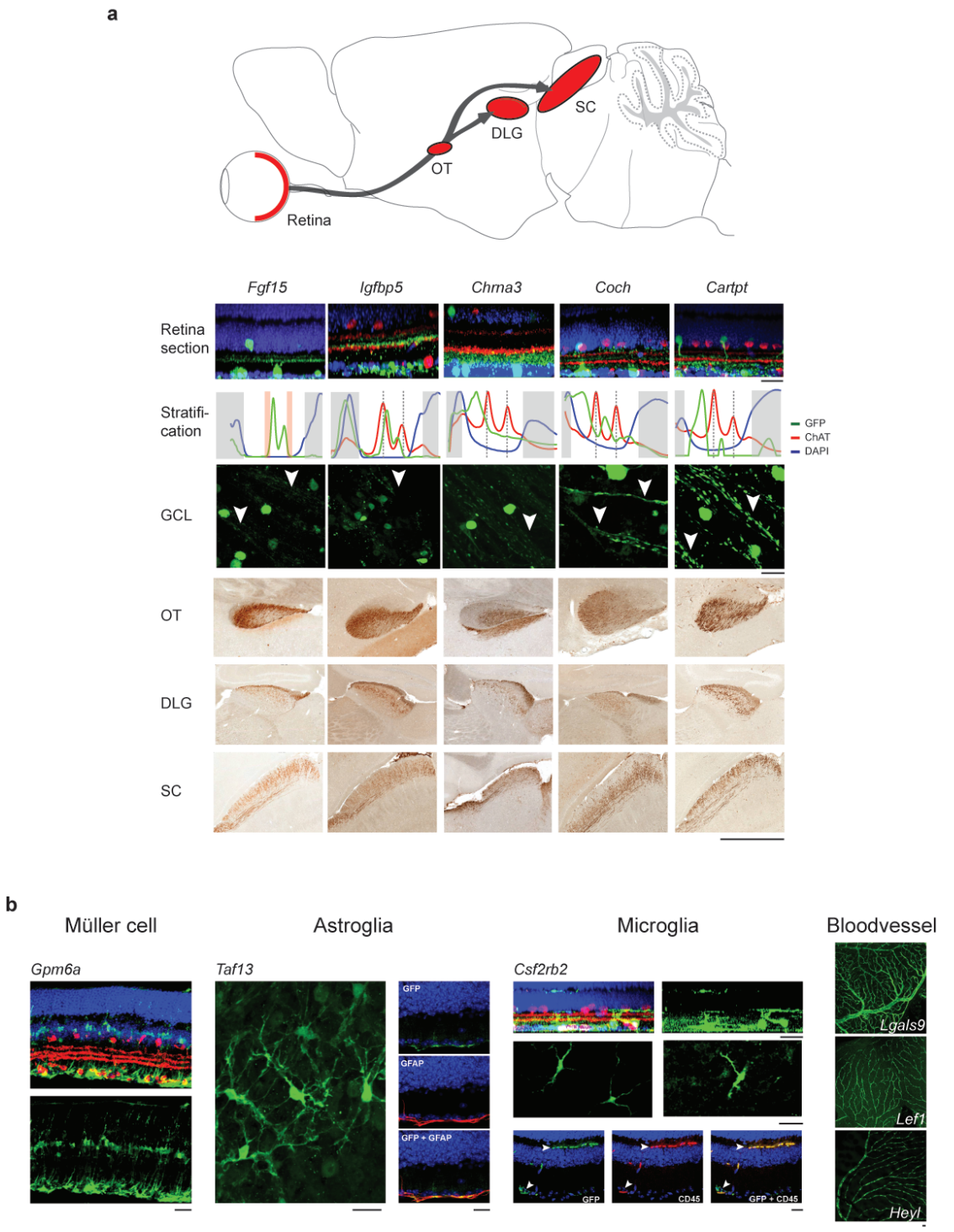

Figure 10. Identification of GFP labeled ganglion cell types. **a**, Example of five transgenic mouse lines which express GFP in subsets of ganglion cells. Top, schematic view of the main ganglion cell projections in the brain. Bottom, GFP is green in the first three rows and brown in the last three rows and DAPI is blue in all panels. First row, optical sections, ChAT is red. Second row, curves represent the fluorescent profiles of GFP, ChAT and DAPI in the IPL. Third row, GFP labeled axons (white arrows). Scale bar, 20 µm. GFP labeling in the optic tract (OT, fourth row), dorsal geniculate (DLG, fifth

row) and superior colliculus (SC, sixth row). Scale bar, 1 mm. **b**, Examples of transgenic mouse lines which label non-neuronal cell classes. First column, typical Müller cell morphology in *Gpm6a* mice. Red, calretinin. Second column, *Taf13* cells are costained with astrocyte marker GFAP. Third column, *Csf2rb2* cells are co-labeled with microglia marker CD45. Fourth column, blood vessels were selectively labeled in *Lgals1*, *Lef1* and *Hey1* mouse lines. Scale bars, 20 μm.

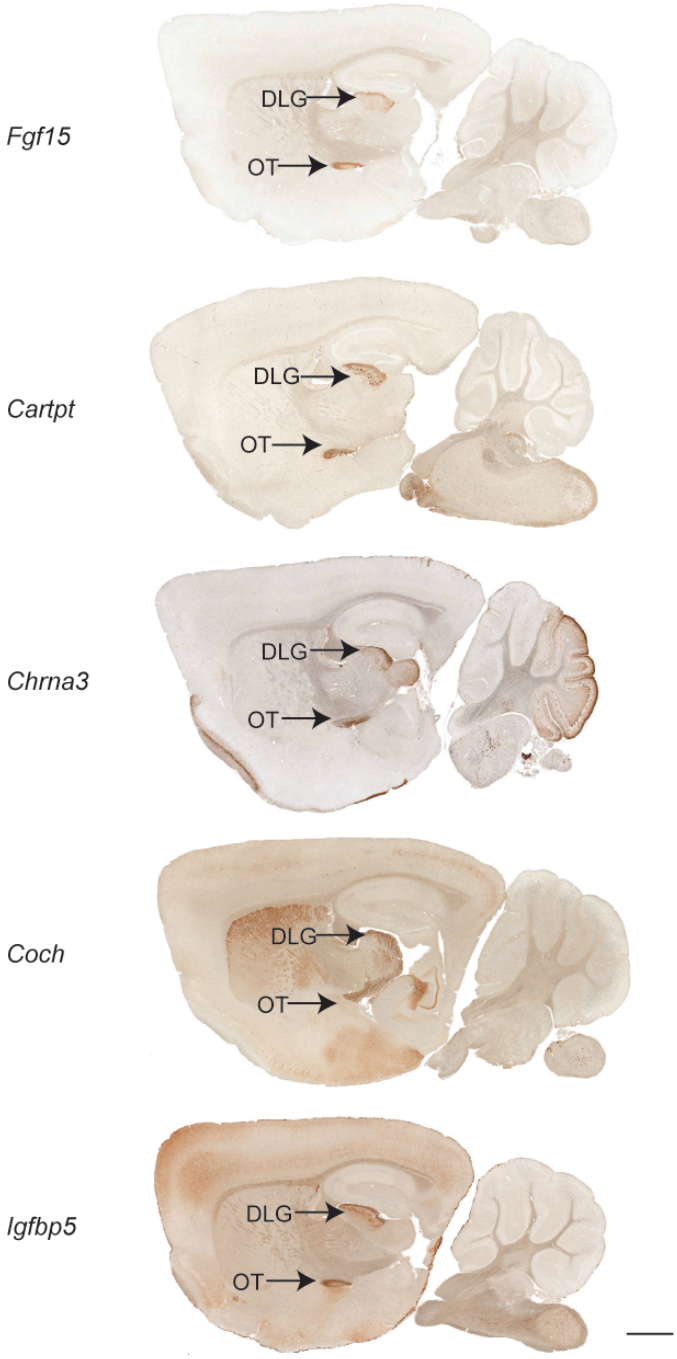

Figure 11. Sparse GFP labeling in the brain allows one to observe the axonal projection of labeled ganglion cells in *Fgf15*, *Igfbp5*, *Chrna3*, *Coch*, *Cartpt* lines. One sagittal section is shown for each mouse line, all section can be downloaded from www.gensat.org. Arrows point to optic tract (OT) and the dorsal geniculate (DLG). Scale bar 1 mm.

Finally, our screen yielded markers for all four non-neuronal cell classes in the retina (**Fig. 10b**). In several mouse lines Müller cells were labeled (**Supplementary Table 9**). Astrocytes were marked in *Taf13*, microglia in *Csf2rb2* and blood vessels in *Lgals9*, *Lef1* and *Heyl* (**Supplementary Table 10)**.

Equivalent stratification groups and connectivity maps

We found that some mouse lines have similar stratification patterns. To quantify this similarity, we divided the IPL into 10 strata using antibody markers (**Fig. 3**, Experimental Procedures) and determined which strata were GFP labeled. In each scan, the depth of the GFP labeled processes within the IPL was normalized to the ChAT labeled strata [18] (see Experimental Procedures and **Supplementary Fig. 15**). We assigned a binary string for every stratification pattern (**Supplementary Table 1**–**10**). The first entry of the binary string represented the OPL and the next ten the different IPL strata. If the strata had a GFP peak, the entry was "1", otherwise the entry was "0". We defined an equivalent stratification group as a set of mouse lines that had the same binary string. We have found 16 equivalent stratification groups. In two of them all 10 strata in the IPL were broadly labeled with or without the OPL. In the remaining 14, specific strata or combination of strata were labeled (**Fig. 12a**).

An equivalent stratification group may include different BACs which label the same cell type, for example the starburst cells (group VIII) or BACs which label different cell types but with the same stratification pattern. An example for the latter is shown in group VI. The cell types of this group stratify in stratum 1, 2 and 8, but *Pus10* represents amacrine cells and *Lmo2* ganglion and amacrine cells.

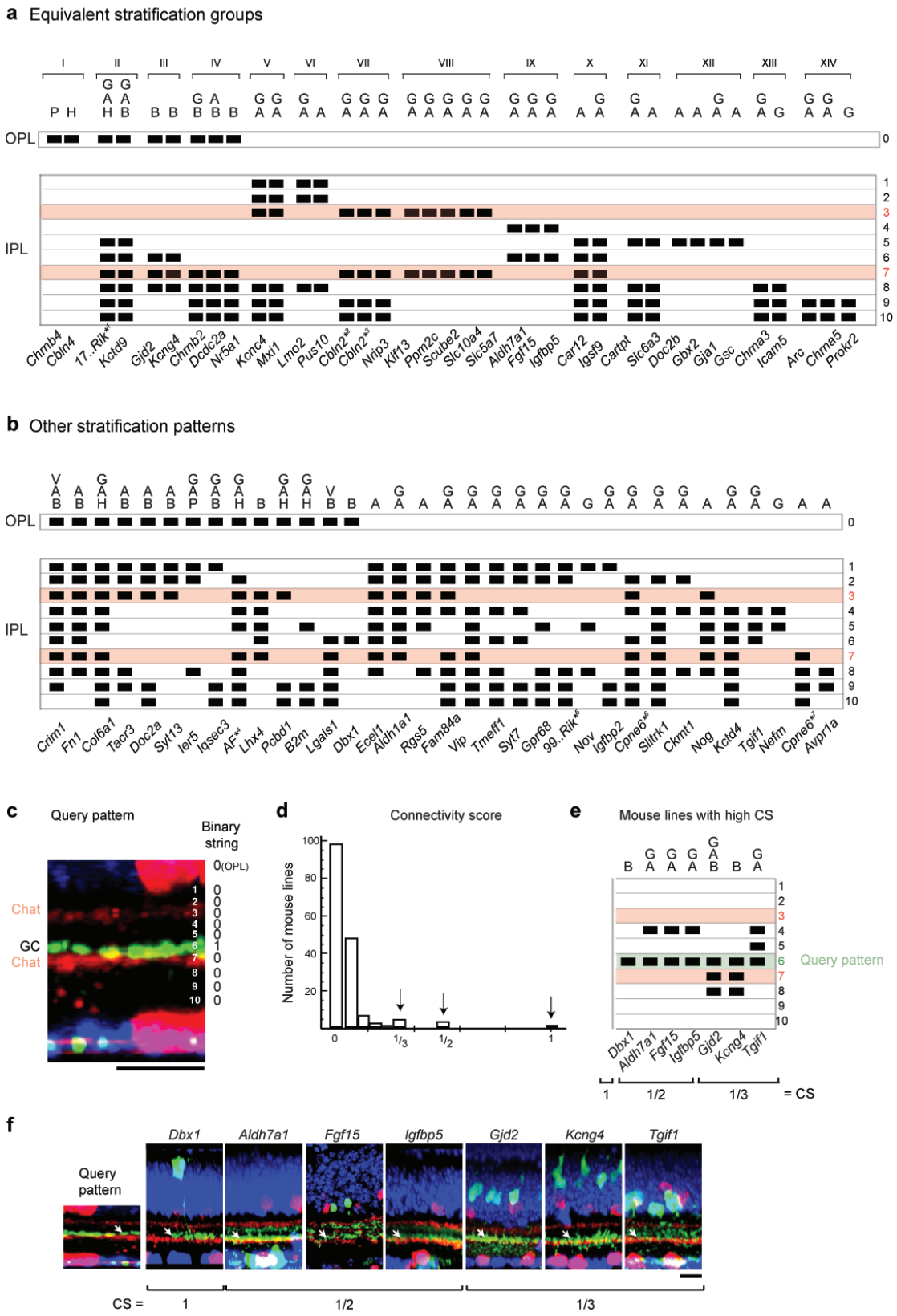

Figure 12. Stratification analysis of different cell types. **a**, Equivalent stratification groups based on the assigned binary strings (see Experimental Procedures). Mouse lines which have the same stratification pattern in the IPL (groups summarized by Roman numerals) are depicted. GFP labeled strata are

represented by black boxes. The ChAT strata are labeled in red. (*[1] *1700054N08Rik*, *[2] *Cbln2_IF376*, *[3] *Cbln2_IF387*) **b**, Unique stratification patterns. (*[4] *AF529169*, *[5] *9930013L23Rik*, *[6] *Cpne6_JS29*,*[7] *Cpne6_JS7*) **c**–**f**, The connectivity score allows one to find potential synaptic partners of a query pattern. **c**, A GFP labeled ganglion cell is shown (query pattern) with processes in one stratum. **d**, Histogram of connectivity scores between the query pattern and all other candidate patterns is shown (see Experimental Procedures). Seven mouse lines had scores larger than or equal to ⅓ (indicated by a black arrows). **e**, The stratification diagram for the eight candidate-connected cells labeled in different mouse lines. **f**, Vertical sections shown for each candidate pattern. GFP (green), ChAT (red) DAPI (blue). P: photoreceptor; H: horizontal cell; B: Bipolar cell; A: amacrine cell in INL; G: Cell in GCL; V: blood vessels. Scale bars, 10 μm.

The example of group XIV with bipolar, amacrine and ganglion cells in the same stratum raises the possibility that those cell types might be connected with each other in a neuronal circuit. In the inner retina, two cell types can only be synaptically connected if their processes co-stratify in at least one IPL stratum. Using this principle we searched for GENSAT mouse lines with labeled cells which are potentially connected. In the example presented in **Figure 12c**, we searched for mouse lines where at least one GFP positive IPL stratum was the same as the dendritic stratification of a ganglion cell type of interest labeled in another mouse line (“query pattern”, **Fig. 12c**).

Since candidate mouse lines with one or few GFP positive strata are more useful than lines with broad IPL labeling, we assigned a connectivity score to each search hit (**Fig. 12d**–**f**). The score is “1” if the stratification patterns of the query and the hit are identical. With increasing number of unmatched GFP strata the score is decreasing towards zero (see Experimental Procedures). This methodology enables one to define a hypothetical circuit that could be rigorously tested by other

methodologies [28] (see Discussion). However the approach may have limited use in candidate mouse lines with both ganglion and amacrine cells labeled in more than one stratum. It may not be possible to separate the contribution of amacrine and ganglion cell processes, as the co-stratification of the candidate cells with the query ganglion cell may simply reflect two ganglion cell types in the same stratum.

Live recordings from labeled cells

The different BAC transgenic mouse strains provide an opportunity to record from a variety of cell types in a targeted way. To visualize GFP positive cells for targeted recordings the excitation of choice is the two photon (2P) laser which does not bleach the photopigments of the retina. To test if the GFP expression is strong enough to be detected by 2P microscopy we chose eight mouse lines and examined isolated wholemount retinas. Among the lines was one (*Fam81a*) that had the weakest staining in the GFP antibody labeled retina library and others that were medium or strongly labeled. **I**n all tested lines the labeled cells were visible under the 2P microscope (**Fig. 13a)**. Moreover, the strength of fluorescence under live conditions correlated with the strength of fluorescence in antibody stained retinas (correlation coefficient = 0.5) (**Fig. 13b**).

We then performed 2P targeted patch clamp recordings in retinal slices (**Fig. 13c**) and in whole mount retinas (**Fig. 13d**). In both tissue preparations light responses could be recorded from GFP marked cells. When the patch-electrodes were filled with Lucifer yellow or neurobiotin the processes of the GFP labeled cells could be investigated with greater detail (**Fig. 13e**–**f**). These results suggest that it may be feasible to target and record from GFP marked cells of most lines in the mouse library.

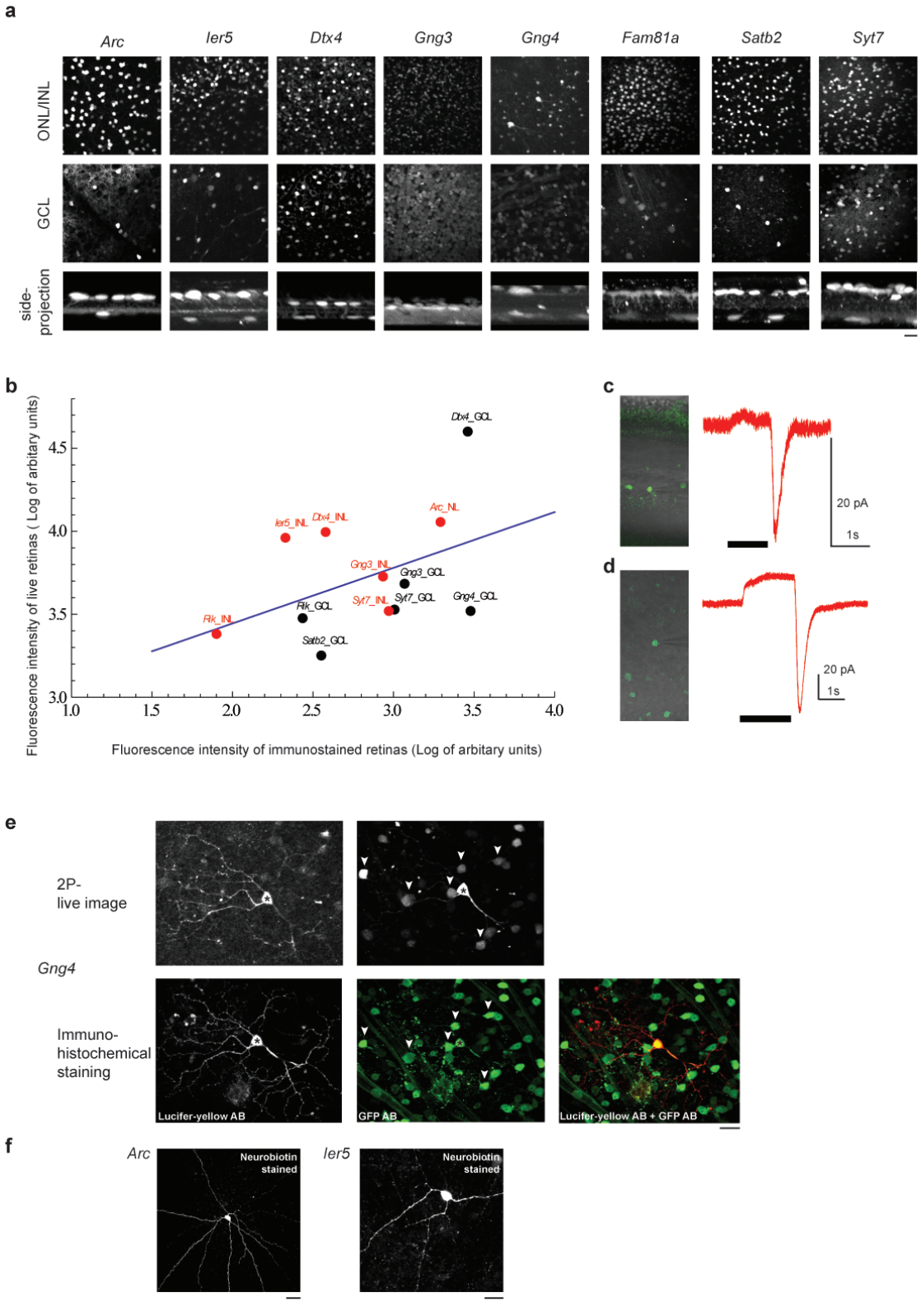

Figure 13. 2P live imaging of the GFP labeled cells in eight transgenic mouse lines. **a,** 2P image of GFP positive cell bodies in adult wholemount retina in the INL and the GCL. Top, top-down projections of GCL and INL, bottom, vertical projections. The laser intensity and PMT settings were optimized for the different lines shown. **b**, Relationship between the average fluorescence in immunostained retinas

scanned with a confocal microscope and in live conditions scanned with 2P microscope. Fluorescence was quantified separately in the INL and GCL. Unlike in (**a**) the laser intensity and PMT settings were the same for all 2P and confocal scans and were done on the same day. INL, red, GCL, black. **c**–**d,** 2P laser targeted electrophysiological recordings of light evoked currents from Arc mice in retinal sections (**c**) and in wholemount retina (**d**) The left pictures show overlaid infrared and 2P images that are used to navigate the pipette to patch the labeled cells. The right panel represents light evoked currents which were measured in voltage clamp at -60 mV holding potential. The timing of the light stimulus is indicated by the black bar. **e,** The top row shows live 2P image of Lucifer yellow filled cell in the *Gng4*-EGFP mouse focusing at different planes. The lower row shows immunohistochemical staining for GFP (green) and Lucifer yellow (white, red) of the previous live-imaged Lucifer-yellow filled cell. The asterisk marks the position of the filled cell body. The arrows indicate GFP positive cell bodies which were visible in the 2P images as well as in the immunohistochemical staining. **f,** Neurobiotin-filled cells in the *Arc*-EGFP and the *Ier5*-EGFP mice. Neurobiotin was visualized with Alexa-555 coupled to streptavidin. Scale bars, 20 µm.

In vivo marked strata and cell types can also be utilized for developmental studies [29]. In five tested lines the GFP labeled cells were clearly visible at postnatal day 0 using 2P microscopy (**Fig. 14**). Therefore strata targeting or postsynaptic partner choice can be studied in these and other lines that express GFP at early time points.

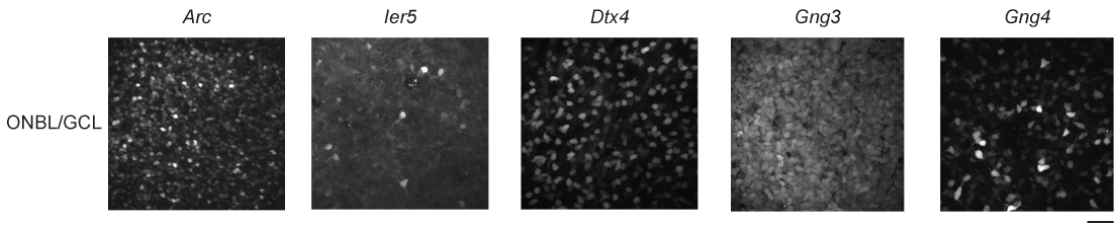

Figure 14. 2P live imaging of GFP labeled cells in five transgenic mouse lines at postnatal day 0 or 1. The pictures show top-down projections of the outer neuroblastic layer (ONBL). Scale bar, 20 µm.

Stability of expression patterns across generations.

In order to be useful for physiological investigations the retinal expression patterns should be stable through different generations. We therefore compared the expression patterns from our screen with the expression patterns of six mouse lines ordered from the public repository of GENSAT mice (MMRRC). The mice were passed through a minimum of four and a maximum of nine generations. In all six lines the retinal GFP expression patterns, based on stratification and cell class labeling, were identical to the GFP labeling of the retinas that were used in our screen (results not shown).

Discussion

We took advantage of the stratification rules of the retina to search GENSAT mouse lines for GFP labeled retinal cell types. We have described ~100 mouse lines with either defined strata or more specifically retinal cell types marked with GFP. To make our data accessible to the research community, we organized the image stacks obtained from the 3D retinal confocal scans in a publicly available database (*http://www.gensat.org/retina.jsp*). The user can search the retina database for cell classes and/or cell processes located in specific IPL strata. Furthermore, it is possible to search for mouse lines where the labeled cells ("candidates") are potentially connected to a cell type of interest ("query"). The resulting candidates are ranked according to the number of strata that are co-labeled with the query cell type. One use of this search is to find the excitatory and inhibitory cell types that give synaptic input to a genetically labeled ganglion cell type [23-26, 30]. Many of the BAC transgenic mice can be ordered at *www.mmrrc.org* and the GFP modified BACs can be ordered at *bacpac.chori.org*.

Note that in few cases MMRRC supplies the BAC-GFP lines in FVB/N-Swiss Webster hybrid background, which is homozygous for the retinal degeneration (rd) allele Pde6b^{rd1}. Since in the recessive eye disease, rd, the photoreceptor layer degenerates, mice have to be backcrossed with for example C57BL/6J mice that lack the Pde6b^{rd1} allele. Most of the strains are sent as B6-FVB hybrids, which do not have rd but carry the recessive disease allele, therefore crossings should be performed with for example the C57BL/6J line. In our hands the backcross of three FVB/N-Swiss Webster hybrid strains to C57BL/6J did not have an effect on the expression pattern of GFP and in all three lines we were able to measure light responses (results not shown). Detailed information about mouse strains with retinal degeneration can be found at *www.jax.org*.

In a few retinal circuits the participating cell types are already established by electron microscopic methods [31, 32]. However targeted recordings were not possible due to the lack of mouse lines with selectively GFP labeled cell types. For example, in the "classical" rod circuit, information flows from rod bipolar cells to AII and A17 amacrine cells. Our screen resulted mouse lines with either GFP labeled AII or A17 cells. Since a mouse line labeling rod bipolar cells has already been described [33], all components of this circuit can now be targeted for functional studies.

The variety of stratum- and cell type-specific mouse lines also creates the opportunity to study the development in distinct strata and cell types, their neural connectivity and axon guidance. The differential axon termination patterns, for example of the *Coch* and *Fgf15* ganglion cells in the distinct strata of the superior colliculus, allow axon guidance investigations for different ganglion cell types [23-26, 30, 34]. When individual cell types are sparsely and brightly labeled, like in the case of type 5 bipolar cells of *Dbx1* or the AII cells of *Slc18a3*, *in vivo* or *in vitro* imaging of retinal strata targeting by individual cell types is feasible [35]. Furthermore, fluorescent

activated cell sorting (FACS) of labeled cell types [36] or individual cell picking followed by gene chip experiments [37] at different stages of development could provide insight into the molecular machinery underlying neural circuit formation. Note that the expression patterns in our screen are from adult mice. It is possible that some lines do not express GFP early enough to be useful for developmental investigations.

GFP expression from BACs may reflect the endogenous expression of the protein encoded by the unmodified BAC however this might not always be the case. The expression pattern may depend on integration site and copy number. Furthermore the endogenous promoter might be longer than the sequence included in the BAC. Further work should clarify which GFP patterns reflect the endogenous expressions of the corresponding gene.

In summary, we screened for retinal cell types in a BAC transgenic mouse line library based on the arrangement of retinal cells and their processes in different layers of the retina as well as known antibody markers. Since many other brain structures like the neocortex and the superior colliculus are also layered structures, a similar screen could result in the identification of mouse lines that label individual cell types in those brain areas.

Supplementary Table 1–10. Summary of all GENSAT mouse lines with patterned GFP expression. The binary stratification string (see Experimental Procedures) and a binary code for labeled cell types (see top for cell type order) is shown. The code for a cell type is 1 if the cell type is labeled and 0 if not. The grey bar indicates the OPL, the red bars the ChAT strata. An asterisk behind the "1" in the binary code for "cells in GCL" indicates that axons are detectable and therefore at least some of the cells in the GCL are ganglion cells.

	Gene	Founder	Stratification (OPL | IPL)	Cell class (Photoreceptor, Horizontal cell, Bipolar cell, Müller cell, Amacrine cell, Cells in GCL, Blood vessel, Microglia, Astrocyte)
Photoreceptors	*Cckbr*	KR80	{1,0,0,0,0,0,0,0,0,0}	{1,0,0,0,0,0 ,0,0,0}
	Chrnb4	CL200	{1,0,0,0,0,0,0,0,0,0}	{1,0,0,0,0,0 ,0,0,0}
	Rac3	JZ58	{1,0,0,0,0,0,0,0,0,0}	{1,0,0,0,0,0 ,0,0,0}
	Cdk5r2	KZ220	{1,0,0,0,0,0,0,0,0,0}	{1,0,0,0,0,1 ,0,0,0}
	Gabarapl1	KY110	{1,0,0,0,0,0,0,0,0,0}	{1,0,0,0,0,1*,0,0,0}
	Ier5	IG267	{1,1,1,0,0,0,0,0,1,0,0}	{1,0,0,0,1,1 ,0,0,0}
	Arhgdib	KY11	{1,1,1,1,1,1,1,1,1,1,1}	{1,0,0,0,1,1 ,1,0,0}
Horizontal cells	*Cbln4*	IG145	{1,0,0,0,0,0,0,0,0,0,0}	{0,1,0,0,0,0 ,0,0,0}
	Sucnr1	LD94	{1,0,0,0,0,0,0,0,0,0,0}	{0,1,0,0,0,0 ,0,0,0}
	Sucnr1	LD99	{1,0,0,0,0,0,0,0,0,0,0}	{0,1,0,0,0,0 ,0,0,0}
	Lmo1	KN8	{1,0,0,0,0,0,0,0,0,0,0}	{0,1,0,0,0,1 ,0,0,0}
	Tubb4	KR607	{1,1,1,1,1,1,1,1,1,1,1}	{0,1,0,0,1,0 ,0,0,0}
	1700054N08Rik	LB209	{1,0,0,0,0,1,1,1,1,1,1}	{0,1,0,0,1,1 ,0,0,0}
	Ablim2	KX71	{1,0,0,0,0,0,0,0,0,0,0}	{0,1,0,0,1,1 ,0,0,0}
	AF529169	KR488	{1,0,1,1,1,1,0,1,1,1,1}	{0,1,0,0,1,1 ,0,0,0}
	Atp6v1b2	IE336	{1,0,0,0,0,0,0,0,0,0,0}	{0,1,0,0,1,1*,0,0,0}
	B2m	IM76	{1,0,0,0,0,1,0,0,0,1,1}	{0,1,0,0,1,1 ,0,0,0}
	Col6a1	JB13	{1,1,1,1,1,0,1,1,1,1,1}	{0,1,0,0,1,1 ,0,0,0}
	Gad1	JC163	{1,1,1,1,1,1,1,1,1,1,1}	{0,1,0,0,1,1 ,0,0,0}
	Lss	JR102	{1,0,0,0,0,0,0,0,0,0,0}	{0,1,0,0,1,1 ,0,0,0}
	Pcbd1	IJ269	{1,0,0,1,0,0,0,0,0,1,1}	{0,1,0,0,1,1 ,0,0,0}
	Peg3	KA50	{1,1,1,1,1,1,1,1,1,1,1}	{0,1,0,0,1,1 ,0,0,0}
	Zfp238	LW144	{1,1,1,1,1,1,1,1,1,1,1}	{0,1,0,0,1,1 ,0,0,0}
	Anxa2	JY66	{1,1,1,1,1,1,1,1,1,1,1}	{0,1,0,0,1,1 ,0,1,0}
	Prox1	KY221	{1,0,0,0,0,0,0,0,0,1,1}	{0,1,1,0,1,0 ,0,0,0}
	Pttg1	JC120	{1,0,0,0,0,0,0,0,0,1,1}	{0,1,1,0,1,0 ,0,0,0}
	Sqle	IM104	{1,1,1,1,1,1,1,1,1,1,1}	{0,1,1,0,1,1 ,0,0,0}

Supplementary Table 1

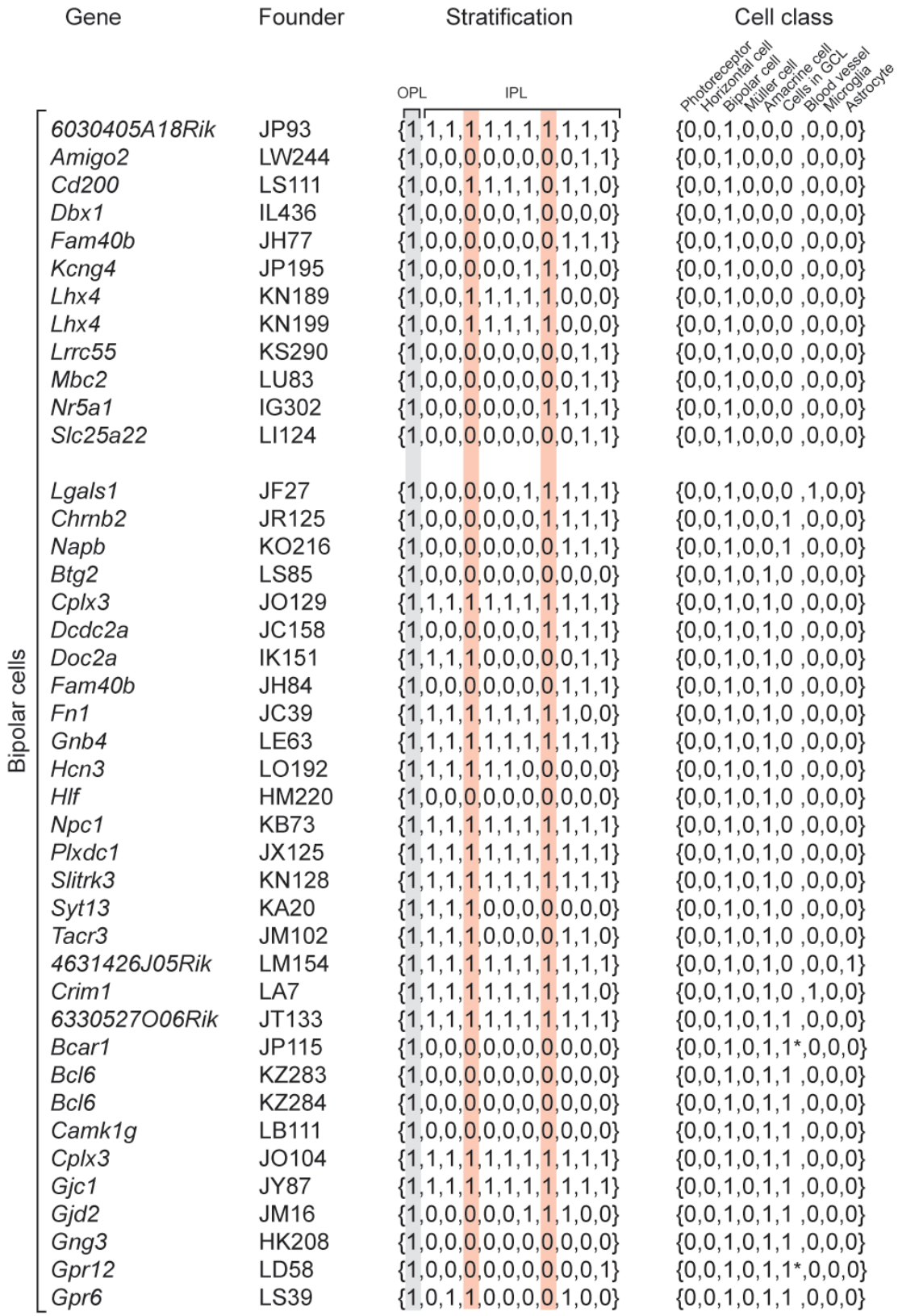

Supplementary Table 2

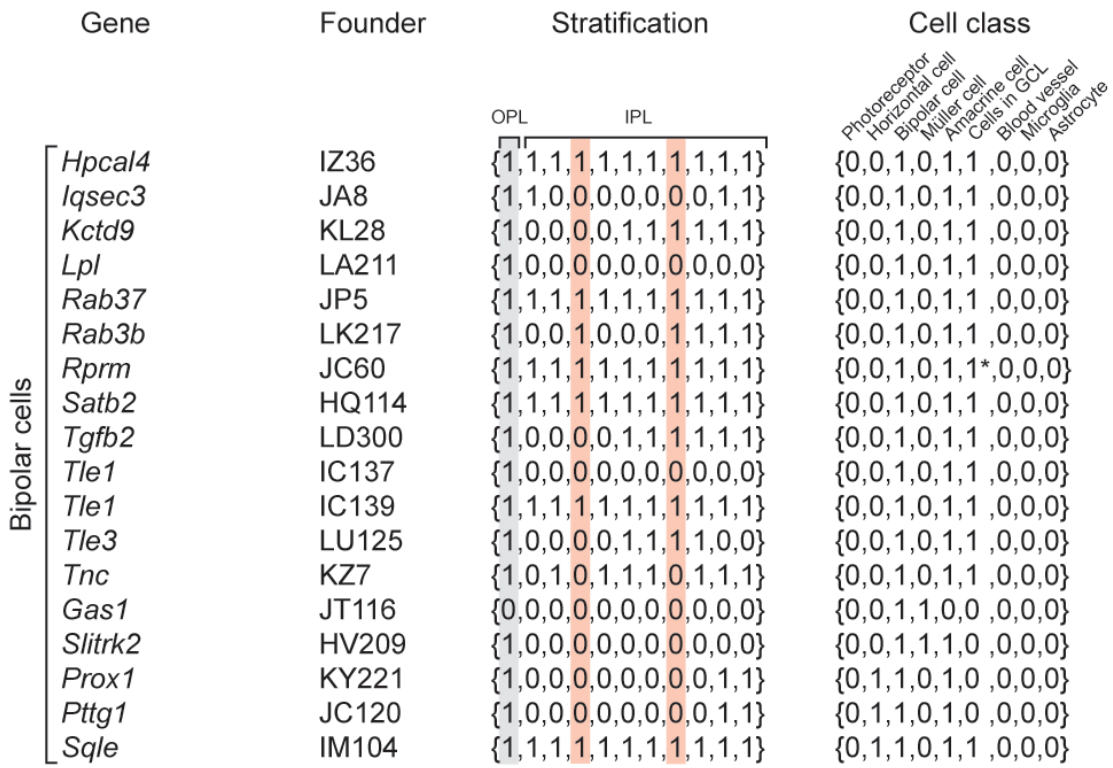

Supplementary Table 3

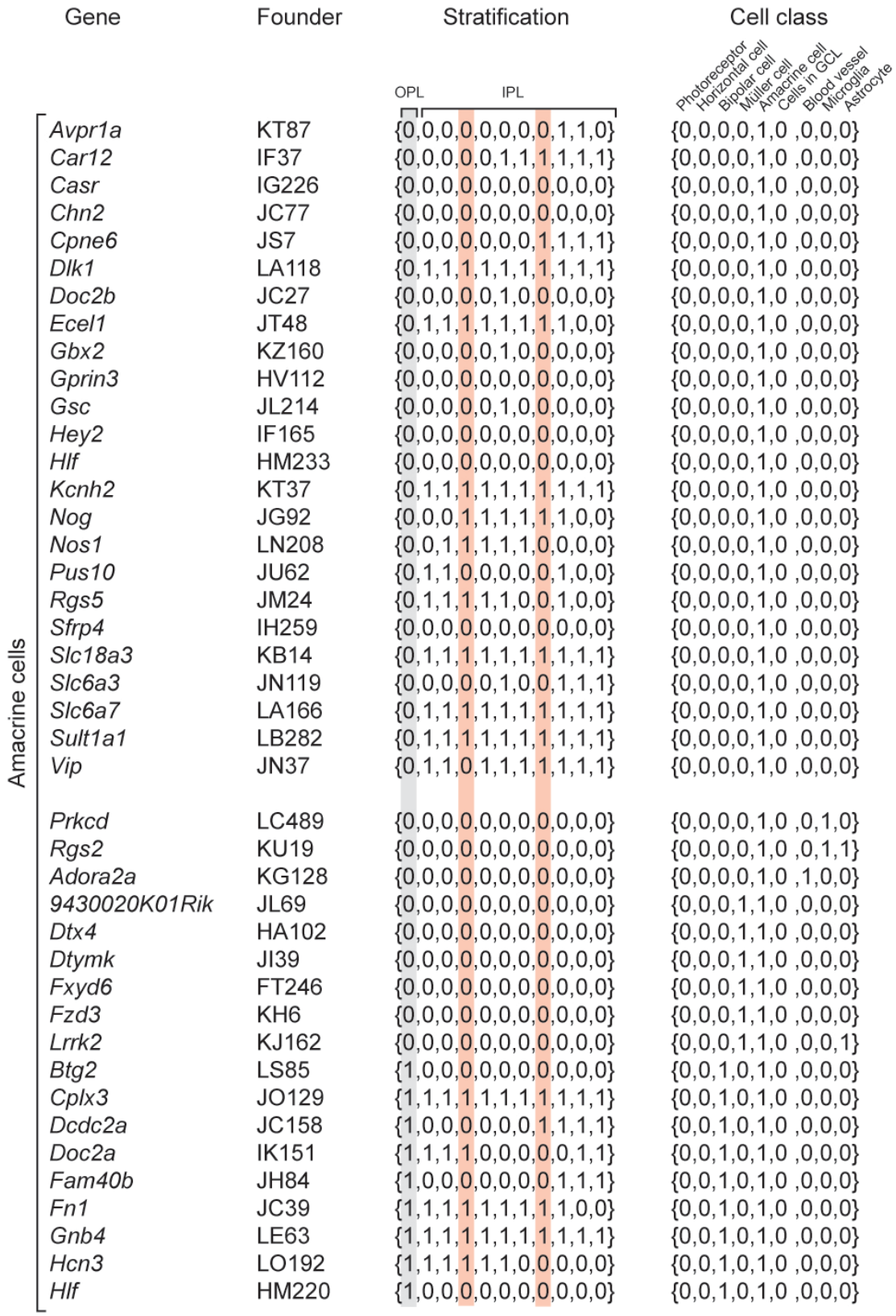

Supplementary Table 4

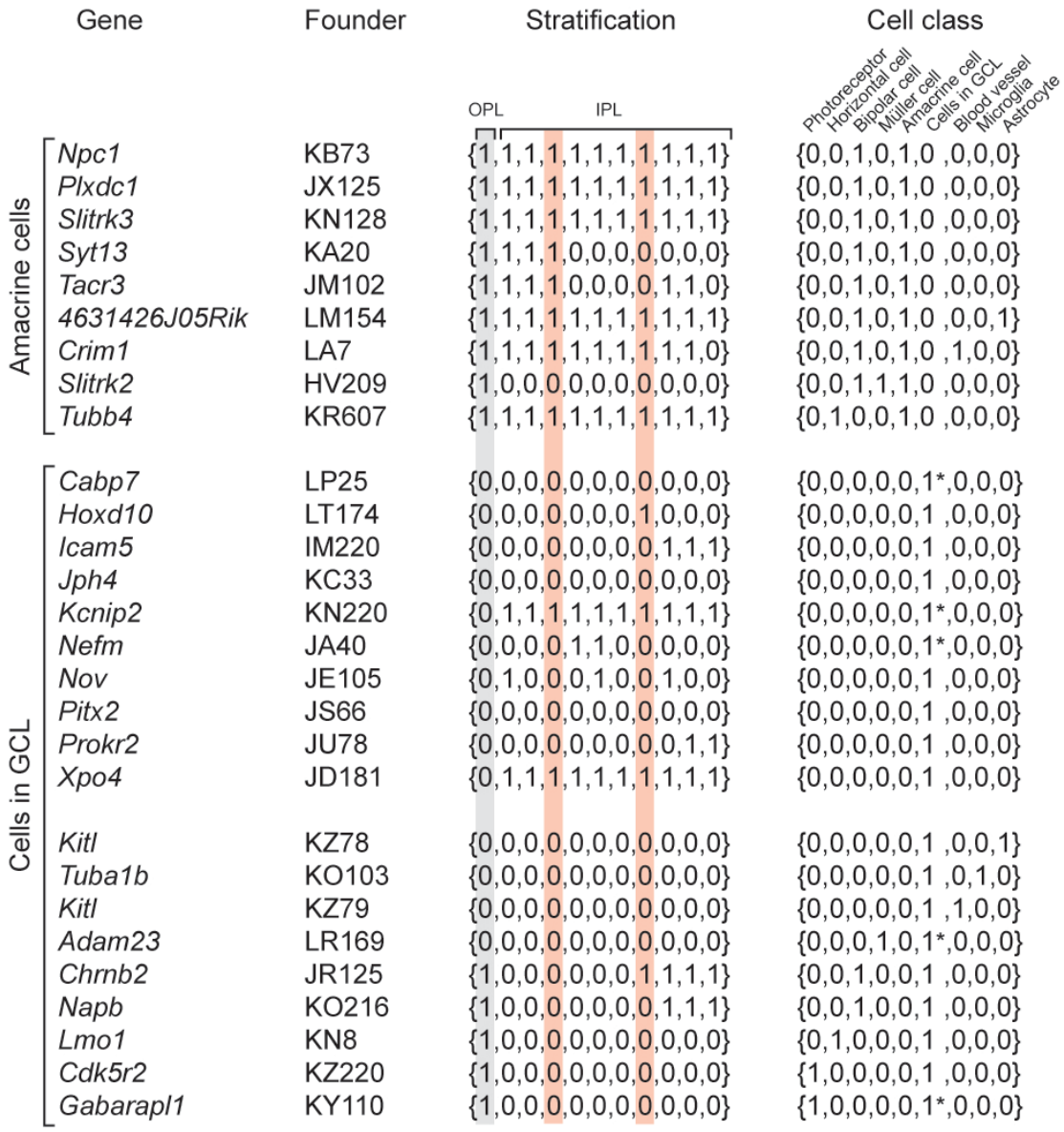

Supplementary Table 5

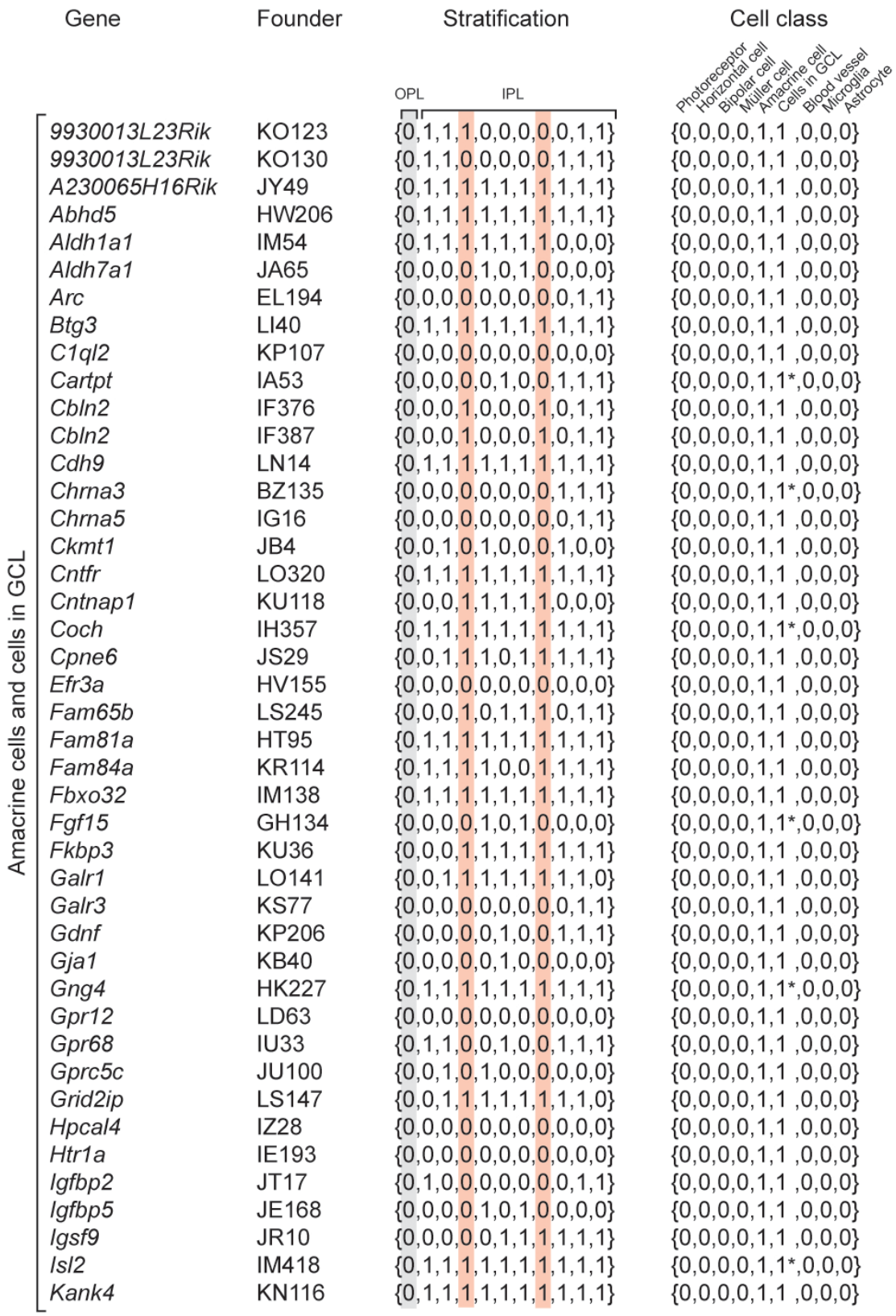

Supplementary Table 6

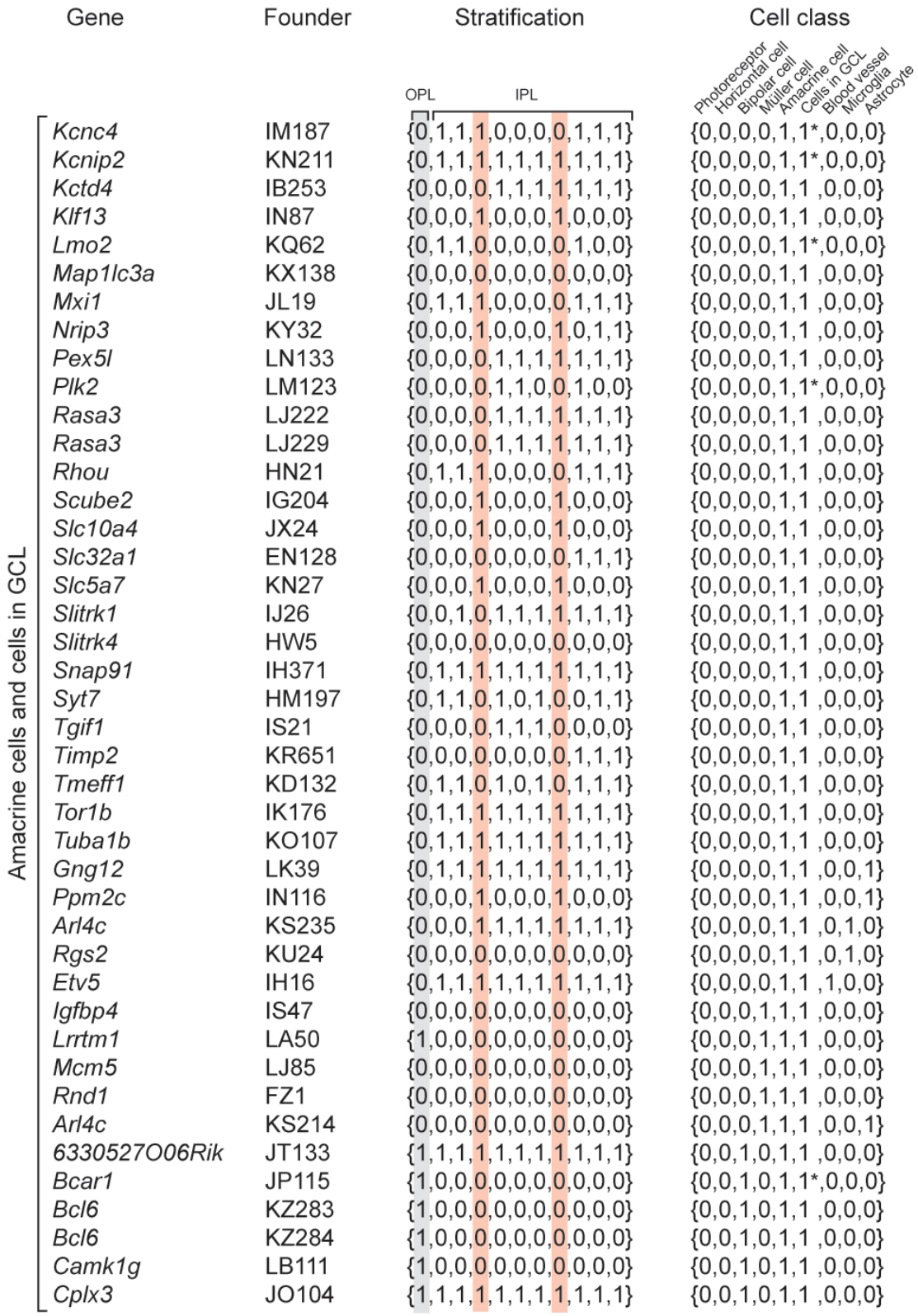

Supplementary Table 7

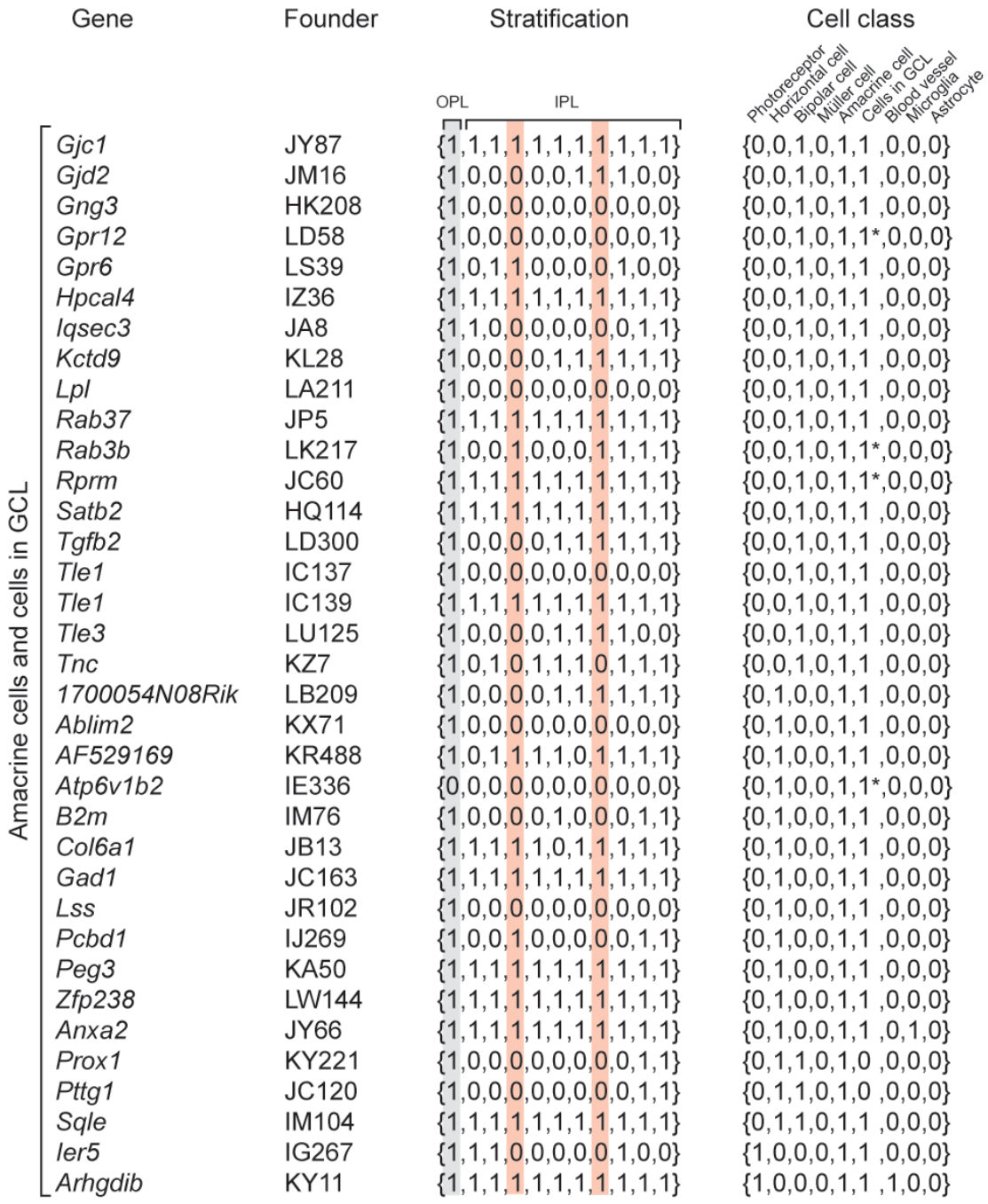

Supplementary Table 8

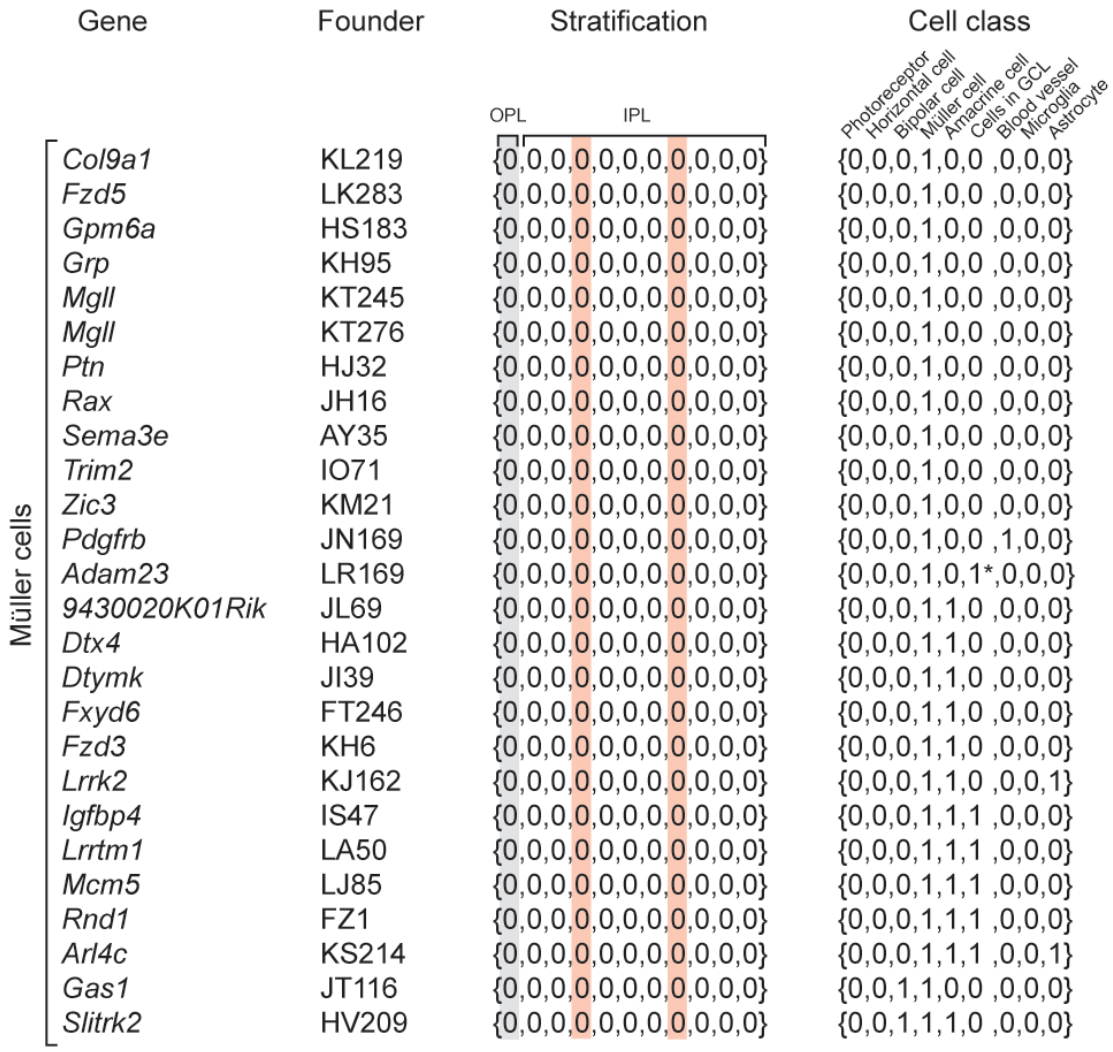

Supplementary Table 9

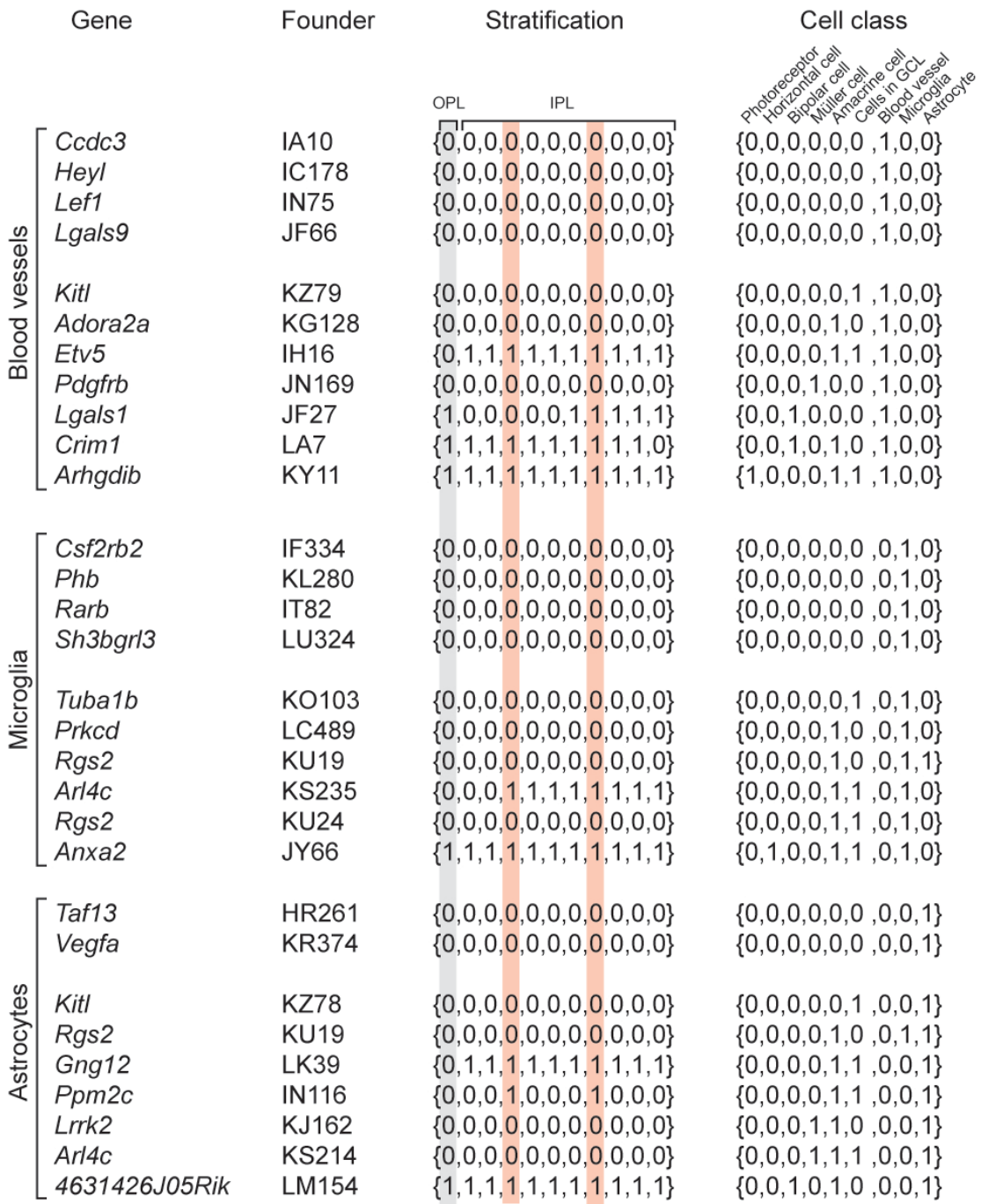

Supplementary Table 10

The molecular logic of retinal cell types

Introduction

Neuronal cell types develop from a general progenitor. One common model is that a progenitor is activated by different "competence stages", which leads the progenitor to induce a certain cell fate [4, 5]. It is known that for each of the competence stages, a set of genes is up- and down-regulated [38, 39]. This specific gene pattern causes a unique genetic fingerprint for the cell type during development. But does a cell type maintain such a unique fingerprint in adulthood when it has reached its defined role in a neuronal circuit? If this is the case, would we also see an overlap in the fingerprints of cell types that belong to the same cell class?

So far, it has not been possible to answer these kinds of questions satisfactorily due to experimental difficulties. When the analysis of single-cell genomes became feasible, researchers randomly selected single, unlabeled, dissociated cells and characterized their genetic identities [40-42]. This approach offers unique opportunities to examine gene expression profiles of progenitors during development, but dissociated cells cannot be distinguished any more by their morphology and function. To circumvent those problems, other researchers isolated cells from transgenic mouse lines in which specific cell types were labeled in different brain regions. This allowed them to collect morphologically and physiologically identified cell types, as well as to isolate higher amounts of RNA for gene profiling. These studies compared cell types chosen from different brain regions like the cingulate cortex, somatosensory cortex, hippocampus, amygdala and thalamus [43].

Our goal was to compare the genetic profile of cell types within one brain area, the retina, in order to understand how functionally related, closely packed but different cell types are specified at the level of gene expression. In the first part of my

thesis, I have shown that we found approximately 150 transgenic mouse lines expressing GFP in individual cell types, or a mixture, within the retina [44]. We selected 14 transgenic mouse lines that are representatives from each cell *class* and labeled a single cell *type* or a combination of few cell types and determined the gene expression profile.

Results

Cell types used for genetic profiling

We selected 14 transgenic mouse lines in which either a specific cell type or a combination of a few types was labeled with GFP (**Fig. 15, Table 1, Supplementary Fig. 1-11**). Each retinal cell class was represented by at least one transgenic mouse line. For the photoreceptor cell class, we chose the rod_{b2} mouse line that selectively labeled the rods (**Supplementary Fig. 1**), and the $cone_{Chrnb4}$ and $cone_{d4}$ mouse lines that marked cones (**Supplementary Fig. 2-3**). In $cone_{Chrnb4}$ and $cone_{d4}$ mice, cones were labeled using different promoters. For the second retinal cell class, the bipolar cells, we selected a transgenic mouse line that labeled all types of ON bipolar cells (ON_{mGluR6}), including rod and cone bipolar cells. The second mouse line for this class labeled the rod bipolar cell type, which is a subset of the ON bipolar cells. Ninety-six percent of the GFP-positive cells in this mouse line (rod bc_{Pcp2}) were the rod bipolar cell type shown by immunostaining against protein kinase C, which exclusively label rod bipolar cells [17] (**Supplementary Fig. 4**).

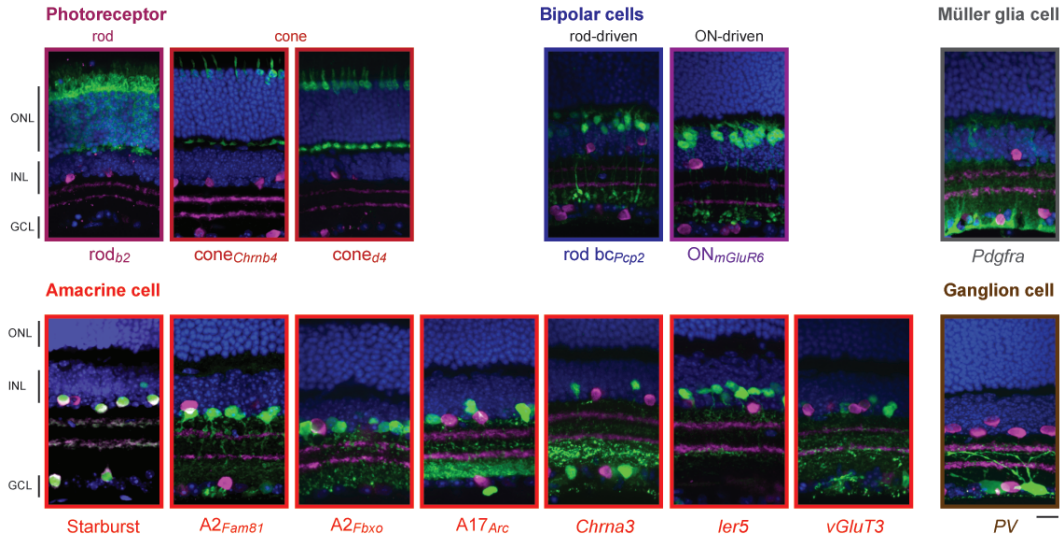

Figure 15. Transgenic mouse lines selected for gene profiling. Immunostained vibratome sections, blue: DAPI, green: GFP or RFP, purple: ChAT. Scale bar: 10 μm.

Abbrevation	Mouse line	P	H	B	M	A	G	Mg	As	Axon	Stratification code										Electrophysiology	GABA	Glycine
rod_{b2}	b2-Cre x Rosa26-LSL-RFP	x	-	-	-	-	-	-	-	-	1	0	0	0	0	0	0	0	0	0	nd	-	-
$cone_{Chrnb4}$	Chrnb4-GFP	x	-	-	-	-	-	-	-	-	1	0	0	0	0	0	0	0	0	0	nd	-	-
$cone_{d4}$	d4-Cre x Rosa26-LSL-RFP	x	-	-	-	-	-	-	-	-	1	0	0	0	0	0	0	0	0	0	nd	-	-
rod bc_{Pcp2}	Pcp2-GFP	-	-	x	-	-	-	-	-	-	0	0	0	0	0	0	0	1	1	1	ON (data not shown)	-	-
ON_{mGluR6}	mGluR6-Cre x Rosa26-LSL-RFP	-	-	x	-	-	-	-	-	-	0	0	0	0	0	0	0	1	1	1	ON (data not shown)	-	-
$A2_{Fam81}$	Fam81a-GFP	-	-	-	-	x	x	-	-	x	0	1	1	1	1	1	1	1	1	1	ON	-	x
$A2_{Fbxo}$	Fbxo32-GFP	-	-	-	-	x	-	-	-	-	0	1	1	1	1	1	1	1	1	1	ON	-	x
$A17_{Arc}$	Arc-GFP	-	-	-	-	x	x	-	-	-	0	1	0	0	0	0	0	1	1	1	ON	x	-
Chrna3	Chrna3-GFP	(x)	-	-	-	x	x	-	-	-	1	1	0	0	0	0	0	1	1	1	ON	-	-
Starburst	ChAT-Cre x Rosa26-LSL-RFP	-	-	-	-	x	x	-	-	-	0	0	0	1	0	0	0	1	0	0	0	nd	x	-
Ier5	Ier5-GFP	(x)	-	-	-	x	x	-	-	-	1	1	1	1	0	0	0	1	0	0	0	ON	-	x
vGluT3	vGluT3-Cre x Thy-LSL-YFP	-	-	-	-	x	x	-	-	x	0	1	1	1	1	1	1	1	1	1	nd	x	x
PV	PV-Cre x Thy-LSL-YFP	-	-	-	-	-	x	-	-	x	0	1	1	1	1	1	1	1	1	1	ON and OFF	-	-
Pdgfra	Pdgfra-Cre x Rosa26-LSL-RFP	-	-	-	x	-	-	-	-	-	0	0	0	0	0	0	0	0	0	0	nd	-	-

Table 1. Transgenic mouse lines used for genetic profiling. “Abbrevation”: naming of the mouse line in the paper. “Mouse line”: exact name of the mouse line. P: photoreceptor; H: horizontal cell; B: bipolar cell; M: Müller glia cell; A: amacrine cell; G: ganglion cell; Mg: microglia; As: astrocyte. Axon: see axonal processes towards the optic disc. “Stratification code” like described in Siegert *et al.* “Electrophysiology”: description of the response properties on a fullfield black-and-white stimulus of individual fluorescence-positive cells in wholemount or in slice voltage-clamp recording. “GABA” and “Glycine” immunohistochemical staining. “x” means positive, “-“ negative, “(x)”: some isolated cells seen, nd: not determed, ON or OFF: ON or OFF response, respectively.

The next cell class was the amacrine cells. The different cell types within this class can be distinguished first by the kind of inhibitory neurotransmitter they are releasing (glycine or GABA), second by the stratification of their neuronal processes within the IPL, and third by the area that is covered by the processes of these neurons. We included three transgenic mouse lines showing GFP expression in glycinergic amacrine cell types: *Ier5*, $A2_{Fam81a}$ and $A2_{Fbxo}$. The latter two of these mouse lines labeled the majority of A2 amacrine cell types. We confirmed this observation with colocalization analysis using the Dab1 antibody, a specific marker of A2 amacrine cells. At least 65% of the GFP-positive cells were also Dab1 positive

(**Supplementary Fig. 5-6**). The *Ier5* mouse line, described in the GENSAT screen (**Fig. 5)** [44], primarily labeled a cell type whose neuronal processes were located within IPL strata 1, 2, and 8 (**Supplementary Fig. 9**). We also selected transgenic mouse lines that showed fluorescence expression in GABA-releasing amacrine cells: the first transgenic mouse line was the *Starburst* mouse line, which labeled cholinergic amacrine cells [45] (**Supplementary Fig. 10a**). The neuronal processes of these cell types colocalized with the *ChAT* antibody staining. The $A17_{Arc}$ mouse line marked a putative A17 amacrine cell type (**Supplementary Fig. 7**). A17 amacrine cells locate their neuronal processes within IPL strata 9 and 10 [46]. A similar stratification pattern was observed for a cell type labeled in the *Chrna3* mouse line (**Supplementary Fig. 8**). Additionally, we noticed in this mouse line a 3:1 cone photoreceptor to amacrine cell type ratio of GFP expression (**Supplementary Fig. 12**). The next selected mouse line (*vGluT3*) showed GFP expression mostly in GABAergic amacrine cell types, but also in some ganglion cell types. Neither for the amacrine nor for the ganglion cell types in the *vGluT3* could we observe a distinct stratification pattern (**Supplementary Fig. 10b**). Surprisingly, this mouse line did not express GFP in the vGluT3 amacrine cell type (data not shown).

For genetic profiling of the ganglion cell class, we included in our study the *PV* mouse line, which has been previously described [47]. This mouse line expressed GFP in eight distinct ganglion cell types (results will be published elsewhere by Tim Viney). Finally, we included in our screen a mouse line that showed fluorescence expression in Müller glia cells (*Pdgfra*) **(Supplementary Fig. 11**).

These 14 mouse lines represented five retinal cell classes.

Experimental design

We used fluorescence-activated cell sorting (FACS) of dissociated retinal cells to purify the GFP or RFP-labeled cell types (**Fig. 16a-b**).

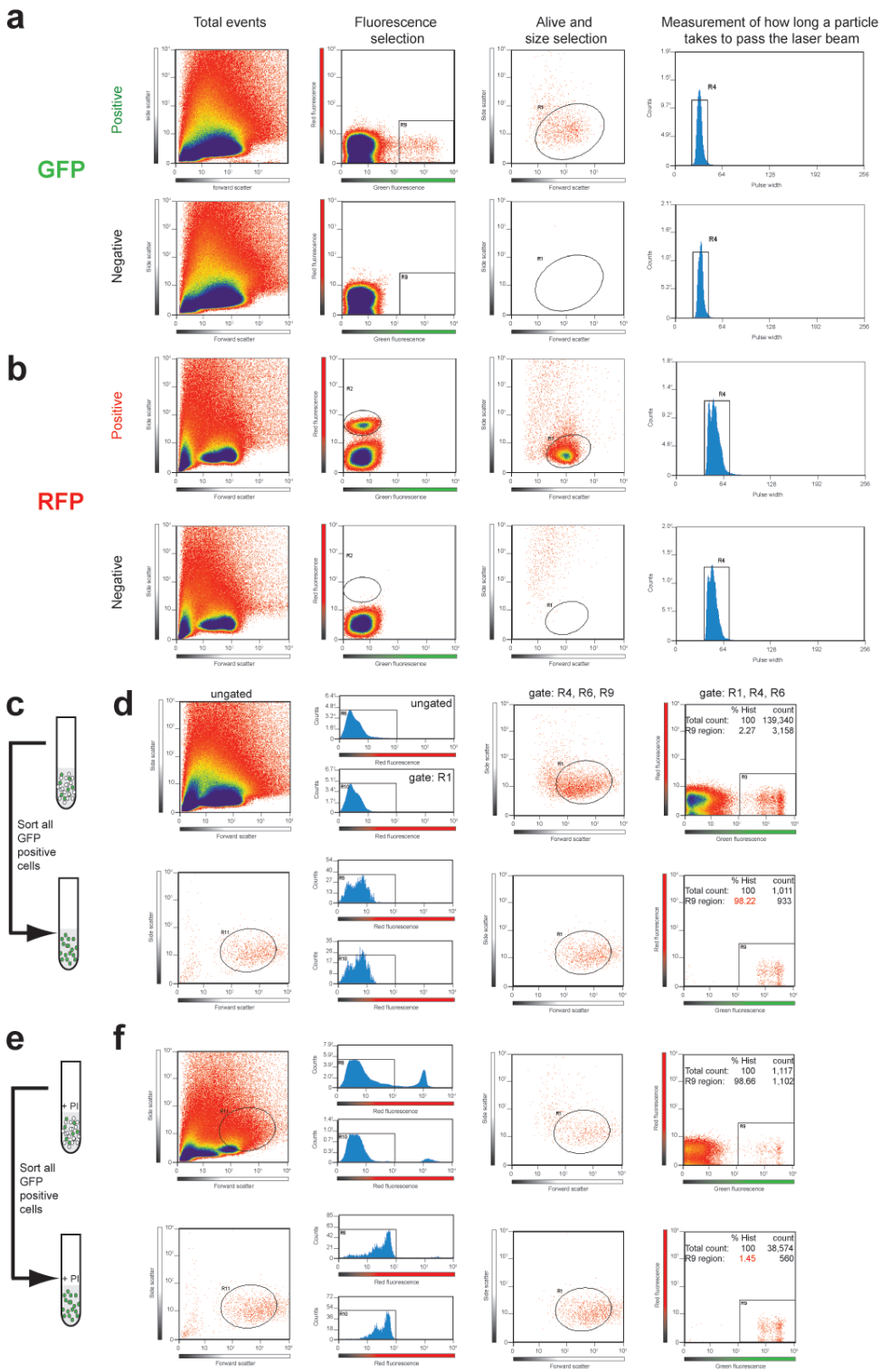

Figure 16. Example plots for gates setting for fluorescence-activated cell sorting (FACS). Transgenic mouse line positive (upper panel) and negative (lower panel) for **a**, GFP and **b**, RFP. First column represents size and granularity of all sorted events (ungated). Fluorescence-positive cells are gated in the fluorescence plot in the second column. Then, they are gated against the size and granularity plot of the first column. Here, a second gate is set based on size and viability of the cells. The third gate is set based on the pulse width (last column). **c**, **e**, Schematic view of the experimental set-up. **c**-**d**, Purity sort. **d**, Measuring the amount of cells in the first round (1st row) and re-sort of the GFP-positive cells (2nd row). **e**-**f**, Analysis the number of dead cells by adding propidium iodide (PI). Measuring the amount of cells in the first round (1st row) and re-sort of the GFP-positive cells (2nd row).

The FACS analysis of each biological triplicate is shown in the supplementary figures. Two concerns about using FACS are the purity of the sorted cells and the fraction of dead cells. In FACS, cells are sorted drop-wise. If a positive event like our cell of interest is measured at the same time as a negative event, then the sorter electronics judge this event as positive and sorts both events within the same drop. To avoid such a purity lost, we performed all our sorts in “single-cell-mode” meaning that a drop is only sorted when a single event of interest is centered within the drop. Additionally, we measured the purity of our sorted cells by first sorting all GFP-positive cells from a retina and then re-sorting this population again. We found that 98.2% of the re-sorted cells were GFP-positive (**Fig. 16c-d**). To estimate the fraction of dead cells among the sorted cells, we added propidium iodide, a DNA binding-dye that is membrane-impermeable and excluded from viable cells. We found that less than 1.5% of the cells were propidium iodide positive (**Fig. 16e-f**).

One factor that causes variability of gene expression comes from the genetic background of animals [48] [49] (**Fig. 17**). For example, a known recessive eye disease that causes photoreceptor degeneration in common laboratory mouse strains could give rise to significant variation in retinal gene expression. Many of the BAC-GFP

strains we used were FVB/N-Swiss Webster hybrids that are known to harbor this recessive mutation. Therefore, we crossed all FVB/N-Swiss Webster mice with C57BL/6J mice and used the F2 generation for genetic profiling (**Fig. 17a**).

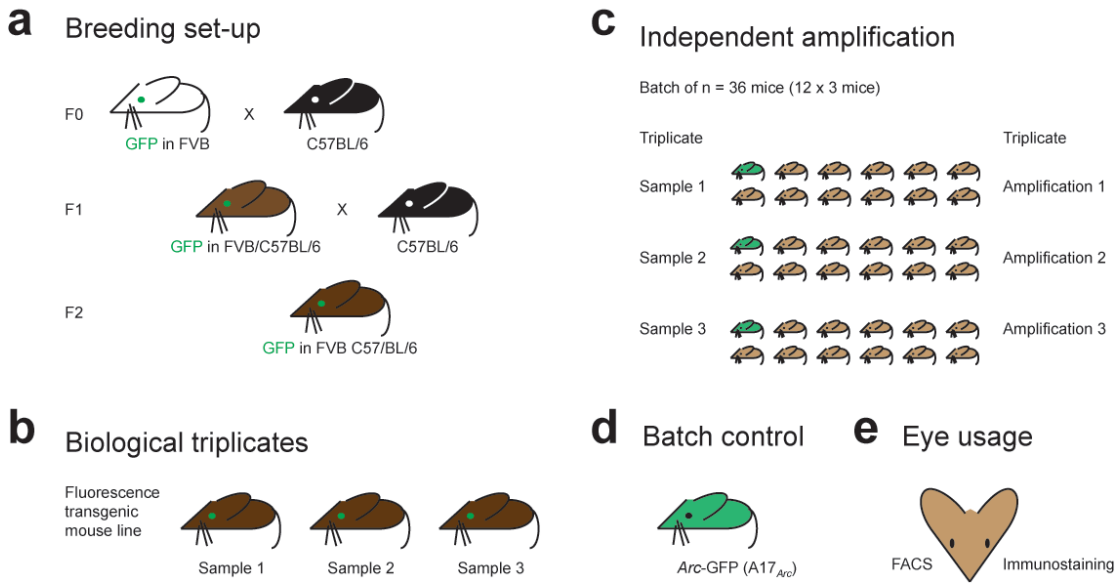

Figure 17. Schematic overview of the experimental design. FVB: FVB/N-Swiss Webster hybrid background. F0, F1, F2: founder generation 0, 1, 2.

For each mouse line (except that of the *PV* mouse), we sorted 200 cells from three different mice (**Fig. 17b**). *PV* mice have a limited number of labeled cells in the retina and we therefore sorted cells from several retinas. To exclude RNA amplification batch artifacts, the three biological samples were independently amplified (**Fig. 17c**).

Due to the high number of samples (19 × 3) that had to be converted to cDNA, amplified, and hybridized, we performed the procedure in two batches. In order to ensure that both batches were consistent, we included the $A17_{Arc}$ mouse line in each batch (**Fig. 17d**).

The expression of many retinal genes depends on the phase of the circadian rhythm [50]. To exclude transcriptional differences caused by the circadian rhythm we prepared the retina and sorted the labeled cells at the same time each day, between 9.30 and 10.30 a.m. All animals were adult, with an average age of 66 days, and the sexes were randomly mixed. We always used the right eye to sort out the labeled cells. For each sort, we confirmed the retinal expression pattern by immunohistochemically staining the left retina. (**Fig. 17e**).

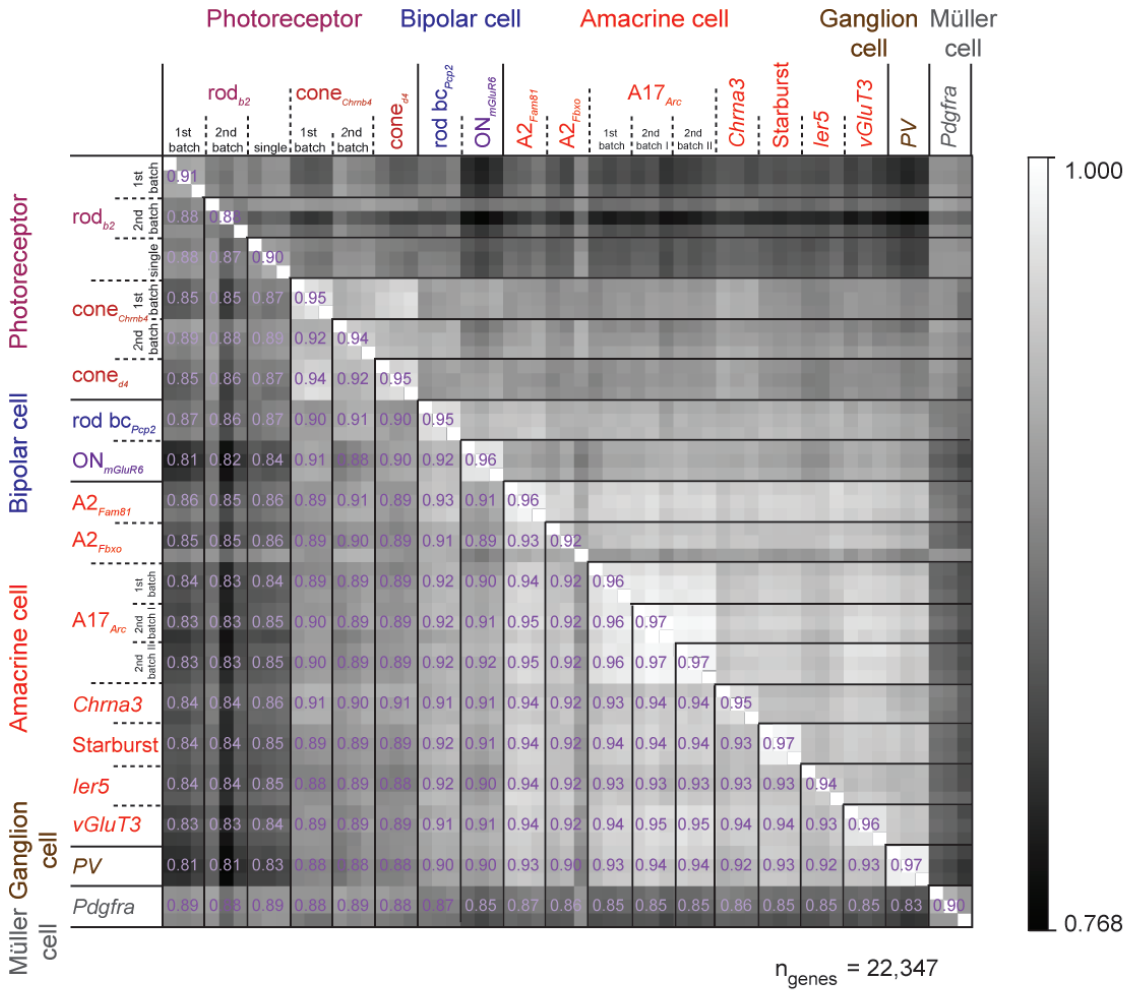

Figure 18. Pairwise-correlation plot of expressed genes across all mouse lines. The grey scale intensities show the Pearson-correlation coefficient of log2 expression values as indicated by the scale bar. The purple numbers show the average Pearson-correlation coefficient of log2 expression values of the triplicate. n indicates the number of total genes.

To measure the reliability of our procedure, we calculated the Pearson correlation coefficient (PCC) between all gene expression patterns (**Fig. 18**). The average PCC of each triplicate was above 0.94 with the exception of the rod_{b2} and the *Pdgfra* mouse lines. This high correlation within biological triplicates suggests that both the genetic state of these sorted cells and the amplification procedure is repeatable from mouse to mouse. The PCC between gene expression patterns belonging to our batch control, $A17_{Arc}$ cells, amplified in the different batches was 0.96. This high inter-batch correlation allowed us to analyze the two batches together without any adjustments. Due to the lower PCC, we repeated amplifications with rod_{b2} in one of the following two ways: either the triplicates were prepared on the same day (**Fig. 18**, rod_{b2} 2nd batch), or the triplicates were prepared on different days but at the exact same time (9.30 a.m.) in the morning (**Fig. 18**, rod_{b2} single). Neither approaches improved the correlation within the biological triplicate. Finally, we quantified the noise in gene expression by summing up the standard deviation for each gene that passes the threshold divided the total by the mean of the gene across all cell types (**Fig. 19**). Rod_{b2} and *Pdgfra* had the noisiest expression patterns.

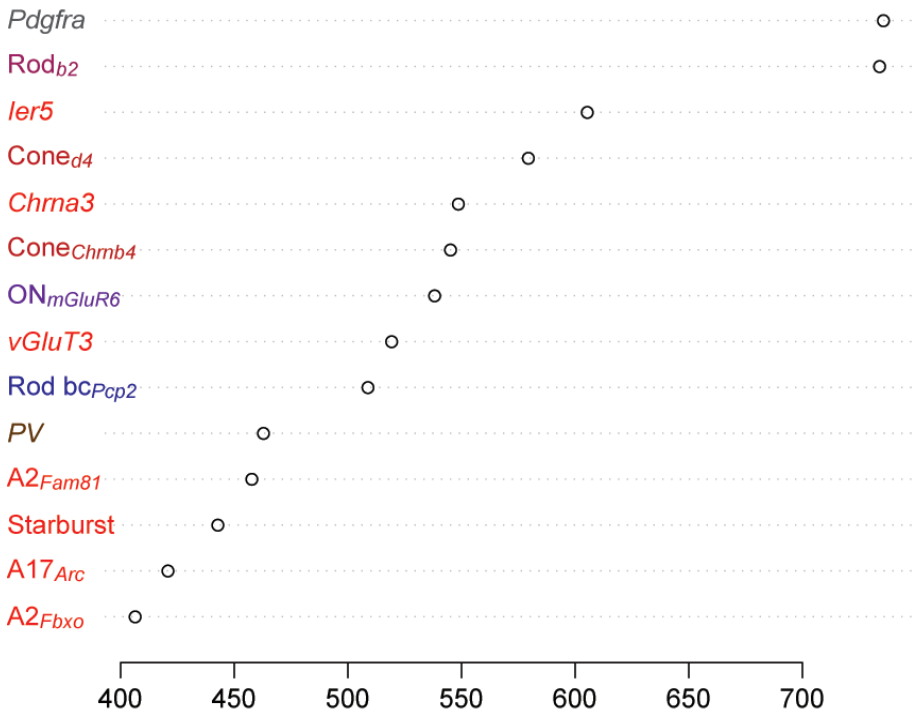

Figure 19. Noise level of each transgenic mouse line. Each dot represents the level of noise for a particular mouse line.

Photoreceptors showed expected gene pattern

The conversion of light into voltage change in photoreceptors, the "phototransduction cascade", is performed by a number of proteins. Several studies have described the genes that encode the proteins of the phototransduction cascade, as well as other genes that are specifically expressed either only in rods or only in cones or in both [51]. We used these genes to validate our method of determining gene expression patterns. To reveal the most specific and highly expressed 25 genes of one cell type, we first asked which genes have a high expression value in our selected cell type, e.g. photoreceptors, versus the non-selected cell types (not photoreceptors); second, how big is the fold-change between the selected and the non-selected cell types; and third, how significant is the expression within the biological triplicates. Using this approach, we found more than 25 genes that are exclusively expressed in all photoreceptors (rod_{b2}, $cone_{Chrnb4}$, $cone_{d4}$, **Fig. 20a**). Out of the 25 highest expressed genes, we found 13 genes that had already been described in the literature as photoreceptor-specific (**Fig. 20a**). Among these are well-known genes like Recoverin (*Rcvrn*) [52] and Guanylyl cyclase-activating protein (*Guca1a*) [53].

Several gene families, like the opsins, phosphodiesterases (PDEs) and cyclic nucleotide-gated ion channels (CNGs), are known to have a specific subunit exclusively expressed in rods or cones [51]. We found that many of these rod- or cone-specific genes had a high expression value and a high fold-change within our dataset (**Fig. 20b-c**). In the case of rods, we repeated cell sorting and amplifications from biological triplicates of the rod_{b2} mice three times (1st and 2nd batch, and single analysis).

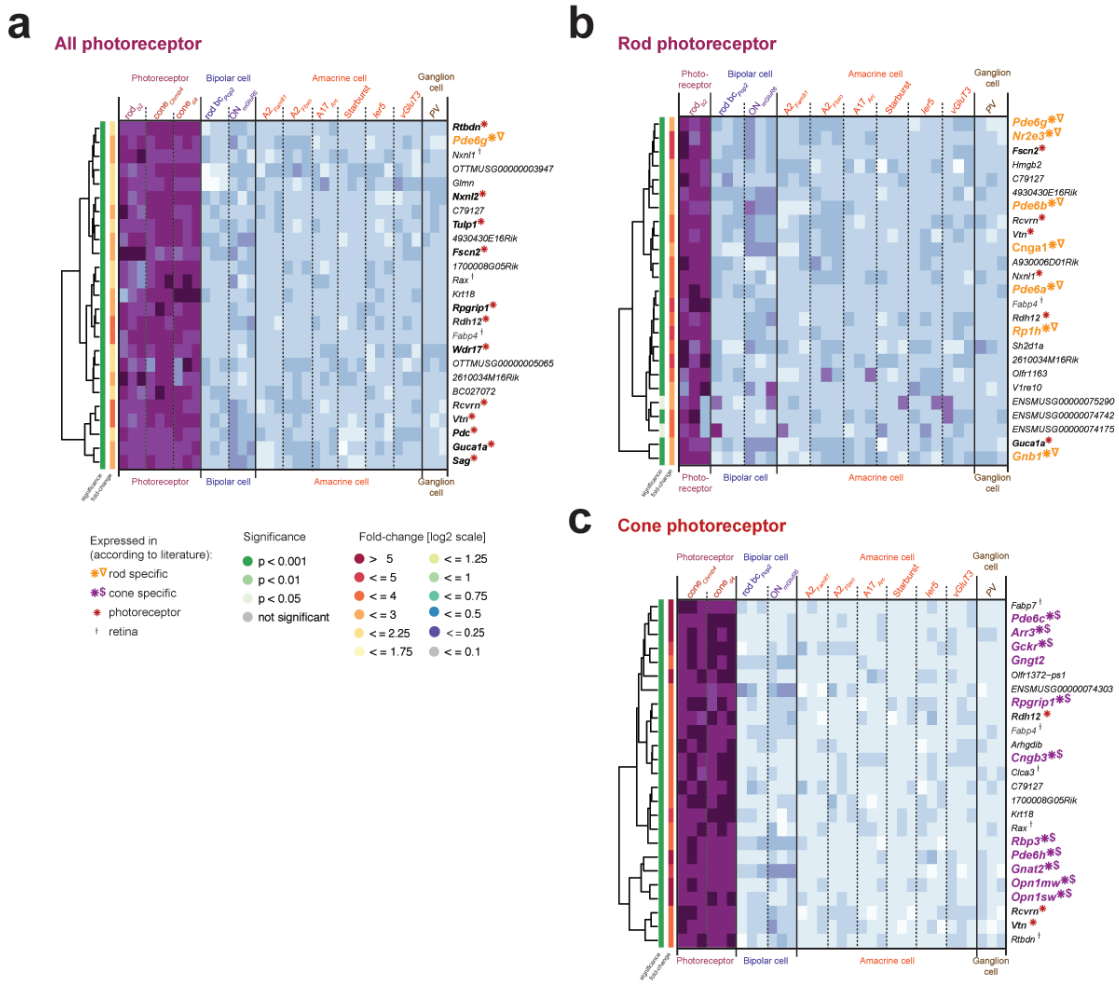

Figure 20. Hierarchical clustering of the 25 highest enriched genes that have a high expression in **a**, photoreceptors, **b**, rod- or **c**, cone photoreceptors. White and purple indicate relatively low and relatively high expression levels, respectively. The bars on the left of the heatmap color-code the significance within the biological triplicate and the fold-change of a particular gene.

After we identified the genes for each of the rod_{b2} repetitions that passed the threshold of log1.75 and intersected the lists, we found the same set of genes among the highest expressed genes (**Fig. 21a**). For cone photoreceptors, we had two mouse lines available which express a fluorescent protein in cones, but each of them under a different promoter. We found many known genes among the ones that were the same between these two lines (**Fig. 21b**). In summary, many of the known photoreceptor-, rod- and cone-specific genes were highly and specifically expressed in the same cells in our dataset. This finding we took as a validation of our approach.

a

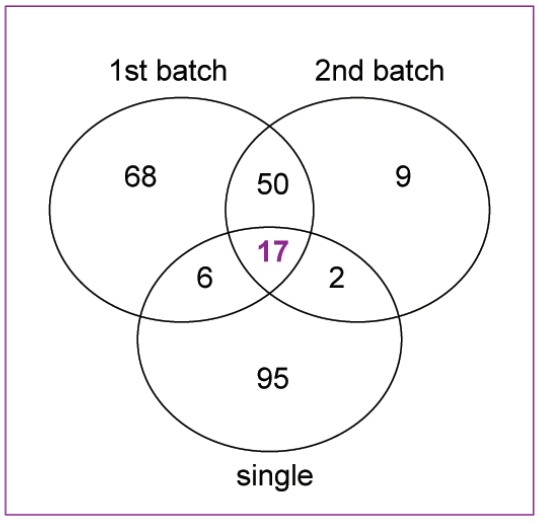

Genes shared within all sets

A930006D01Rik	*Olfr1163*
Cnga1	*Pde6a*
EG270499	*Pde6b*
EG384594	*Polg2*
Faim	*Rho*
Gnat1	*Rp1h*
Gnb1	*Susd3*
Guca1b	*Svs3b*
Nr2e3	

b

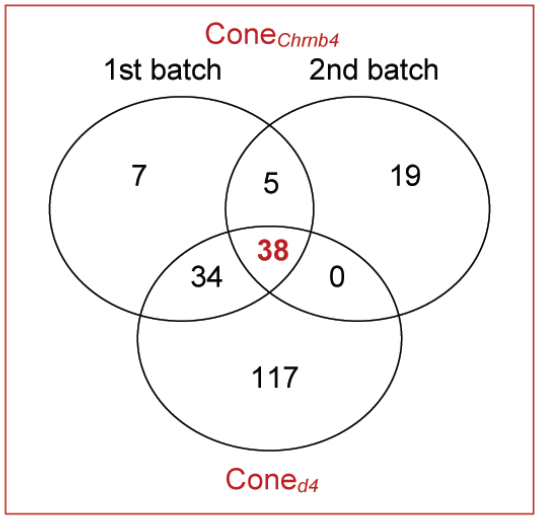

Genes shared within all sets

1110002B05Rik	*Hspb6*
1700008G05Rik	*Igj*
1700113O17Rik	*Jam3*
2310026E23Rik	*Lcn2*
2810002I04Rik	*Mfge8*
4930434E21Rik	*Mogat1*
9330129D05Rik	*Olfr1372-ps1*
Agr2	*Opn1mw*
Arhgdib	*Opn1sw*
Arr3	*Osgep*
Cd59a	*Otop3*
Clca3	*Pde6c*
Cngb3	*Pde6d*
Crxos1	*Pde6h*
ENSMUSG00000	*Pnp1*
074303	*Pnp2*
En2	*Ppm1j*
Fabp7	*Ppp1r14d*
Gnat2	*Ttc35*
Gngt2	

Figure 21. Venn-Diagrams of photoreceptors. **a**, Comparison of the 1st, 2nd batch and single for rod$_{b2}$. **b**, Comparison of cone$_{Chrnb4}$ (1st and 2nd batch) and cone$_{d4}$. The list next to the diagram shows the genes that are shared between all three datasets.

Each cell type has its own genetic profile

How much adult cell types differ from each other in gene expression is not known. Here, we compared each of the 14 groups of cells with each other to address this question.

First, we analyzed bipolar cells of the rod bc_{Pcp2} and ON_{mGluR6} lines. We found a few genes exclusively expressed in rod bc_{Pcp2} or ON_{mGluR6} cells, but the fold-change of most of the genes was very low and had high variability within the biological triplicate (**Fig. 22a, b**).

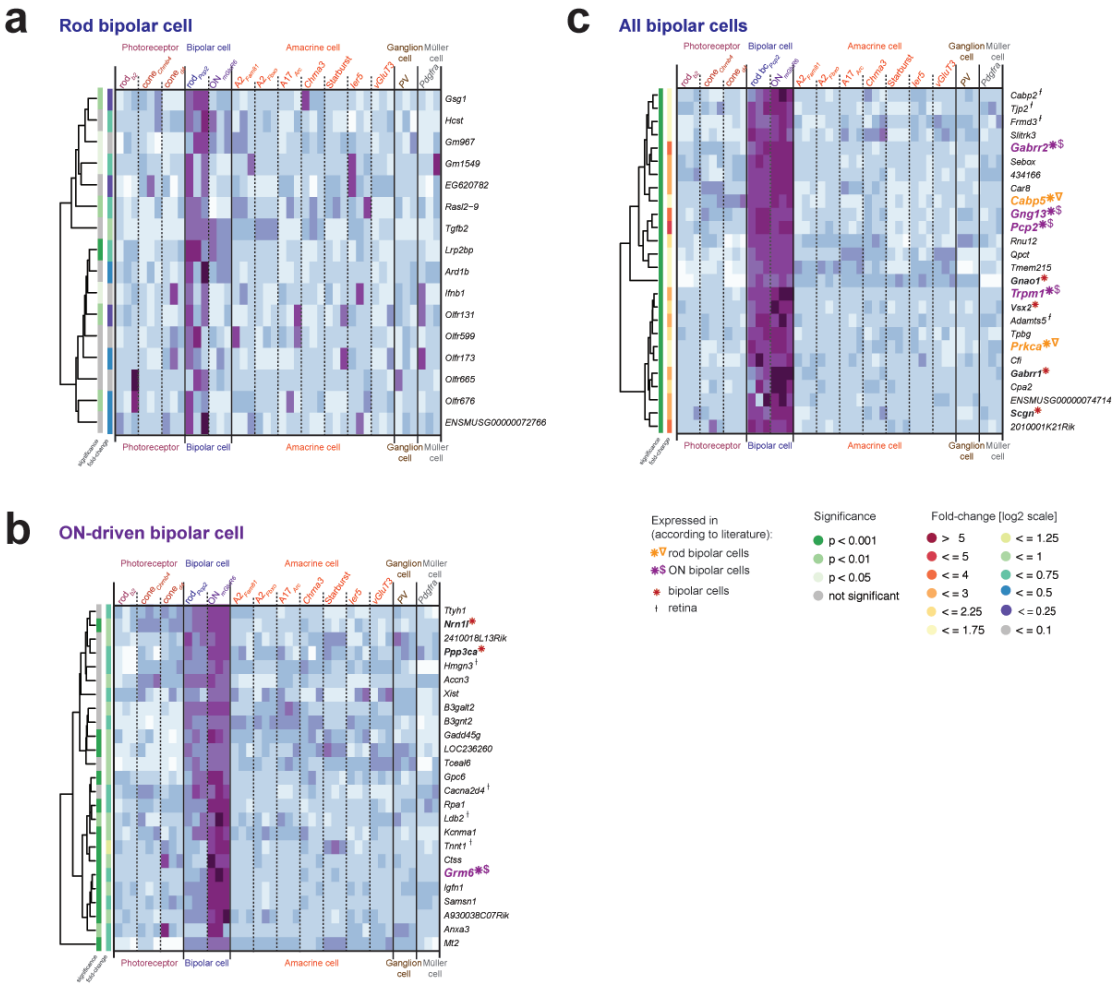

Figure 22. Hierarchical clustering of the 25 highest enriched genes that have a high expression in **a**, rod bipolar cells (rod bc_{Pcp2}), **b**, ON bipolar cells (ON bc_{mGluR6}), **c**, both bipolar cells. White and purple indicate relatively low and relatively high expression levels, respectively. The bars on the left of the heatmap color-code the significance within the biological triplicate and the fold-change of a particular gene.

This result is not unexpected, since rod bipolar cells belong to the subclass of ON bipolar cells and, therefore, rod bc_{Pcp2} cells are subsets of ON_{mGluR6} cells (**Supplementary Fig. 4**). Therefore, we grouped together data from rod bc_{Pcp2} and ON_{mGluR6} cells and searched for genes that were exclusively expressed in those two cell groups. We found at least 25 genes with a high expression value and a high fold-change that were expressed in this group (**Fig. 22c**). Six genes have been described in the literature as being specifically expressed in ON-responding bipolar cells, like the transient receptor potential cation channel (*Trpm1*) [54]. Two of these genes are even more restricted: they are rod bipolar cell-specific (protein kinase C, alpha (*Prkca*) [17] and the calcium binding protein 5 (*Cabp5*) [55]).

Amacrine cells make up approximately 50% of all cell types in the retina. For six amacrine cell types or type combinations we found specifically expressed genes (**Fig. 23**). Interestingly, GABAergic amacrine cells have many highly expressed genes with high fold-change (**Fig. 23b-d**, **f**), whereas the genetic profile of glycinergic amacrine cells is less unique (**Fig. 23a, e**). The *Starburst* amacrine cells are one of the best-described retinal cells [6]. Out of the 25 most expressed genes, we found four genes which are, according to the literature, expressed in cholinergic cells: the GABA receptor subunit D (*Gabrd*) [56]; the vesicular acetylcholine transporter (*VaChT, Slc18a3*) [57]; the regulator of G-protein signaling 6 (*Rgs6*) [58]; and the orphan carrier protein (*Slc10a4*) [59]. Several other genes in the list have been described as being expressed in the retina but have not yet been specifically assigned to *Starburst* cells (**Fig. 23d**). The second GABAergic amacrine cell type is the A17 amacrine cell that is marked in the $A17_{Arc}$ [44]. Previous work has described A17 amacrine cells expressing the gap junction protein Cx45 (*Gjc1*) [46]. Our gene data reveals that this gene is highly expressed in the $A17_{Arc}$ cells (**Fig. 23b**). The A2 amacrine cells serve as a relay station between the rod and the cone pathway [11].

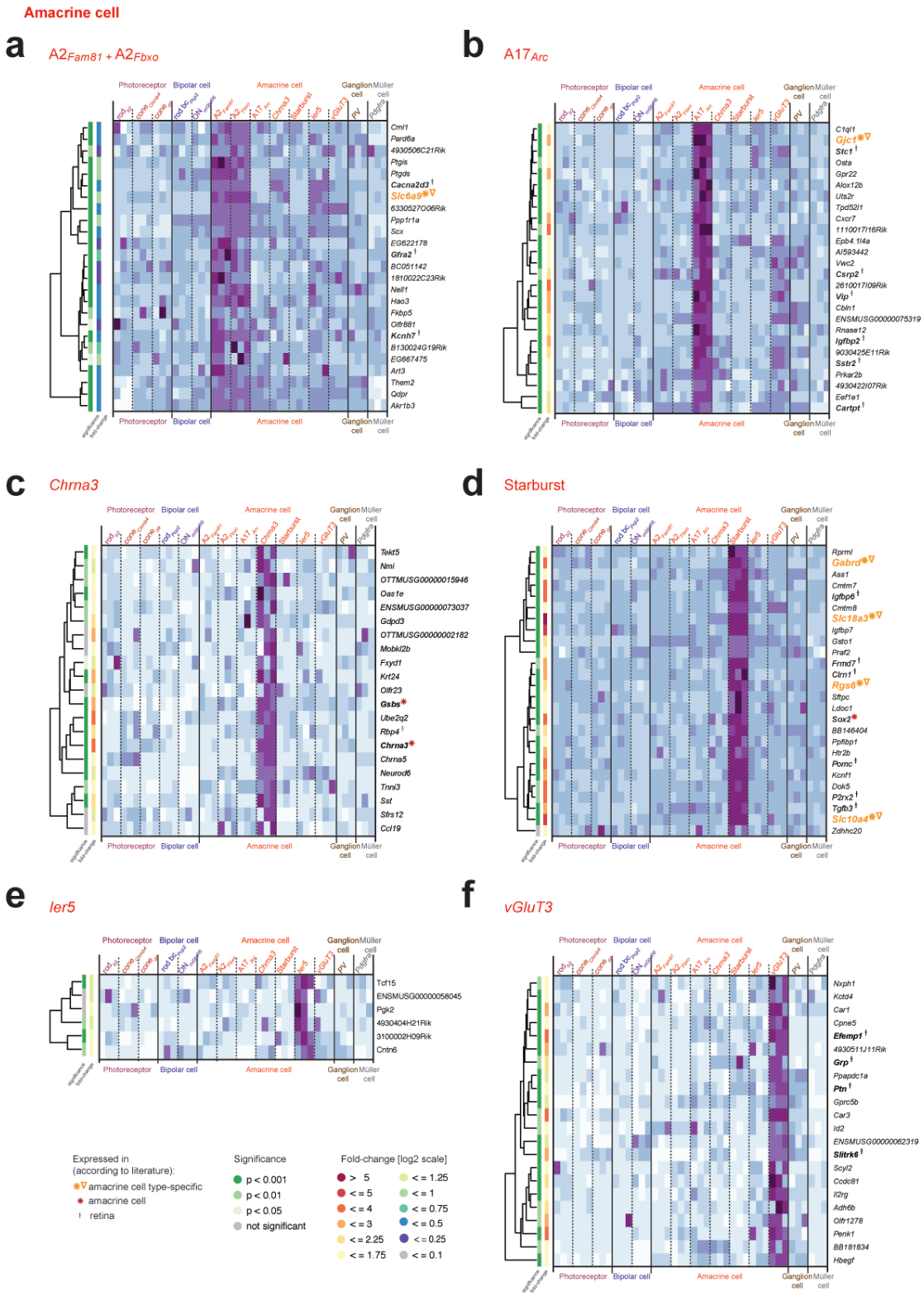

Figure 23. Hierarchical clustering of the 25 highest enriched genes that have a high expression in the amacrine cells. **a**, $A2_{Fam81}$ and $A2_{Fbxo}$, **b**, $A17_{Arc}$, **c**, *Chrna3*, **d**, *Starburst*, **e**, *Ier5* and **f**, *vGluT3*. White and purple indicate relatively low and relatively high expression levels, respectively. The bars on the left of the heatmap color-code the significance within the biological triplicate and the fold-change of a particular gene.

Our study included two mouse lines that have been shown in the GENSAT screening to express GFP in A2 amacrine cells (**Fig. 7**). We confirmed this morphological observation by quantifying the number of GFP- and Dab1-positive cells. Dab1 is a specific marker of A2 cells. The majority of the GFP-positive cells in $A2_{Fam81a}$ and $A2_{Fbxo}$, were positive for Dab1, but an additional population of ganglion cells was found in the $A2_{Fam81a}$, and a population of amacrine cells was found above the A2 amacrine cells in the $A2_{Fbxo}$ (**Supplementary Figure 5-6**). Because the majority of the cells were A2 amacrine cells in both mouse lines, we treated these two lines as a single group (**Fig. 23a**). Even the most specific genes had a lower fold-change and a higher variability than GABAergic cells. The same was true for *Ier5* amacrine cells. Both A2 and *Ier5* are glycinergic cells.

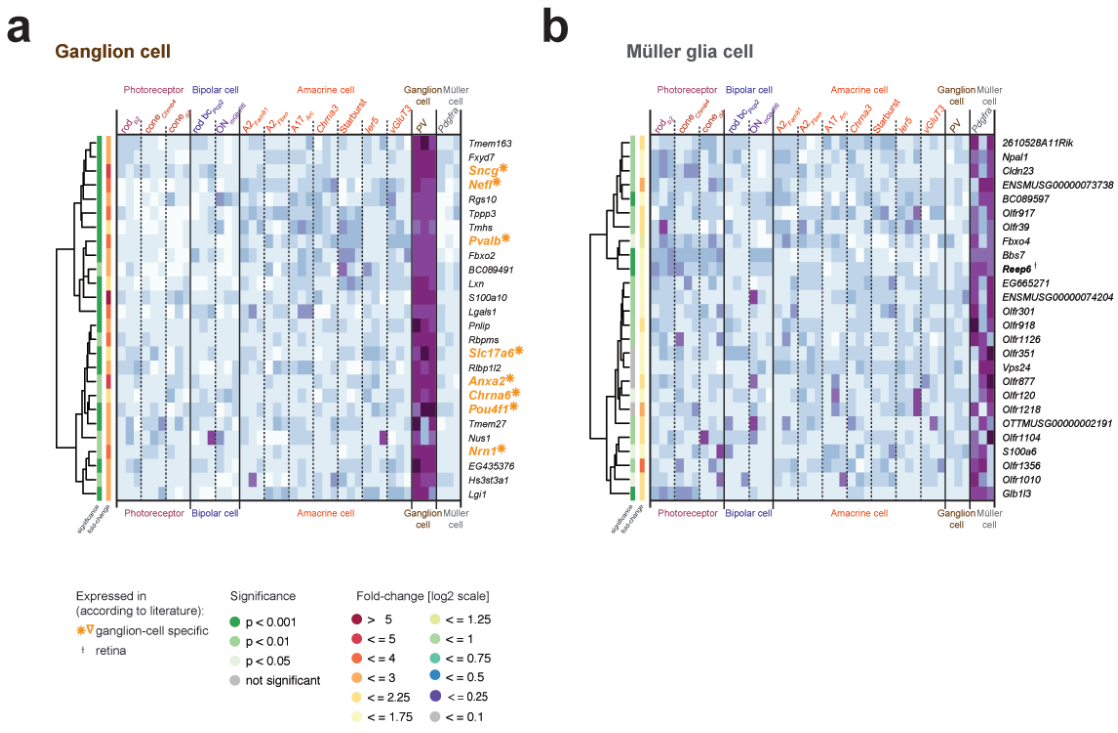

Figure 24. Hierarchical clustering of the 25 highest enriched genes that have a high expression in **a**, ganglion cells (*PV*) and **b**, Müller glia cells (*Pdgfra*). White and purple indicate relatively low and relatively high expression levels, respectively. The bars on the left of the heatmap color-code the significance within the biological triplicate and the fold-change of a particular gene.

For the next cell class, the ganglion cells (*PV*), we found many highly and specifically expressed genes (**Fig. 24a**). Eight of these genes have already been described as ganglion-cell specific. For the Müller glia cells (*Pdgfra*), the genetic profile was similar to rods in the sense that the biological triplicates were noisy (**Fig. 24b**).

Rod photoreceptors and Müller glia cells have specific down-regulated genes

Specificity in gene expression can be caused by genes that are up-regulated in a given cell type, but also other genes that are specifically down-regulated. We therefore searched for genes that were transcriptionally repressed in individual cell types. Figure 25 illustrates that the majority of the genes in 12 out of the 14 cell groups are not specifically down-regulated (**Fig. 25**). The fold-change of most of the genes in the group of 12 is very low with a few exceptions: in cone photoreceptors the gene *Vax2*; in bipolar cells *Ppargc1a* and *Mab21l1*; and in the *Ier5* amacrine cell *Neurod1*. Interestingly, these genes have been described in the literature as being involved in early developmental processes [60] [61, 62] [63].

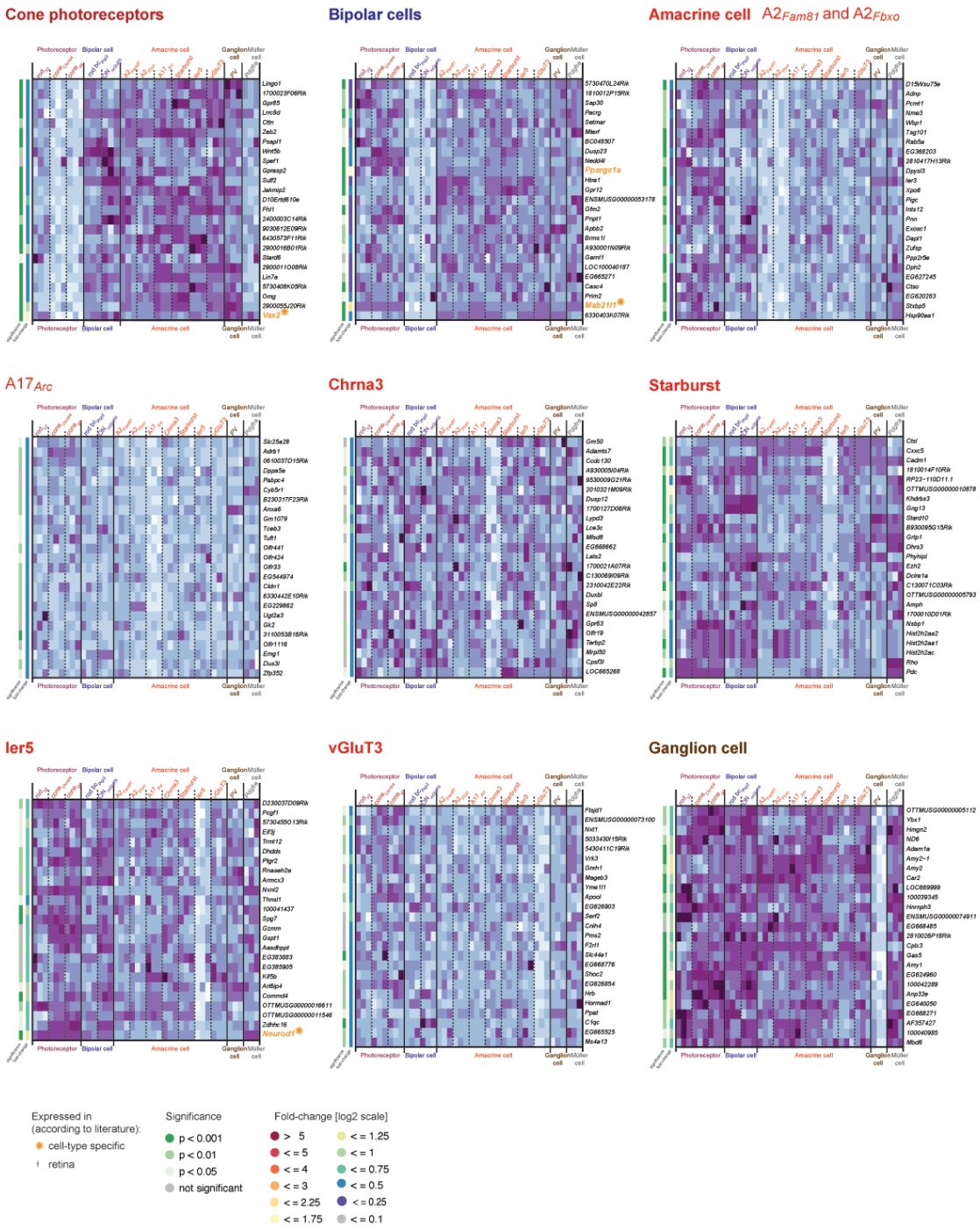

Figure 25. Hierarchical clustering of the 25 highest enriched genes that have a low expression in cone photoreceptors (cone$_{Chrnb4}$ and cone$_{d4}$), bipolar cells (rod bc$_{Pcp2}$ and ON$_{mGluR6}$), amacrine cells (A2$_{Fam81}$ and A2$_{Fbxo}$, A17$_{Arc}$, *Chrna3*, *Starburst*, *Ier5*, *vGluT3*) or ganglion cells (*PV*) but are high expressed everywhere else. White and purple indicate relatively low and relatively high expression levels, respectively. The bars on the left of the heatmap color-code the significance within the biological triplicate and the fold-change of a particular gene.

Unlike the other cells, rods and Müller glia cells have many genes that are significantly down-regulated (**Fig. 26**)

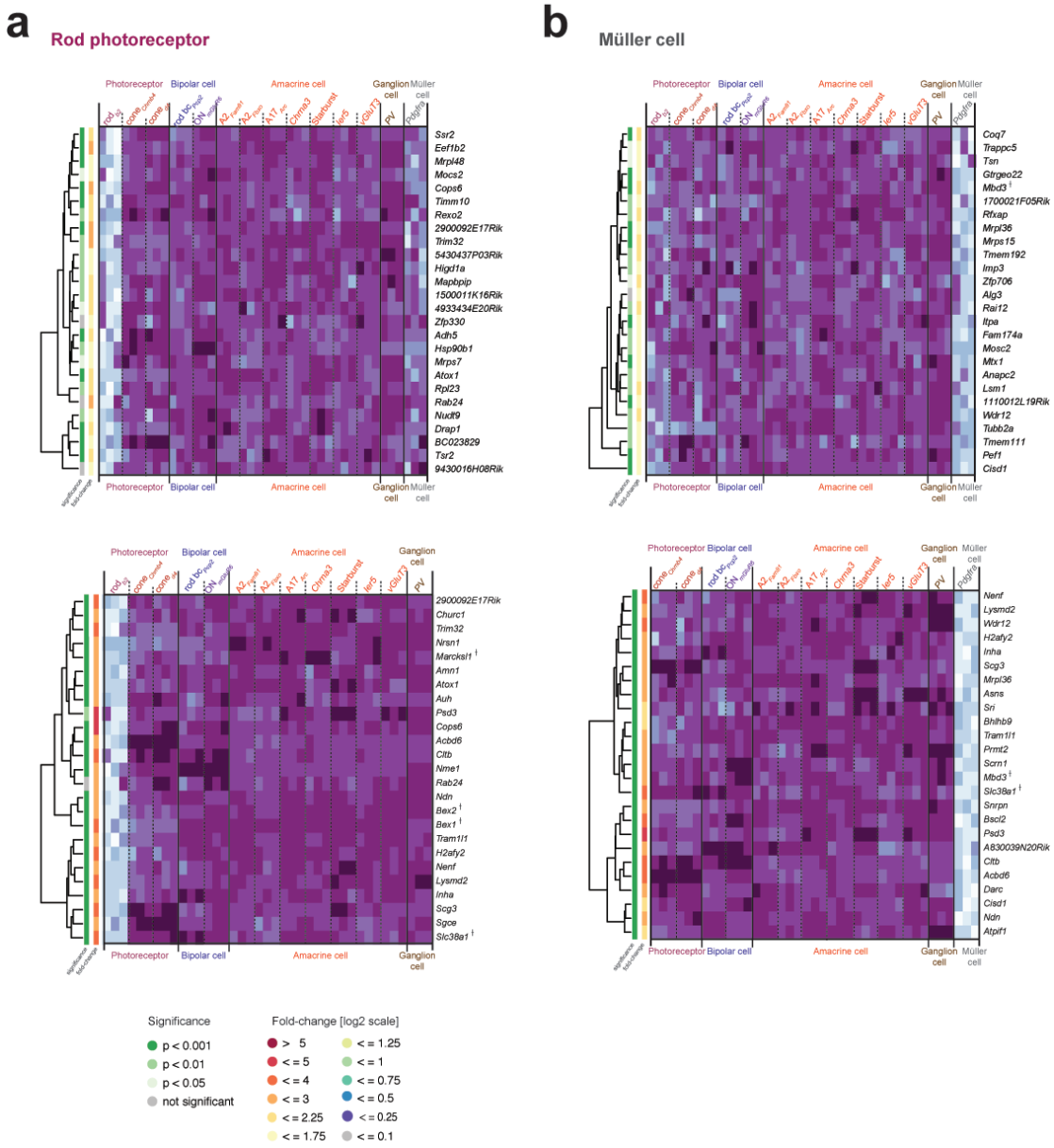

Figure 26. Hierarchical clustering of the 25 highest enriched genes that have a low expression in **a**, rod photoreceptor (rod_{b2}) and **b**, Müller glia cells (*Pdgfra*) but are high expressed everywhere else. White and purple indicate relatively low and relatively high expression levels, respectively. The bars on the left of the heatmap color-code the significance within the biological triplicate and the fold-change of a particular gene. The first row includes all mouse lines. In the second row, *Pdgfra* and rod_{b2} are removed from the rod photoreceptor and Müller glia cells, respectively.

Cell types belonging to a cell class cluster together

We asked if cell types that belong to the same biological class cluster together based on gene expression patterns. Biological cell classes are put together based on morphological and functional similarities. For example, rods and cones belong to the photoreceptor class since they both sense light and also share similar morphological features. **Figure 27** demonstrates that each cell type in our dataset clusters to its expected biological class.

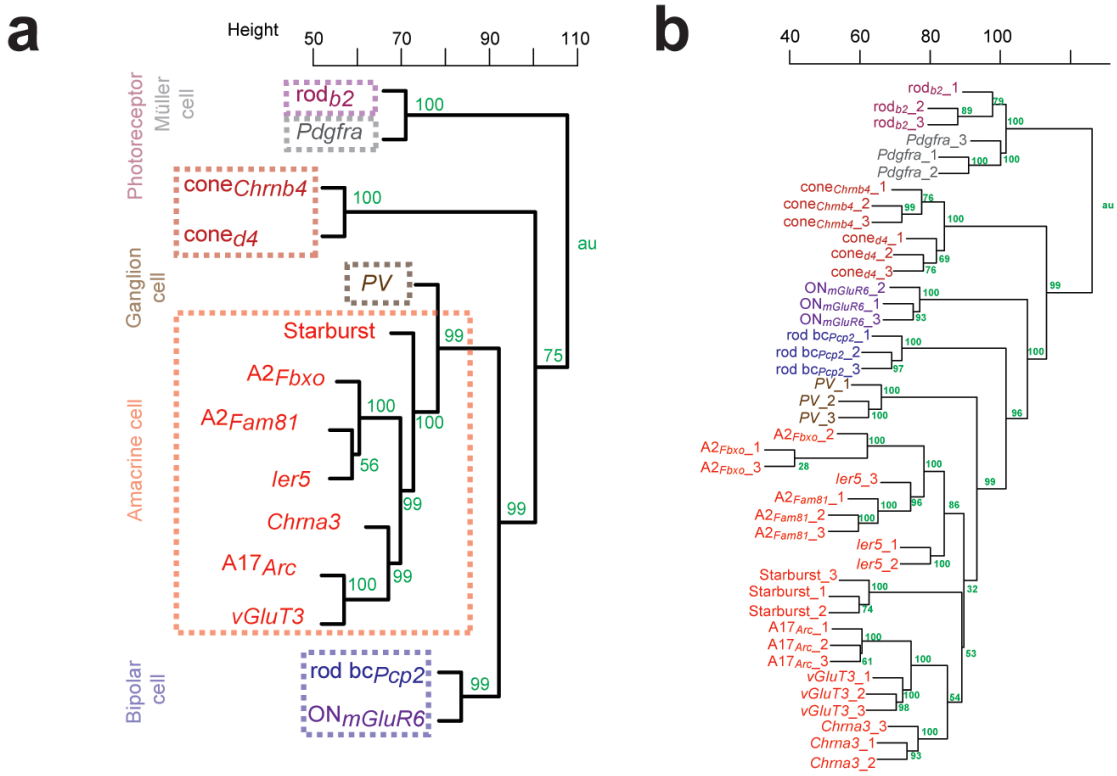

Figure 27. Hierarchical clustering of all mouse lines for **a**, the median of the data and **b**, each triplicate.

Biologically relevant groups share a set of genes

Next we analyzed the genes that are shared between functionally defined subsets of cell types. Amacrine cells can be subdivided in two sub-classes based on the neurotransmitter they are releasing: GABA or glycine. Immunohistochemical

stainings revealed that A2$_{Fam81a}$, A2$_{Fbxo}$ and *Ier5* are glycinergic amacrine cells; whereas the majority of A17$_{Arc}$, *Starburst*, *vGluT3* and *Chrna3* are GABAergic amacrine cells (**Supplementary Fig. 5-9**, **Table 1**). We analyzed the GABAergic amacrine cell types to determine which genes are shared within this group (**Fig. 28a**). One of the genes that had the highest fold-change was *glutamic acid decarboxylase 1* (*Gad1*), an enzyme necessary to transform glutamate into GABA [64]. For the glycinergic combination, we found *Slc6a9*, which is the plasma membrane glycine transporter, to be one of the highest expressed genes (**Fig. 28b**).

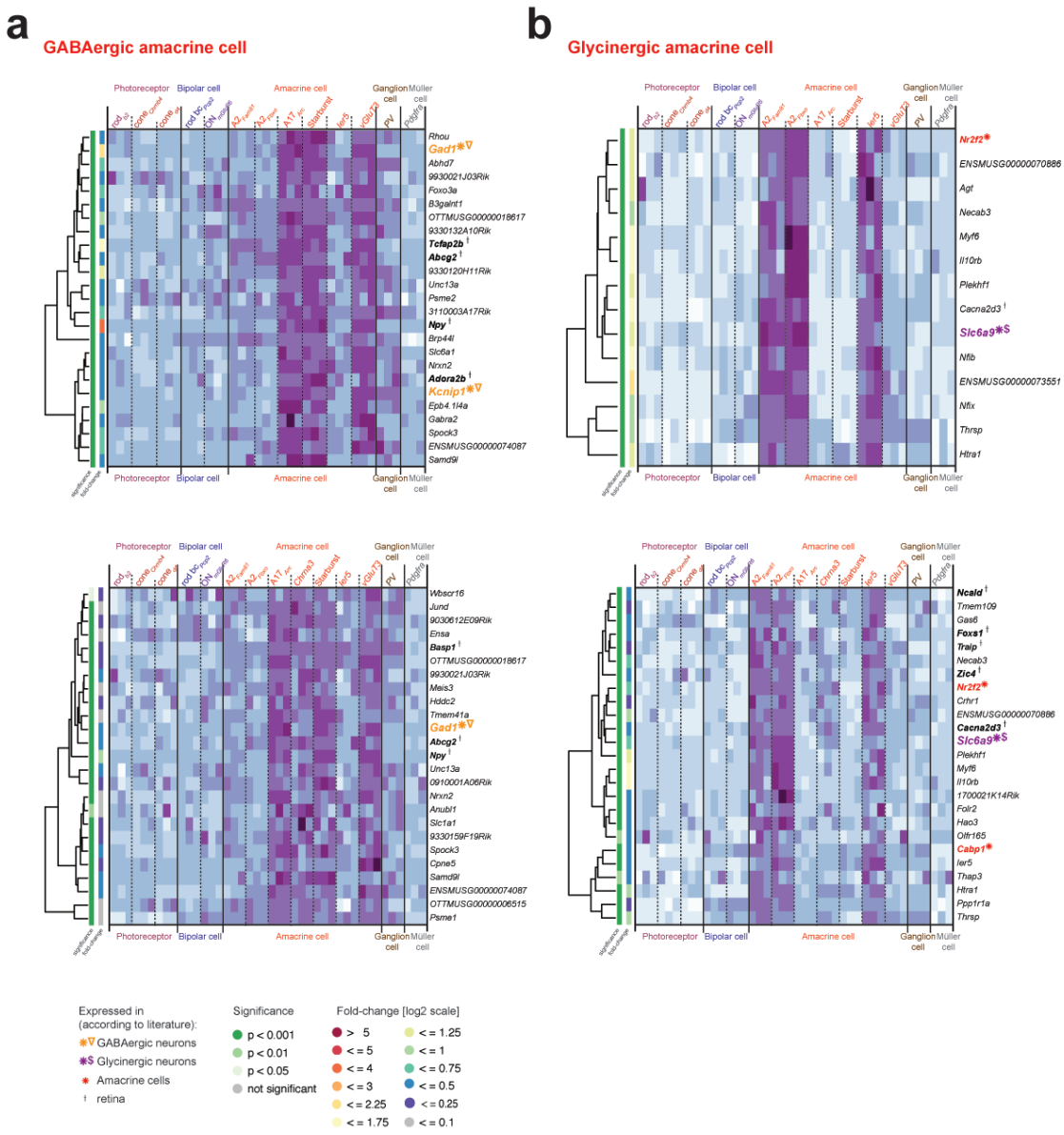

Figure 28. Hierarchical clustering of the 25 highest enriched genes for **a**, GABAergic and **b**, glycinergic amacrine cells. White and purple indicate relatively low and relatively high expression levels, respectively. The bars on the left of the heatmap color-code the significance within the biological triplicate and the fold-change of a particular gene. The upper panel has the column for *Chrna3* removed whereas in the lower part *Chrna3* was included in the analysis.

Most genes that are expressed in all amacrine cells but not in other cell types have a low fold-change, with the exception of the gene *Slc32a1. Slc32a1* is the vesicular GABA/glycine transporter that is known to be expressed only in inhibitory neurons (**Fig. 29a**).

Retinal cell neurons can be divided into two groups based on the type of synapse that the individual cells have. The photoreceptor and bipolar cells in the outer retina are releasing glutamate through a distinct type of synapse called the ribbon synapse [65], while amacrine and ganglion cells in the inner retina make conventional synapses. Comparing these two groups revealed a number of genes specifically expressed in one or the other group (**Fig. 29b**). Two of the highest expressed genes for the ribbon-containing cells are genes known to play a role in the function of ribbon synapses (*Cacna2d4* [66], *Slc17a7* or *vGluT1* [67]). Interestingly, the transcription factor *Otx2* is a marker for ribbon cells and *Pax6* is a marker for non-ribbon cells. These transcription factors have well-defined roles during development. Recent studies have revealed roles for these transcription factors in adult animals [68-70].

In **Figure 20a**, we showed that several genes are exclusively highly expressed in all photoreceptors. We also found at least 25 genes that are strongly down-regulated in photoreceptors and are therefore specific for cells that are not photoreceptors (**Fig. 29c**).

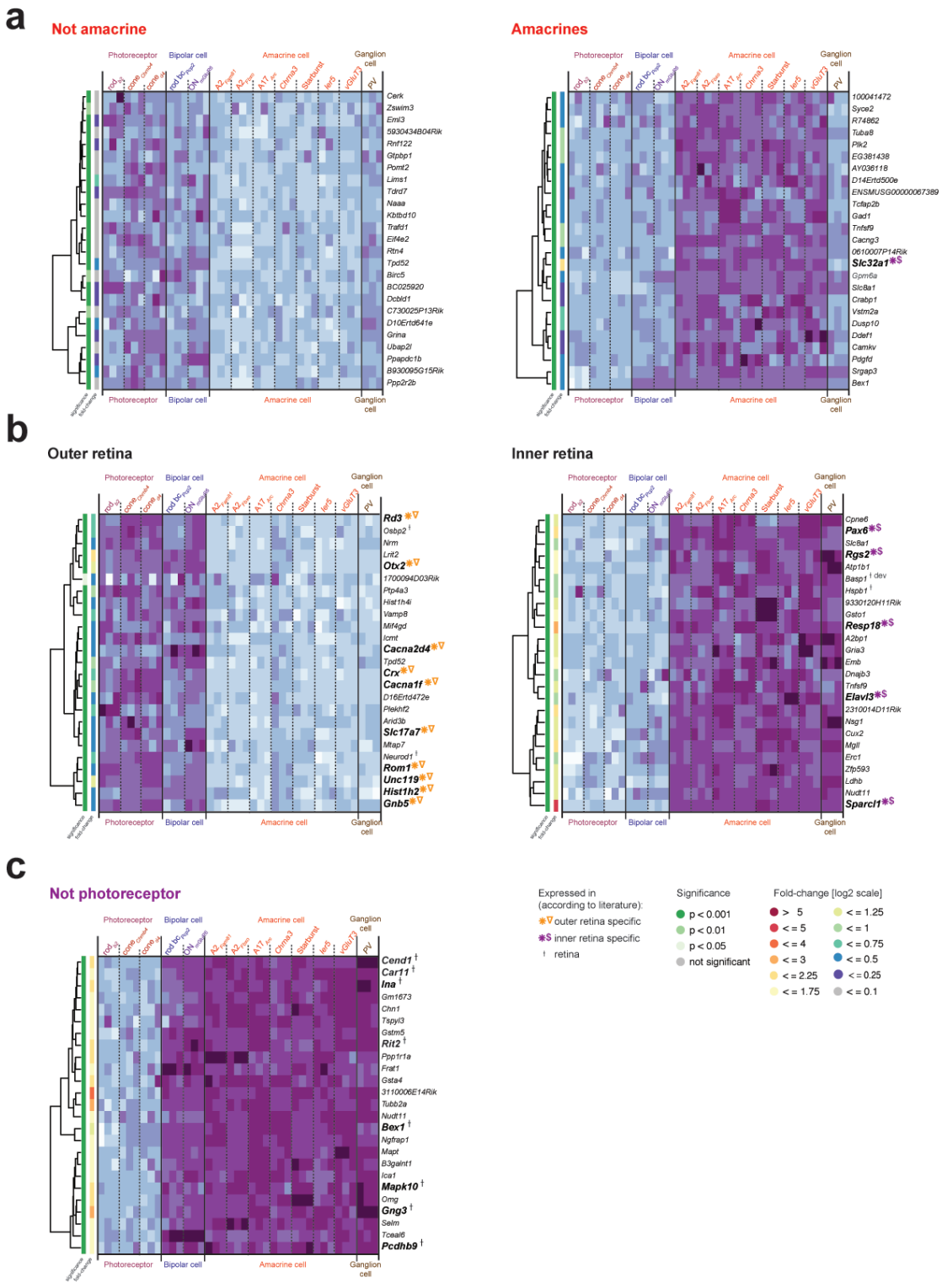

Figure 29. Hierarchical clustering of the 25 highest enriched genes for **a**, non-amacrine vs amacrine-specific, **b**, outer vs inner retina and **c**, non-photoreceptors. White and purple indicate relatively low and relatively high expression levels, respectively. The bars on the left of the heatmap color-code the significance within the biological triplicate and the fold-change of a particular gene.

The transcriptional code of cell types

Transcription factors are responsible for cell type-specific expression of genes. Our dataset includes the expression value of 2000 transcription factors for each mouse line. This allowed us to look for transcription factors that have a high fold-change difference between the different cell groups (**Fig. 30**). For the majority of the cell groups, we found transcription factors that are specific for the cell group (**Fig. 30a**). Among such cell class-specific transcription factors are *Sebox* and *Vsx2* [71] for bipolar cells (**Fig. 30b**), and *Rax* [72] for photoreceptors (**Fig. 30d**). Transcription factors like *Myf6* or *Tcfap2b* [42] are specific to glycinergic and GABAergic amacrine cells, respectively (**Fig. 30c**). In addition, *Otx2*, a transcription factor known to be expressed in photoreceptor and bipolar cells [69], is specifically expressed in those mouse lines (**Fig. 30e**). But we also found transcription factors with a high fold-change that are expressed in all cells but not in individual cell types (**Fig. 30f-g**). This can be shown in particular for the rod photoreceptors and Müller glia cells.

Channels and receptors in the retina

Finally, we screened our dataset for receptors and channels expressed specifically in cell groups (**Fig. 31**). For example, the GABA-receptor rho subunits *Gabrr1* and *Gabrr2* that are expressed in both bipolar cell groups, or *Chrna5* that is expressed in cone photoreceptors (**Fig. 31b**). Surprisingly, we also found several olfactory receptors (Olfr, **Fig. 32**).

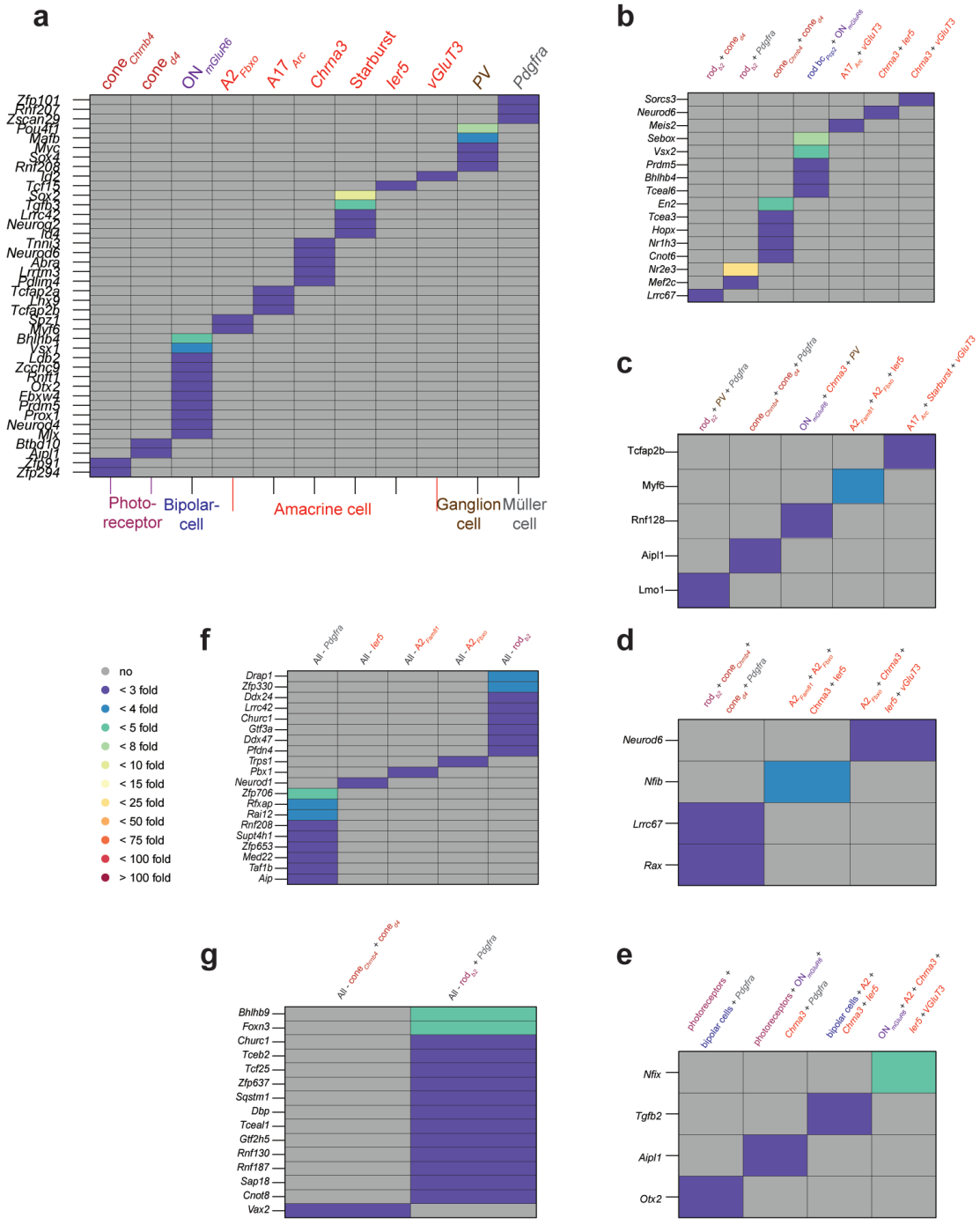

Figure 30. Fold-change plot for transcription factors. Fold-change is color-coded.

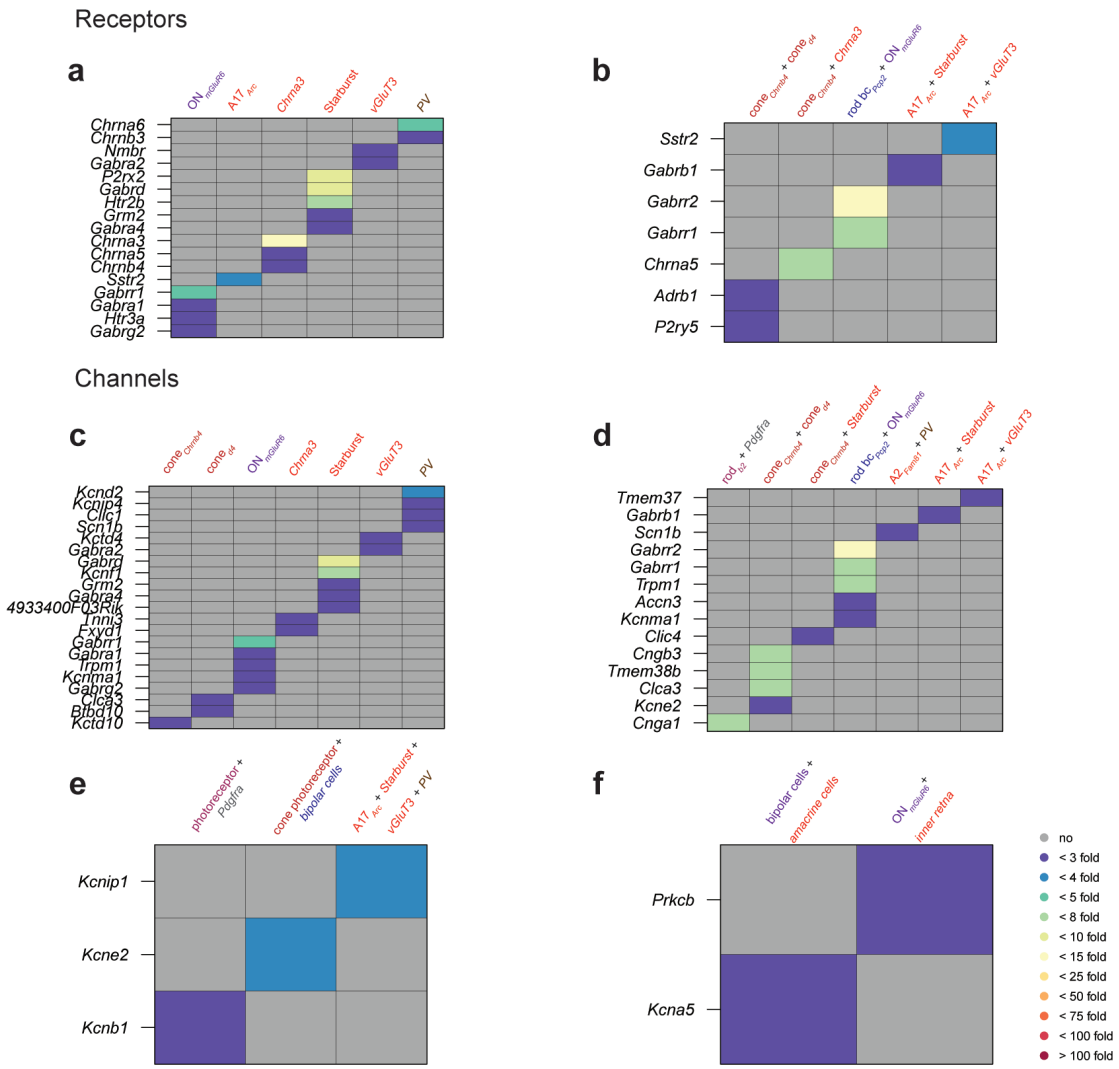

Figure 31. Fold-change plot for **a**-**b**, channels and **c**-**f**, receptors. Fold-change is color-coded.

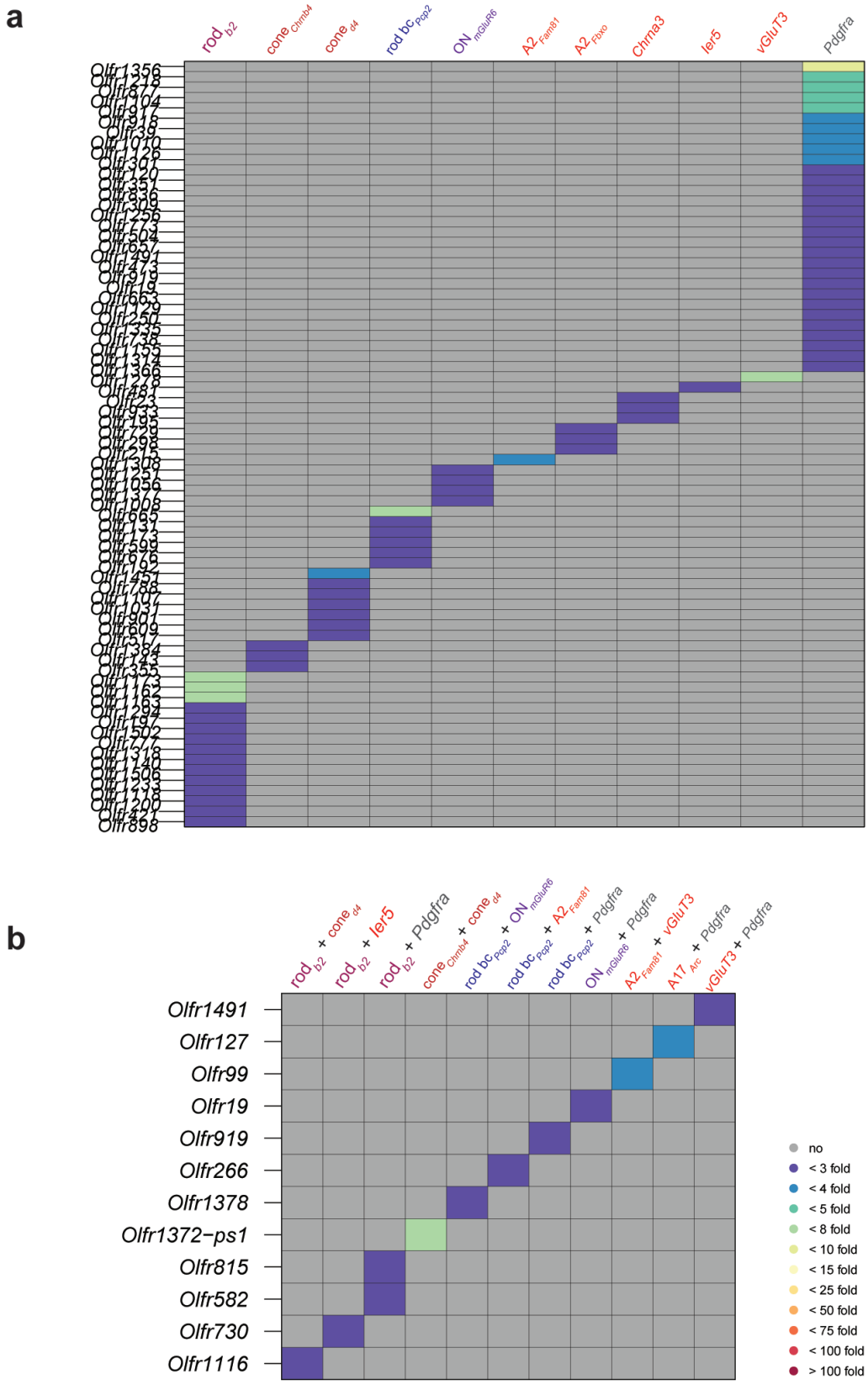

Figure 32. Fold-change plot for olfactory receptors. Fold-change is color-coded.

Discussion

The strategy

One critical step in gene profiling is the time from removing the tissue until collecting and lysing the cells of interest [73]. Ideally, this step should be as short as possible and cause minimal stress for the cell. We established a protocol to dissociate retinal cells within 10 min. For sorting out the cells, we decided to use FACS because most of the fluorescence-labeled cells in the retina in a transgenic mouse make up less than one per cent of the total cell population. Single cell picking would be less efficient and more time consuming. FACS allowed us to sort the cells within less than 3 minutes. Several disadvantages have been described for FACS, but we did not observe them. [2] For most of our mouse lines we could set a very distinct gate for the fluorescence-positive cells (**Fig. 16a**-**b**). Sometimes, for some fluorescence-positive populations like A17$_{Arc}$, we saw a fainter and a stronger fluorescence-positive population. For A17$_{Arc}$, we performed gene arrays from these two populations but we could not see any strong differences within the gene expression pattern, meaning that these cells are either starting to lose GFP or express less GFP (**Supplementary Fig. 13**). Another criticism refers to the purity and viability of the sorted cells. For both variables, we performed control experiments showing that our cells were a pure population and were still viable. The third critical point is the number of sorted cells. In our study, we kept the same amount of cells across all mouse lines. Previous experiments have revealed that the RNA yield of 200 cells is efficient enough to get reliable amplification and expression values for individual genes on the arrays (data not shown). This reliability is shown in the high similarity within the independently amplified biological triplicates of each mouse line. We could further validate our data, when we were looking into genes that are known to be involved in the rod and cone phototransduction cascade [51]. Among such genes,

we found all those which have been described to be specifically expressed in the individual photoreceptor types. We confirmed this result by including two mouse lines that both drive fluorescence expression in cones but use different promoters. Gene expression patterns were highly similar in both mouse strains (**Fig. 21b**).

The role of rod photoreceptors and Müller glia cells

In the case of rod photoreceptors (rod_{b2}) and Müller glia cells (*Pdgfra*), the pairwise correlation plot showed a high transcriptional variability within the biological triplicate (**Fig. 18**). For rod photoreceptors, the transcriptional variability is likely to be a biological phenomenon, and was confirmed by two additional experiments: the repetition of the experiment (rod_{b2}, 2nd batch), and the preparation of each rod_{b2} at the exact same time but on different days (rod_{b2}, single). Neither experiment improved the correlation within the biological triplicates. But all three experiments (rod_{b2} 1st batch, 2nd batch and single) shared a set of highly expressed rod photoreceptor-specific genes (**Fig. 21a**).

We also see high transcriptional noise within the Müller glia cells (*Pdgfra*). But if we look in the set of genes which are highly expressed in rod_{b2} and *Pdgfra* but not in other cells, we found genes like *Rhodopsin* or *Nr2e3* that are known to be rod photoreceptor-specific (**Supplementary Fig. 14**) [74, 75]. This result implies that the dissociation of the Müller glia cells from the rod photoreceptors was probably insufficient. To further explore this possibility, we would have first to repeat the Müller glia cells gene arrays and slightly extent the papain-digestion and, second, add another mouse line that expresses GFP within Müller glia cells.

Another interesting result is the high number of genes that are down-regulated in adult rod photoreceptors (**Fig. 26a**). One explanation for this

phenomenon could be based on development: rod photoreceptors are continuously developing from different progenitors [76, 77], suggesting that the easiest way for a progenitor to develop a rod photoreceptor would be either using transcriptional [78] or epigenetic [39] factors that down-regulate a set of genes and so cause the cells to develop into rod photoreceptors. That development may be the key factor for down regulation might also be confirmed by the down-regulation of genes in other cells. For example, we found individual genes that were down regulated and had a high fold-change difference in cone photoreceptors and bipolar cells. Those genes have in common that they have been described as influencing cell fate generation during development [60-62].

Amacrine cells: GABA versus glycine

We found another intriguing gene pattern for both A2 mouse lines ($A2_{Fbxo}$ and $A2_{Fam81}$). Immunohistochemical staining revealed that the majority of the labeled cells were A2 amacrine cells. We have also shown, in **Figure 19**, that the data have a noise level similar to $A17_{Arc}$ or *Starburst* cells. For the latter two, we found a distinct set of genes with a high expression value and fold change, but for both A2 amacrine cells, the majority of the genes have a low fold change. A similar low fold change was observed for the highest expressed genes in the *Ier5* amacrine cell. Interestingly, both A2 and *Ier5* release glycine as their neurotransmitter, whereas other amacrine cell types release GABA (**Table 1**, **Fig. 28**). It might be that glycinergic amacrine cells have higher transcriptional variety, and this makes it difficult to reveal distinct genes. Glycinergic amacrine cells are narrow-field amacrine cells and often have an intense contact with different cell types. [79] We also know that A2 amacrine cells have a distinct role in day and night vision [47]. It might be that glycinergic amacrine cells serve as a kind of “relay” station, allowing a very flexible switch of gene expression pattern based on light conditions. We only tested our cells at one time point in a day.

To reveal the possibility of different gene expression patterns day and night, we would also have to test animals at different times of day.

Olfactory receptors

It is thought that olfactory receptors, which are responsible for odor detection, are exclusively located in the olfactory sensory neurons. [80] However, we showed that gene and pseudogene members of the olfactory receptors were expressed in distinct cell types, like rods and cones (**Fig. 32**). We did not observe any specific olfactory receptor for a particular cell class. The functional role of olfactory receptor genes and pseudogenes in retinal cells is unknown, and opens an exciting avenue for investigation.

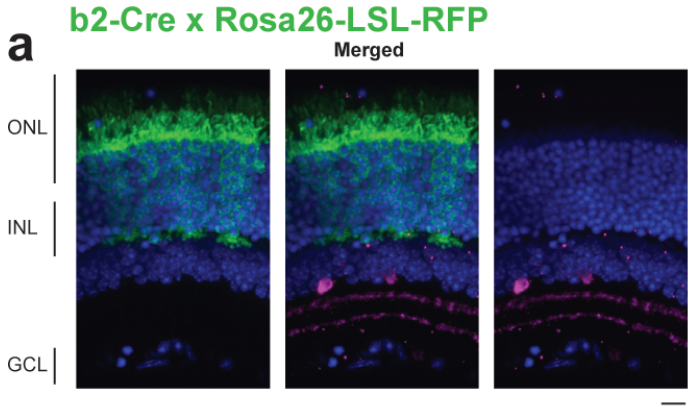

b

GFP positive cells in [cells/ 1 mm2]		
ONL	INL	GCL
365 (+/- 267)	0	0
1985 (+/- 760)	Total cells in region	

Binary code		
cell type	axons	stratification
100000000	no	100000000

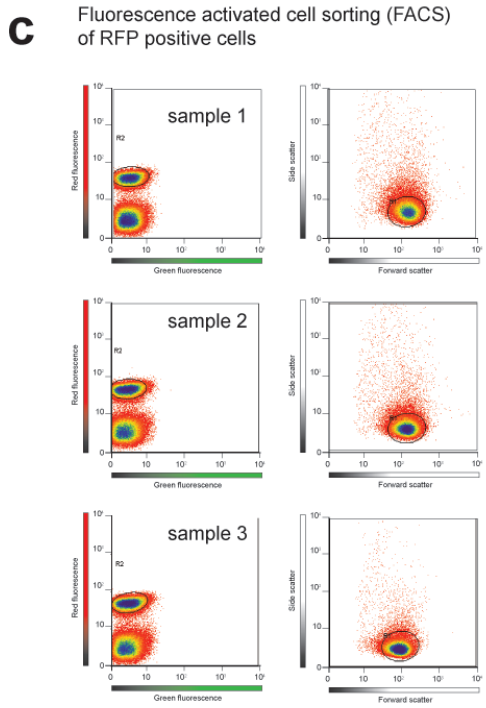

Supplementary Figure 1. Mouse line labeling rod photoreceptors (rod$_{b2}$). **a**, Immunostained vibratome sections, blue: DAPI, green: RFP, purple: ChAT. **b**, Quantification of the number of RFP-positive cells in the nuclear layers and the binary code. **c**, FACS gates for the biological triplicates. The first column plots GFP against RFP to reveal the fluorescence-positive cells. The second column shows the selection for the cell size and granularity of the cells. Scale bar: 10 μm

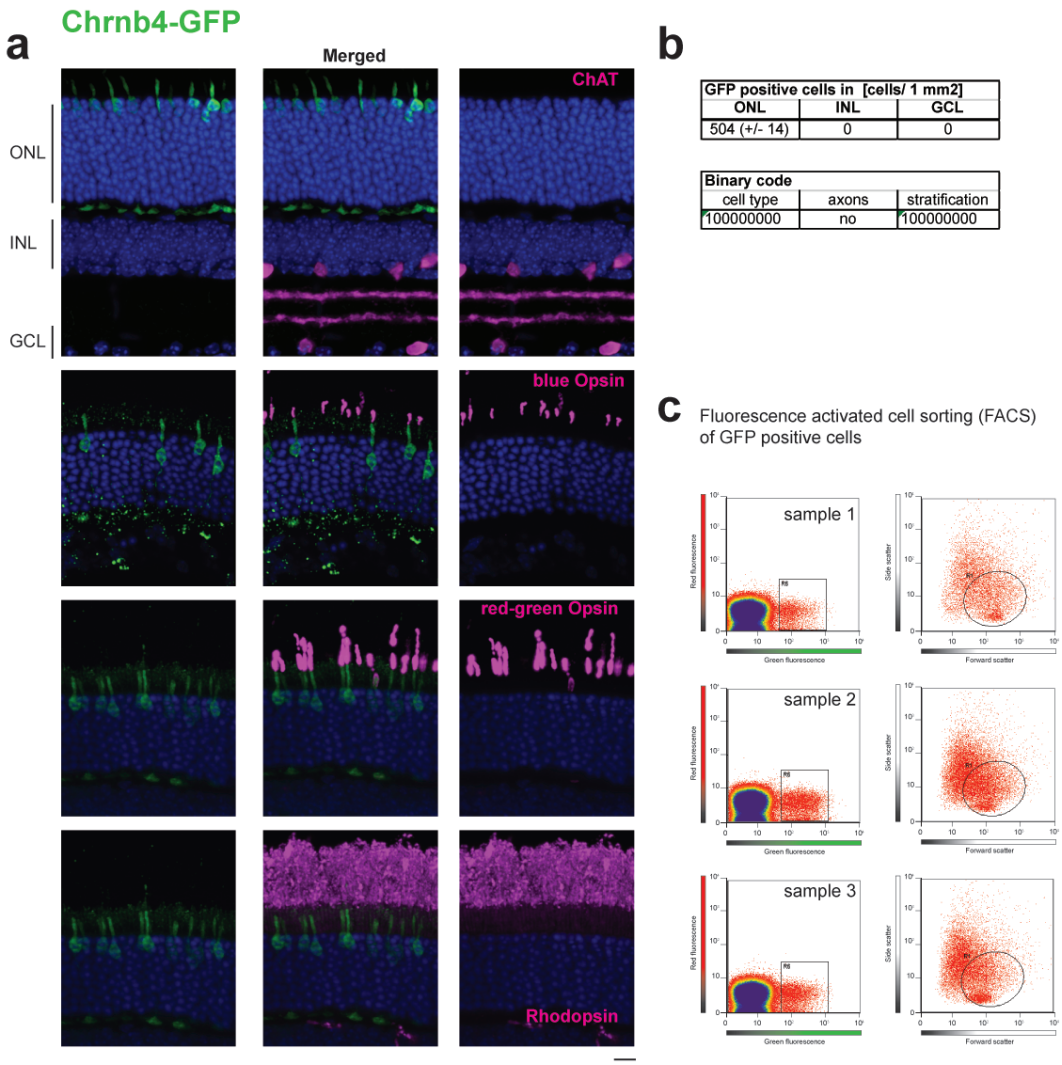

Supplementary Figure 2. Mouse line labeling cone photoreceptors (cone$_{Chrnb4}$). **a**, Immunostained vibratome sections, blue: DAPI, green: GFP, purple: 1st row: ChAT, 2nd row: blue Opsin, 3rd row: red-green Opsin, 4th row: Rhodopsin. **b**, Quantification of the number of GFP-positive cells in the nuclear layers and the binary code. **c**, FACS gates for the biological triplicates. The first column plots GFP against RFP to reveal the fluorescence-positive cells. The second column shows the selection for the cell size and granularity of the cells. Scale bar: 10 μm

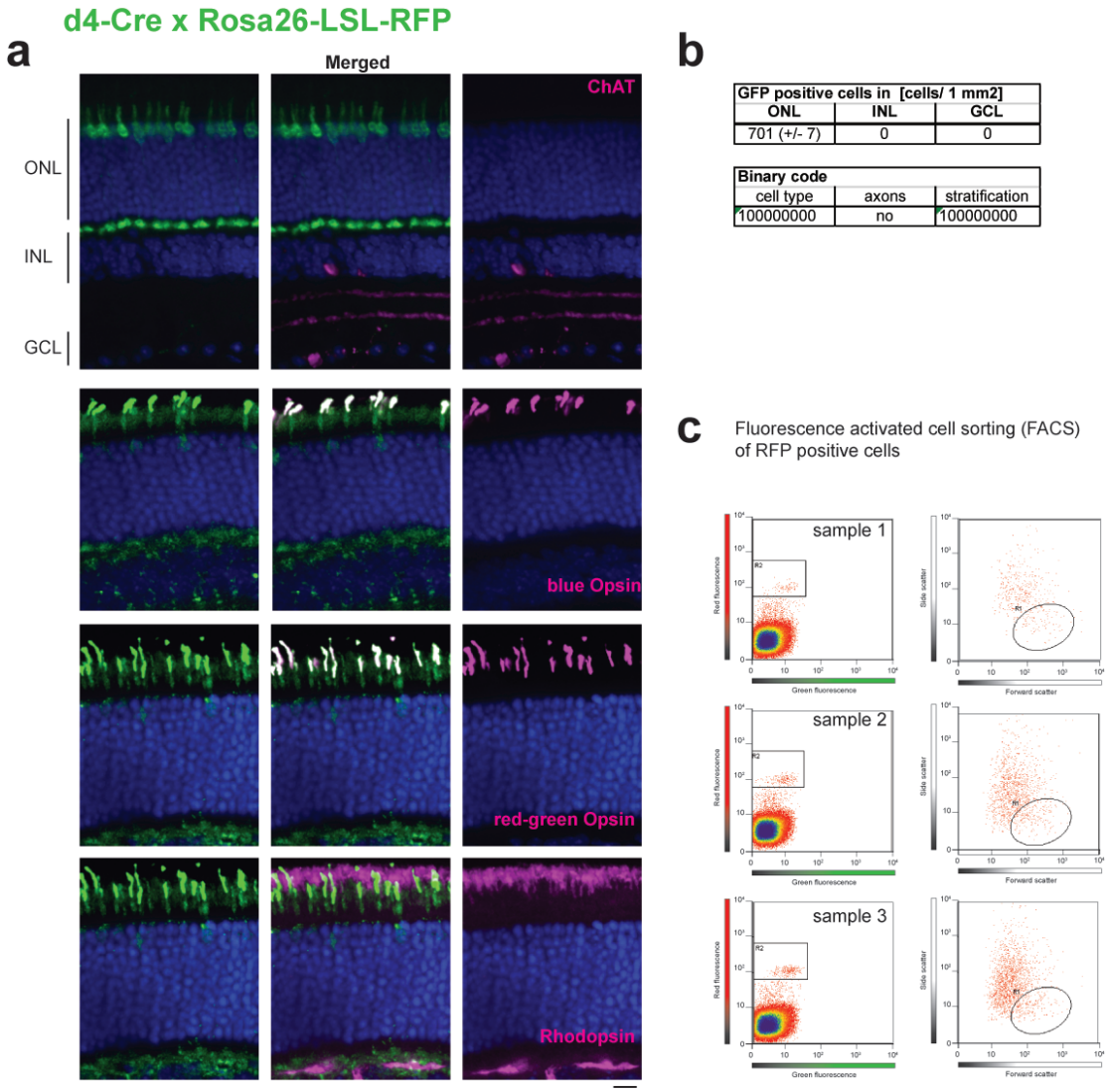

Supplementary Figure 3. Mouse line labeling cone photoreceptors (cone$_{d4}$). **a**, Immunostained vibratome sections, blue: DAPI, green: GFP, purple: 1st row: ChAT, 2nd row: blue Opsin, 3rd row: red-green Opsin, 4th row: Rhodopsin. **b**, Quantification of the number of GFP-positive cells in the nuclear layers and the binary code. **c**, FACS gates for the biological triplicates. The first column plots GFP against RFP to reveal the fluorescence-positive cells. The second column shows the selection for the cell size and granularity of the cells. Scale bar: 10 μm

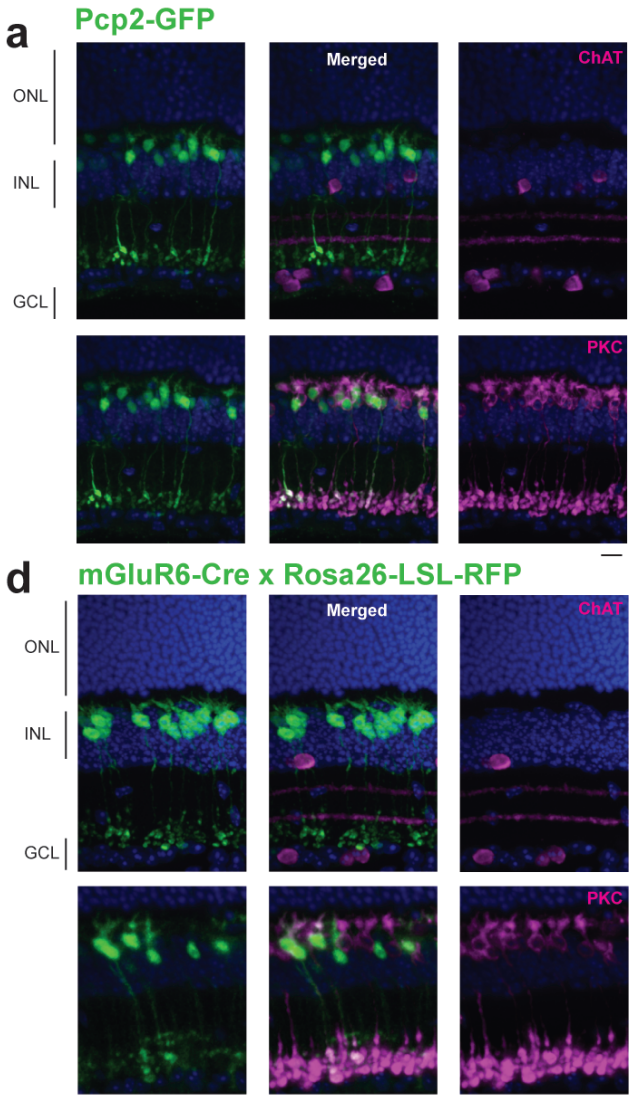

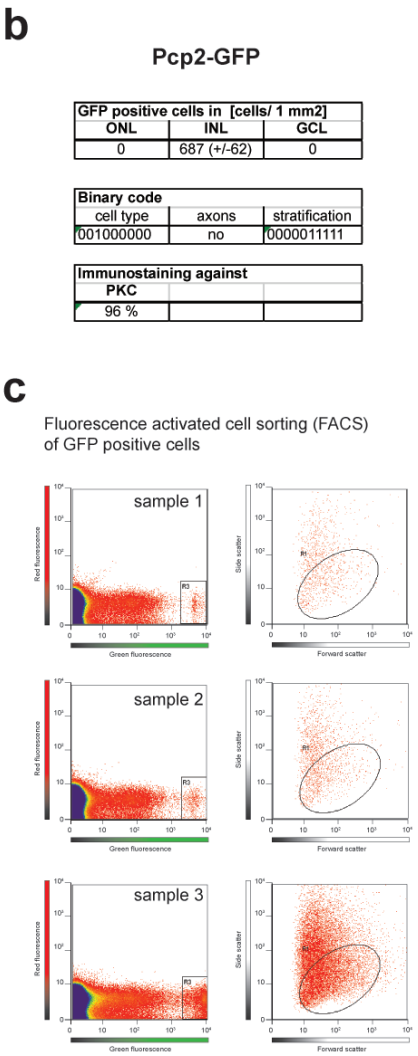

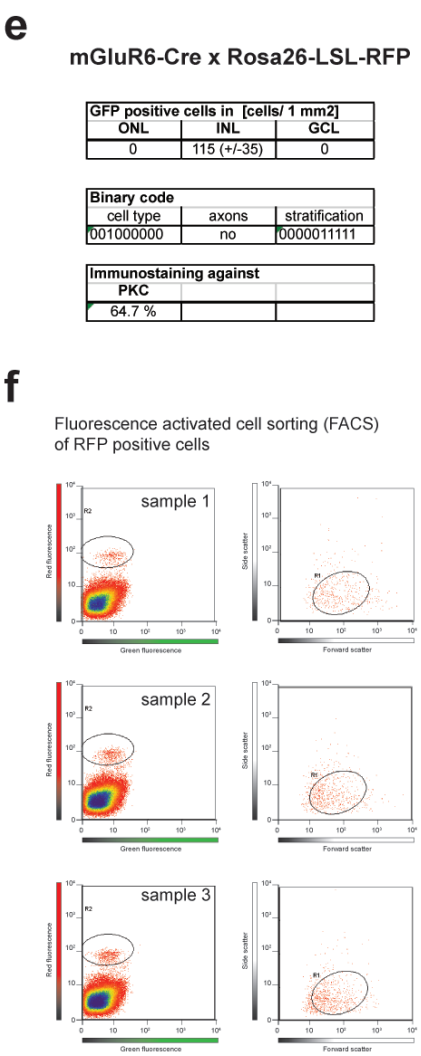

Supplementary Figure 4. Mouse lines labeling bipolar cells. **a-c**, rod bipolar cells (rod bc$_{Pcp2}$), **d-f**, ON bipolar cells (ON bc$_{mGluR6}$). **a**, **d**, Immunostained vibratome sections, blue: DAPI, green: GFP and RFP, respectively, purple: 1st row: ChAT, 2nd row: PKC. **b**, **e**, Quantification of the number of GFP or RFP-positive cells in the nuclear layers and the binary code. **c**, **f**, FACS gates for the biological triplicates. The first column plots GFP against RFP to reveal the fluorescence-positive cells. The second column shows the selection for the cell size and granularity of the cells. Scale bar: 10 μm

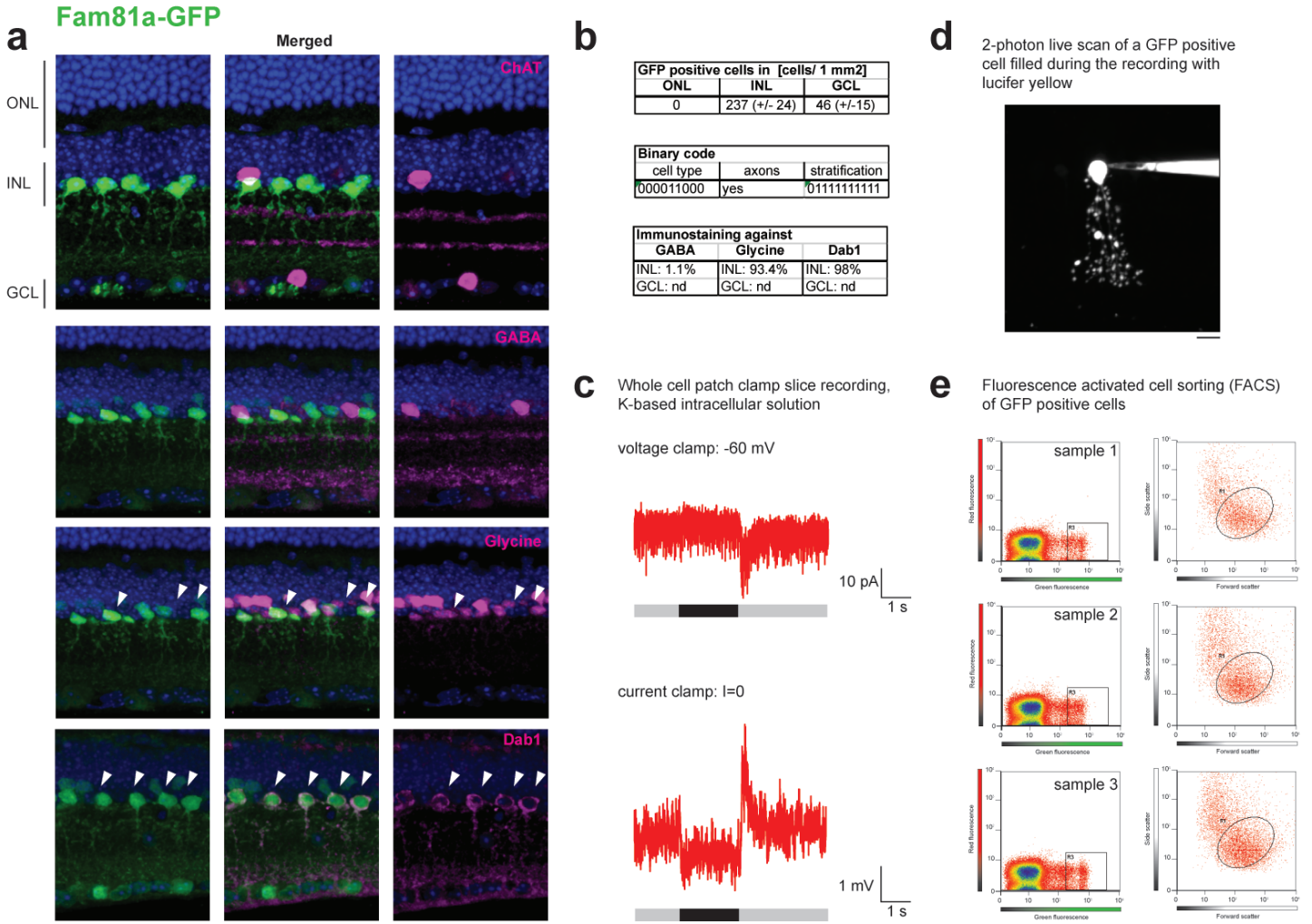

Supplementary Figure 5. Mouse line labeling A2 amacrine cells (A2$_{Fam81}$). **a**, Immunostained vibratome sections, blue: DAPI, green: RFP, purple: 1st row: ChAT, 2nd row: GABA, 3rd row: Glycine, 4th row: Dab1. **b**, Quantification of the number of GFP-positive cells in the nuclear layers and the binary code. **c**, Whole cell patch clamp slice recording. Upper plot: voltage clamp, lower plot: current clamp. **d**, 2-photon live imaging of a Lucifer yellow filled GFP-positive cell. **e**, FACS gates for the biological triplicates. The first column plots GFP against RFP to reveal the fluorescence-positive cells. The second column shows the selection for the cell size and granularity of the cells. Scale bar: 10 μm

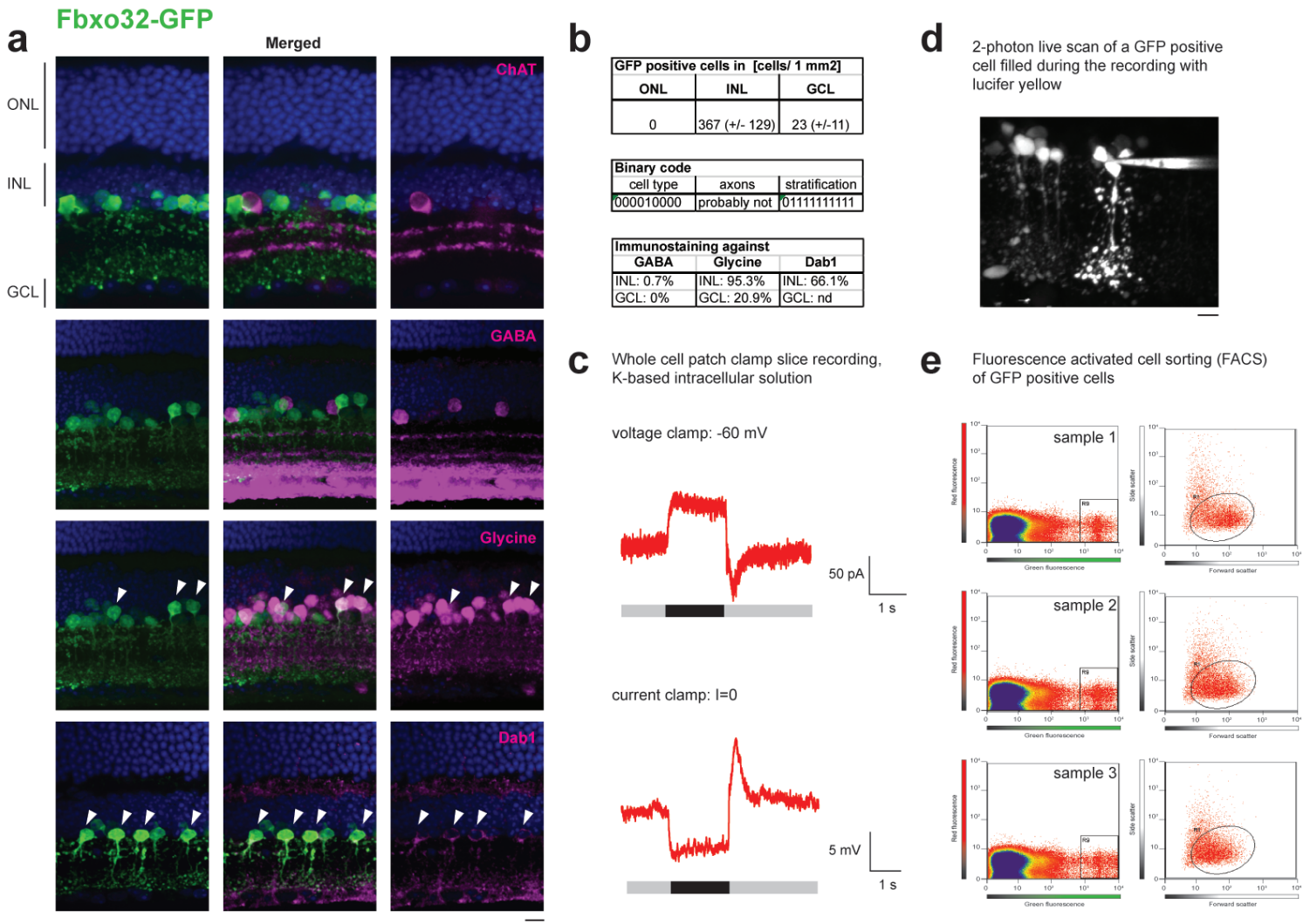

Supplementary Figure 6. Mouse line labeling A2 amacrine cells ($A2_{Fbxo}$). **a**, Immunostained vibratome sections, blue: DAPI, green: RFP, purple: 1st row: ChAT, 2nd row: GABA, 3rd row: Glycine, 4th row: Dab1. **b**, Quantification of the number of GFP-positive cells in the nuclear layers and the binary code. **c**, Whole cell patch clamp slice recording. Upper plot: voltage clamp, lower plot: current clamp. **d**, 2-photon live imaging of a Lucifer yellow filled GFP-positive cell. **e**, FACS gates for the biological triplicates. The first column plots GFP against RFP to reveal the fluorescence-positive cells. The second column shows the selection for the cell size and granularity of the cells. Scale bar: 10 μm

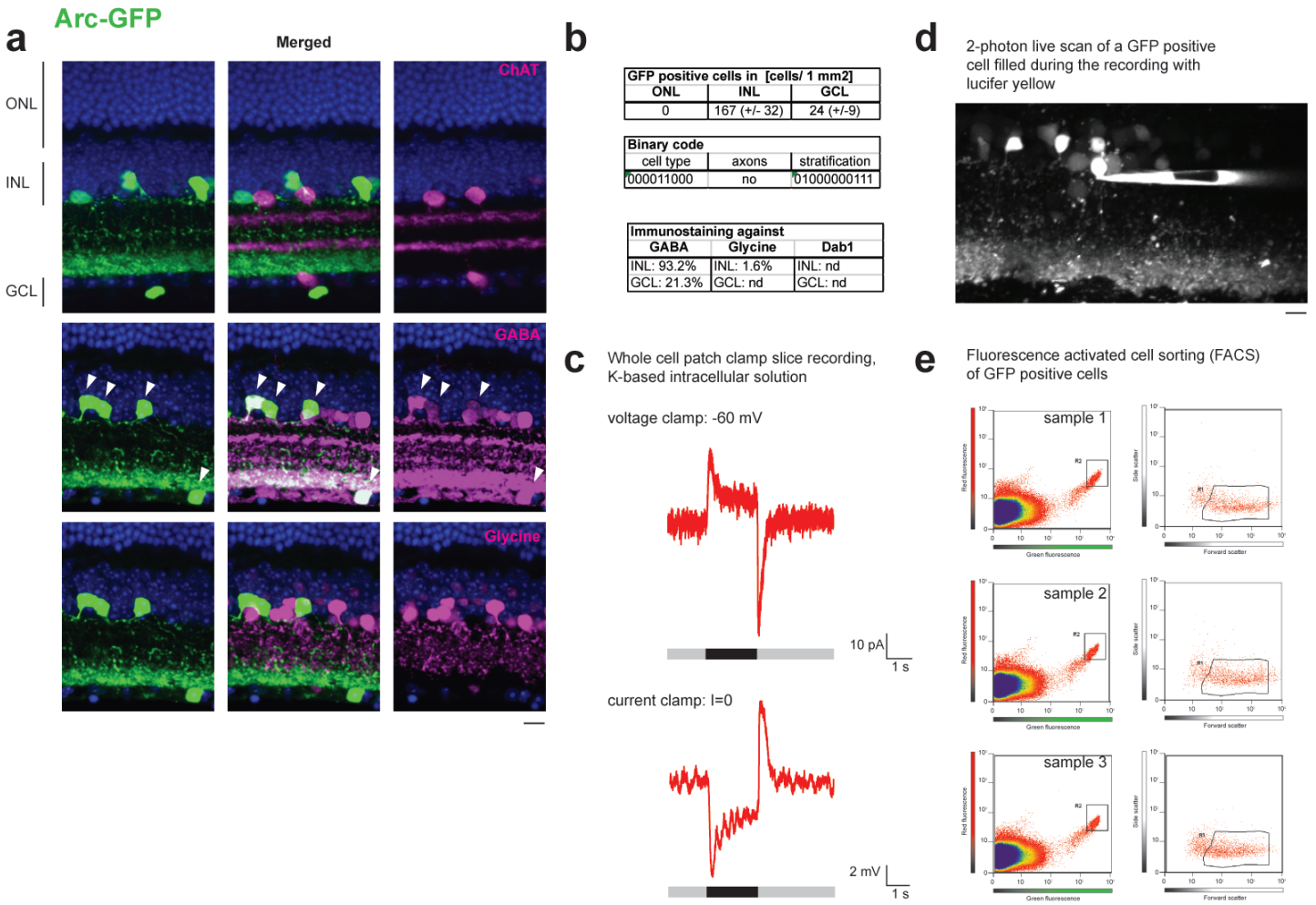

Supplementary Figure 7. Mouse line labeling A17 amacrine cells ($A17_{Arc}$). **a**, Immunostained vibratome sections, blue: DAPI, green: RFP, purple: 1st row: ChAT, 2nd row: GABA, 3rd row: Glycine. **b**, Quantification of the number of GFP-positive cells in the nuclear layers and the binary code. **c**, Whole cell patch clamp slice recording. Upper plot: voltage clamp, lower plot: current clamp. **d**, 2-photon live imaging of a Lucifer yellow filled GFP-positive cell. **e**, FACS gates for the biological triplicates. The first column plots GFP against RFP to reveal the fluorescence-positive cells. The second column shows the selection for the cell size and granularity of the cells. Scale bar: 10 μm

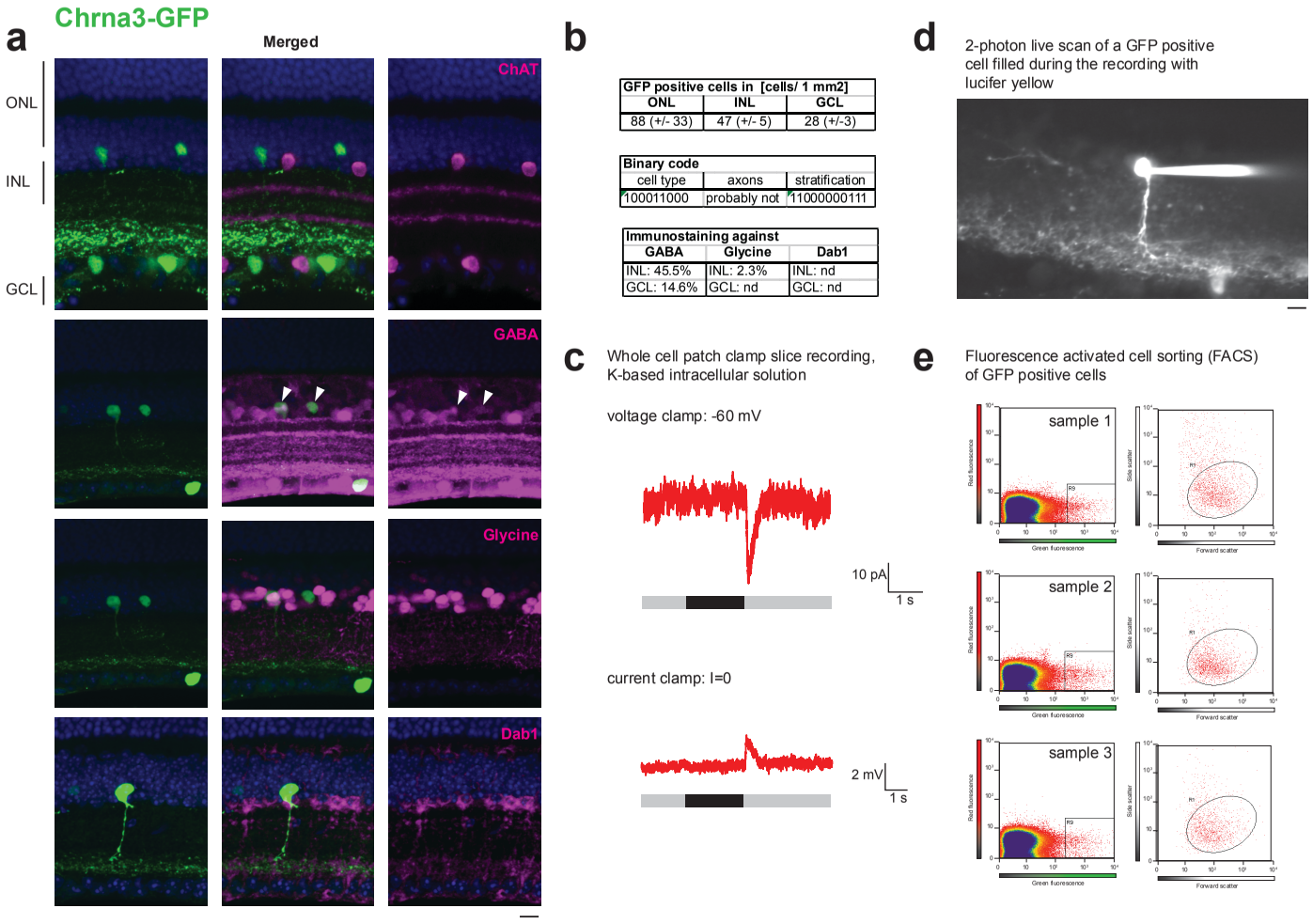

Supplementary Figure 8. Mouse line labeling Chrna3 amacrine cells (*Chrna3*). **a**, Immunostained vibratome sections, blue: DAPI, green: RFP, purple: 1st row: ChAT, 2nd row: GABA, 3rd row: Glycine, 4th row: Dab1. **b**, Quantification of the number of GFP-positive cells in the nuclear layers and the binary code. **c**, Whole cell patch clamp slice recording. Upper plot: voltage clamp, lower plot: current clamp. **d**, 2-photon live imaging of a Lucifer yellow filled GFP-positive cell. **e**, FACS gates for the biological triplicates. The first column plots GFP against RFP to reveal the fluorescence-positive cells. The second column shows the selection for the cell size and granularity of the cells. Scale bar: 10 μm

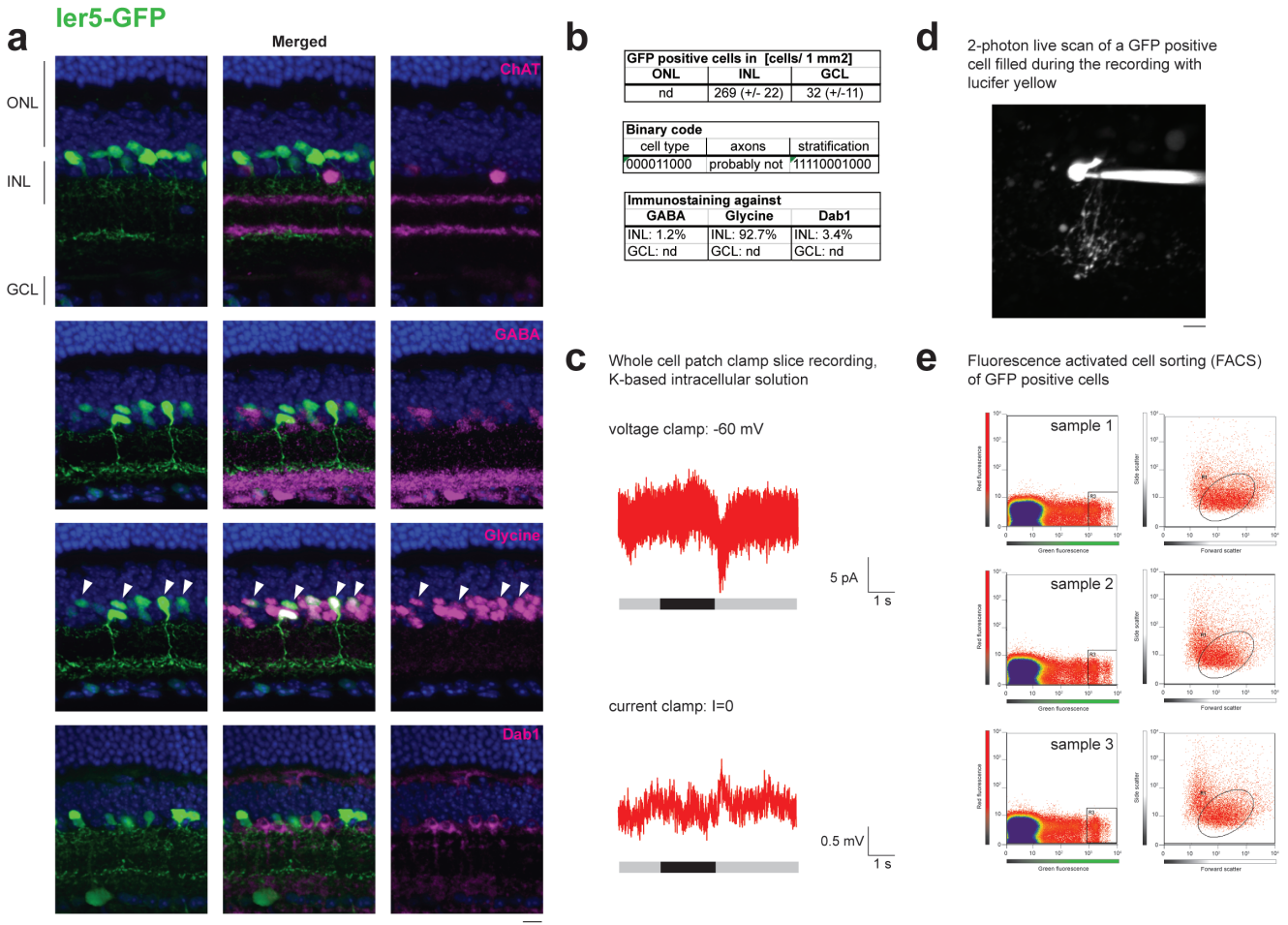

Supplementary Figure 9. Mouse line labeling Ier5 amacrine cells (*Ier5*). **a**, Immunostained vibratome sections, blue: DAPI, green: RFP, purple: 1st row: ChAT, 2nd row: GABA, 3rd row: Glycine, 4th row: Dab1. **b**, Quantification of the number of GFP-positive cells in the nuclear layers and the binary code. **c**, Whole cell patch clamp slice recording. Upper plot: voltage clamp, lower plot: current clamp. **d**, 2-photon live imaging of a Lucifer yellow filled GFP-positive cell. **e**, FACS gates for the biological triplicates. The first column plots GFP against RFP to reveal the fluorescence-positive cells. The second column shows the selection for the cell size and granularity of the cells. Scale bar: 10 μm

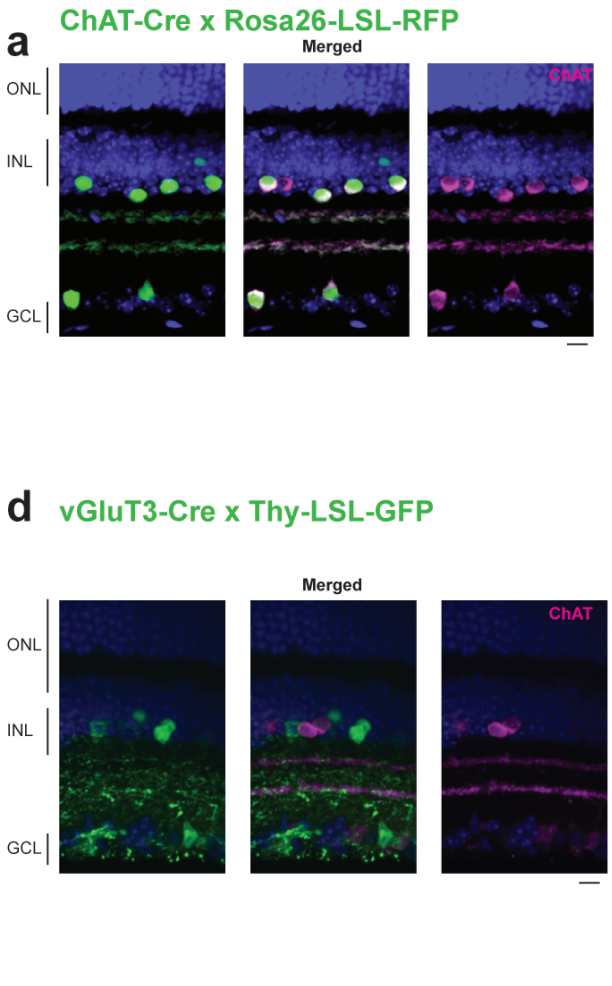

Supplementary Figure 10. Mouse lines labeling amacrine cells. **a**-**c**, Starburst amacrine cells **d**-**f**, vGluT3 amacrine cells. **a**, **d**, Immunostained vibratome sections, blue: DAPI, green: RFP and GFP, respectively, purple: ChAT. **b**, **e**, Quantification of the number of RFP or GFP-positive cells in the nuclear layers and the binary code. **c**, **f**, FACS gates for the biological triplicates. The first column plots GFP against RFP to reveal the fluorescence-positive cells. The second column shows the selection for the cell size and granularity of the cells. Scale bar: 10 μm

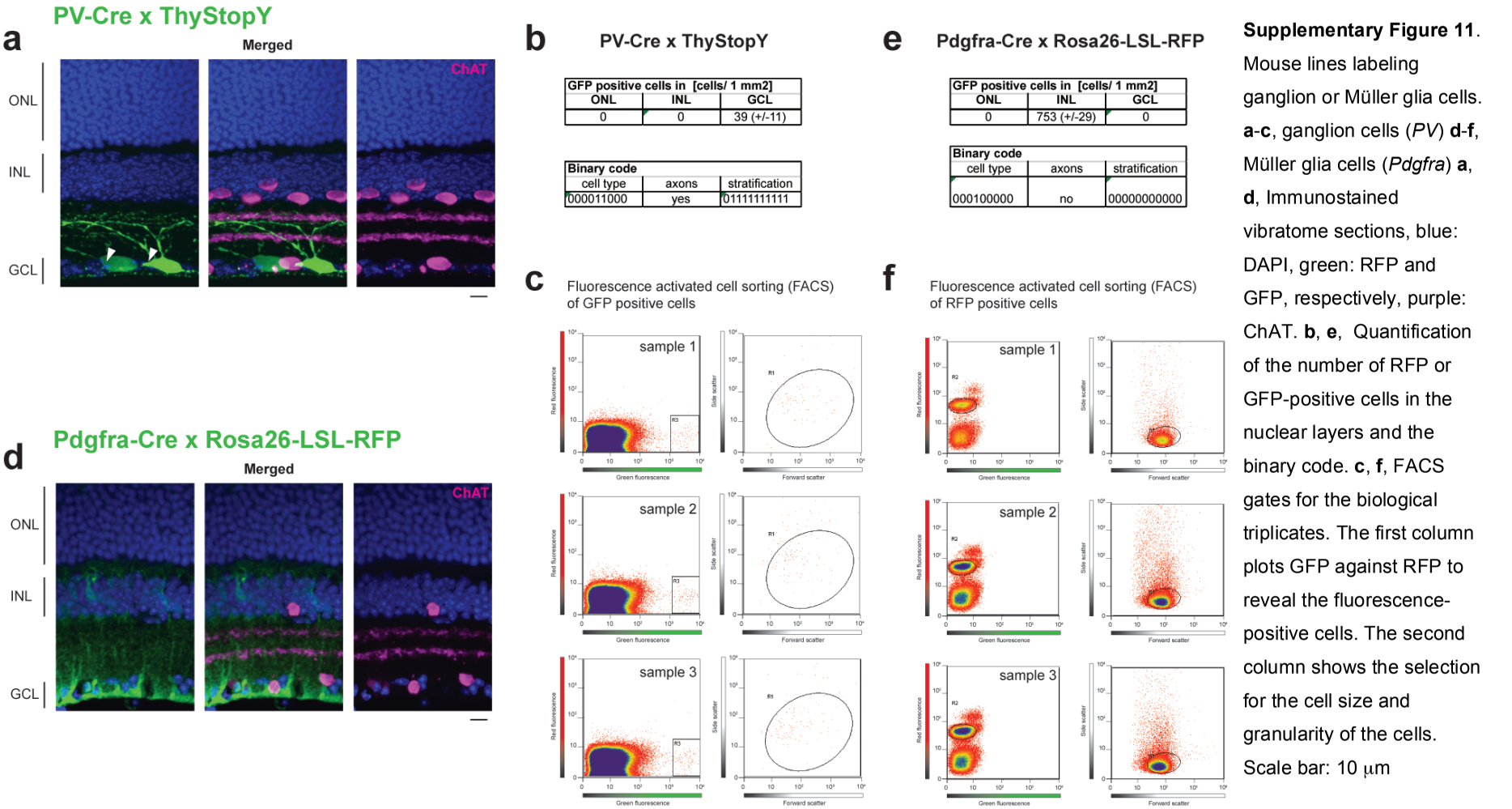

Supplementary Figure 11. Mouse lines labeling ganglion or Müller glia cells. **a**-**c**, ganglion cells (*PV*) **d**-**f**, Müller glia cells (*Pdgfra*) **a**, **d**, Immunostained vibratome sections, blue: DAPI, green: RFP and GFP, respectively, purple: ChAT. **b**, **e**, Quantification of the number of RFP or GFP-positive cells in the nuclear layers and the binary code. **c**, **f**, FACS gates for the biological triplicates. The first column plots GFP against RFP to reveal the fluorescence-positive cells. The second column shows the selection for the cell size and granularity of the cells. Scale bar: 10 μm

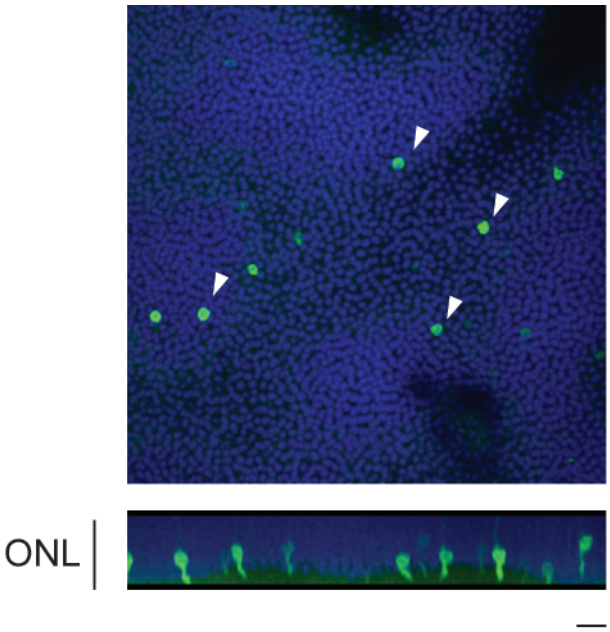

Supplementary Figure 12. Photoreceptor labeling in *Chrna3*. Immunostained wholemount retina, blue: DAPI, green: GFP. Upper panel: Wholemount topview. Lower panel: side-projection. Scale bar: 10 μm

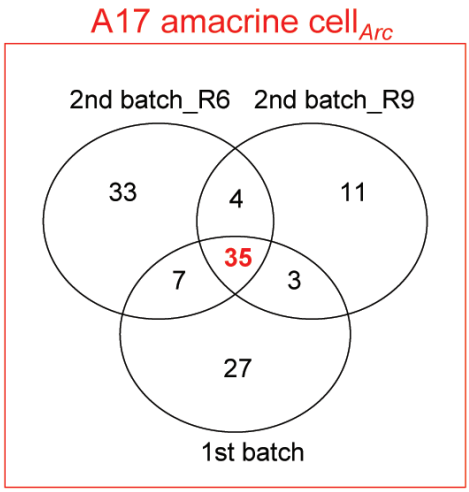

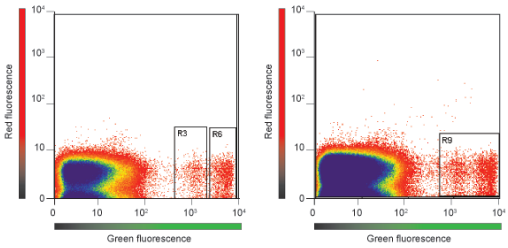

Genes shared within all sets

1110017I16Rik	*Gng8*
2610017I09Rik	*Gpr22*
4930422I07Rik	*Igfbp2*
9030425E11Rik	*Klhl32*
AI593442	*Lhx9*
C1ql1	*Marcks*
Cartpt	*Neto2*
Cbln1	*Osta*
Csrp2	*Pcbd1*
Cthrc1	*Pgam2*
Cxcr7	*Prkar2b*
Dtnbp1	*Sstr2*
ENSMUSG00000	*Stc1*
075319	*Tcfap2a*
Eef1e1	*Tcfap2b*
Epb4.1l4a	*Tpd52l1*
Gdf2	*Uts2r*
Gjc1	*Vwc2*

Supplementary Figure 13. Venn-Diagram of the different Arc batches (1st and 2nd) and different sorting regions for the 2nd batch (R6 and R9). The list next to the diagram shows the genes that are shared between all three datasets.

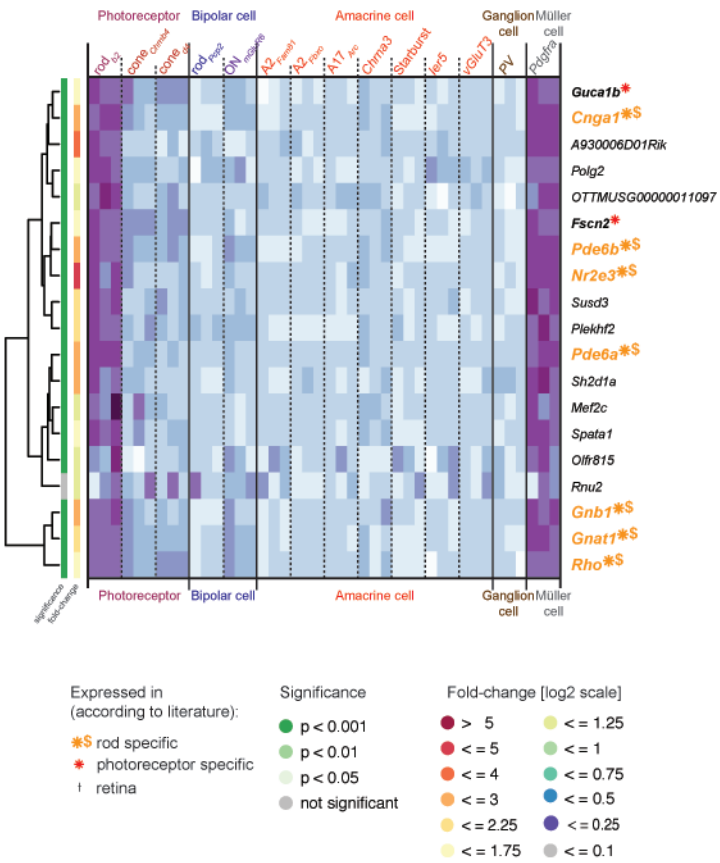

Supplementary Figure 14. Hierarchical clustering of the 25 highest enriched genes for rod photoreceptor and Müller glia cells. White and purple indicate relatively low and relatively high expression levels, respectively. The bars on the left of the heatmap color-code the significance within the biological triplicate and the fold-change of a particular gene.

Experimental Procedures

Animals for live recordings and gene profiling

(The name in square brackets is the abbrevation of the transgenic mouse lines used for genetic profiling): [A2$_{Fam81}$]: Tg(*6430514L14Rik*-EGFP)95Gsat (note new name: *Fam81a*-EGFP), [A17$_{Arc}$]: Tg(*Arc*-EGFP)194Gsat/Mmcd, [*Chrna3*]: Tg(*Chrna3*-EGFP)BZ135Gsat/Mmnc, [cone$_{Chrnb4}$]: Tg(*Chrnb4*-EGFP)1Gsat, Tg(*Dtx4*-EGFP)102Gsat, [A2$_{Fbxo}$] Tg(*Fbxo32*-EGFP)138Gsat/Mmcd, Tg(*Gng3*-EGFP)208Gsat, Tg(*Gng4*-EGFP)227Gsat, [*Ier5*]: Tg(*Ier5*-EGFP)267Gsat, Tg(*Satb2*-EGFP)127Gsat, Tg(*Syt7*-EGFP)197Gsat were purchased from MMRRC (*www.mmrrc.org*). Before starting experiments, we backcrossed these animals at least twice with wild-type C57BL/6J mice that were purchased from RCC Ltd. (Füllinsdorf, Germany). Mouse lines expressing Cre under a cell-specific promoter: [rod$_{b2}$]: b2-Cre (provided by Y-Z Le)[81], [cone$_{d4}$]: d4-Cre (provided by Y-Z Le)[82], [*Starburst*]: 129S6-Chat_tm1(cre)Lowl/J (Jackson, stock: #006410), [ON$_{mGluR6}$]: B6Cf1-Tg(mGlur6-Cre)BR, FMI, [rod bc$_{Pcp2}$]: B6:FVB-Tg(Pcp2-EFP)2Yuza (Jackson, stock: #004690) , [*Pdgfra*]: B6Cf1-Tg(Pdgfra-Cre)BR, Boston, [*PV*]: 129SVCB6(PV-CRE#32)SA-09 (provided by S. Arber), [vGluT3]: B6Cf1-Tg(vGlut3cre)BR. With exception of the PV-Cre vGlut3-Cre mouse lines, all mice have been crossed with the Rosa26-LSL-RFP reporter (provided by H-J. Fehling [83]). PV-Cre and vGluT3-Cre were crossed with C57BL/6-TG(ThystopYFP)JS (provided by J. Sanes). All animal procedures were performed in accordance with the standard ethical guidelines (European Communities Guidelines on the Care and Use of Laboratory Animals: 86/609/EEC) and were approved by the Veterinary Department of the Canton of Basel-Stadt.

Immunohistochemistry

For the genetic address book: 536 eye pairs from different transgenic mouse lines, representing 536 different BACs, of the GENSAT project were tested. Fixation was done by intracardial administration of 4% paraformaldehyde in phosphate buffered saline (PBS). Eyes were enucleated, stored in 4% paraformaldehyde (PFA) (wt/vol) in PBS in New York and after pooling of several eyes sent to Basel. In Basel, retinas were dissected from the eyecup and washed in PBS at 4°C for 1–5 days. Otherwise, eyes were enucleated, the retina dissected from the eyecup, fixed for 20-30 min in 4% PFA/PBS and washed overnight in PBS. Next, retinas were incubated in 30%

sucrose (wt/vol) overnight at room temperature (RT). The retinas were treated with three freeze-thaw cycles and washed in PBS. All further steps are done at RT. The retina was incubated in blocking solution (10% normal donkey serum (vol/vol, Chemicon), 1% bovine serum albumin (wt/vol) and 0.5% Triton X-100 (vol/vol, in PBS, pH 7.4) for 1 h. Primary and secondary antibody applications were done in 3% normal donkey serum, 1% bovine serum albumin, 0.02% sodium acid (wt/vol), and 0.5% Triton X-100 in PBS [84]. Primary antibodies were applied for 3-7 days. After washing the retina three times for 10 minutes in PBS, the retina was incubated in fluorescence-conjugated secondary antibodies and 10 µg/ml of the cell nuclei dye 4', 6-diamidino-2-phenylindole (DAPI, Roche Diagnostics) at a dilution of 1:200 for 2 hrs, followed by three washes in PBS, and mounting on slides with ProLong Gold antifade reagent (Molecular Probes). Retinas for cyrostat section were embedded in Shandon M-1 embedding matrix (Thermo Electron Corporation) and cryosectioned to 25 µm thick slices with Microm HM560 (Leica). Immunohistochemical staining of cryosections were done in Ventana Discovery XT machine with a customized procedure (Ventana Medical Systems, Inc) using different primary antibodies listed below. Retinas for vibratome section were embedded in 3% agarose (wt/vol) (SeaKem Le Agarose, Lonza) in PBS, and 200 µm vertical sections were cut with a Leica VT1000S vibratome. Antibody staining procedure was the same as in whole mounts.

The following primary antibodies were used (in alphabetical order): rabbit anti-Calbindin (1:1000; Swant), mouse anti-Calretinin (1:1000; Chemicon), rat CD45 (1:100; Abcam), goat anti-choline acetyl transferase, ChAT, (1:300; Chemicon), mouse anti C-terminal binding protein 2 (CtBP2, 1:4000; BD Biosciences), rabbit anti-disabled homolog 1 (Dab1, 1:1000; Chemicon), rabbit anti-Gamma-aminobutyric acid (GABA, 1:1000; Sigma), rabbit anti-glutamate decarboxylase 65/67 (GAD65/67, 1:1000; Chemicon), mouse glial fibrillary acidic protein (GFAP,1:200; Sigma), rabbit anti-GFP (1:200; Molecular Probes), sheep anti-GFP (1:200; Biogenesis), rabbit anti-Gy13 (1:200; Margoskec lab), rat anti-Glycine (1:7500; ImmunoSolution), rabbit anti-Opsin blue (1:200, Millipore), rabbit anti-Opsin red/green (1:200; Millipore), lectin peanut agglutin directly coupled to Alexa 568 (1:200; Molecular Probes), goat anti-protein kinase C antibodies (PKC, 1:200; Santa Cruz Biotechnology), mouse anti-protein kinase C antibodies (PKC, 1:200; BD Biosciences) , rabbit anti-RFP (1:200; Chemicon), mouse anti-Thyrosine hydroxylase (Th, 1:200; Chemicon).

For the secondary antibodies, we used in donkey serum raised antibodies either from Invitrogen (Alexa Fluor 405, Alexa Fluor 488, Alexa Fluor 555, Alexa Fluor 633) or from Jackson Laboratory (cy 2, cy3, cy5).

Microscopy

Confocal 3D scans were taken with a Zeiss LSM 510 Meta Axioplan 2 laser scanning confocal microscope using Plan-Apochromat 63X/1.4 or 100X/1.4 oil immersion objective lenses at three excitation laser lines (405 nm for DAPI, 488 nm for GFP and 633 nm for ChAT).

Image and stratification analysis of the GENSAT mice

All original Zeiss 3D scan files ("lsm" format) were deposited without image processing at the GENSAT website. Images were viewed in Imaris (Bitplane). The images shown in this paper were processed in the following ways: All scans were first median filtered either within 3 x 3 x 1 or 3 x 3 x 3 neighbourhoods. Horizontal ONL, INL and GCL sections (**Fig. 4** and **Fig. 8**) were obtained by averaging the image frames corresponding to the different nuclear layers. Vertical sections of **Figure 3b**; **4b**–**c**; **5** (except for *ler5*); **6**; **7**; **8a**–**b**, **h**–**i**; **9**; **10a**–**b**; **12c**, **f**; (**Supplementary Fig. 15**) are optical 30-100 micron thick z-sections from the 3D scans. The rest of the vertical sections are either cryo- or vibratome sections. After obtaining horizontal or vertical projections, the images were exported from Imaris as "tif" files and opened in Adobe Photoshop. Images were next cropped, and if visibility required the contrast was adjusted using the "Curves" command. This later operation was needed in some cases when background "salt and pepper" noise was very high. This background noise was always maximum above the GCL corresponding to the Müller cell end feet and decreased exponentially towards the INL. This noise was only seen in some retinas and probably caused by long (weeks or months) stay in fixative since we could not observe this noise in any of the retinas that were freshly prepared after 30 minutes of fixation. This "salt and pepper" noise could be differentiated from cellular labeling based on feature size and location.

Quantification of stratification was performed in Mathematica (Wolfram Research) by a program written by B.R. (**Supplementary Fig. 15**). The main problem for stratification analysis is the curvature of the mounted retina. This can be corrected using the ChAT strata as reference [18]. The original Zeiss "lsm" scan file with three channels (GFP, DAPI and ChAT) representing the depth in the retina from the ganglion cell side) was imported to Mathematica and stored as a "3 x 512 x 512 x n"

matrix (“3” refers to the GFP, ChAT and DAPI channels, each frame is 512 x 512 pixels, n = 100-200 represents number of frames). This matrix was first trimmed on each side to yield a “3 x 500 x 500 x n” matrix and divided into 10 x 10 pieces (**Supplementary Fig. 15a**) resulting in 100 “3 x 50 x 50 x n” blocks. In each block, each of the three channels was averaged, frame by frame, to yield 100 curves of length “n” for GFP, ChAT and DAPI (**Supplementary Fig. 15b**). First all curves were normalized in amplitude to span a range from zero to one (**Supplementary Fig. 15c**). Next each of the 100 ChAT curves were stretched and shifted to position the two ChAT-peaks at 0 and 100 on the “x” axis. The stretch and shift factors obtained for each ChAT curve were then applied to each of the 100 corresponding GFP and DAPI curves (**Supplementary Fig. 15d**). After this “unbending” procedure the 100 curves of each channel were averaged and yielded the final stratification for GFP labeled processes in the IPL as shown for example on **Figure 3b**. Since all curves were normalized to the ChAT bands, these GFP stratifications could be compared between different mouse lines. A key point in yielding narrow stratification bands was the use of the ChAT peaks for normalization and not the DAPI labeled borders which are locally variable due to protrusion of cell bodies to the IPL. In some cases the “salt and pepper” noise was removed by subtracting a fitted exponential from the GFP curve (*Doc2b* and *Cartpt* of **Fig. 5** and **10**).

Next, each stratification patterns were represented as binary strings for grouping and comparison. The basis for this “digitalization” procedure was shown on **Figure 3a**–**b**. The ChAT, Calretinin, Th and PKC antibodies divide the IPL into nine strata and artificial division of the PKC labeled IPL band into two further strata yields a total of 10 strata. Since the location of the Calretinin, Th and PKC antibody labeled strata are “fixed” compared to the ChAT strata [17] all ten strata can be recovered in each mouse lines with only ChAT labeling. The binary string had 11 entries, the first corresponding to the OPL and the last 10 corresponding to the ten IPL strata. An entry was “1” if a peak of the GFP curve was localized in that stratum and “0” otherwise. For GFP curves that labeled thicker bands the borders were determined and “1” was assigned in strata between the borders. If only or dominantly Müller cells were labeled, we defined the stratification pattern for all strata “0”. The assignment of binary strings to each GFP pattern was not done automatically but assigned by S.S. and B.R. The collection of mouse lines with the same binary string representations was called “Equivalent stratification groups”.

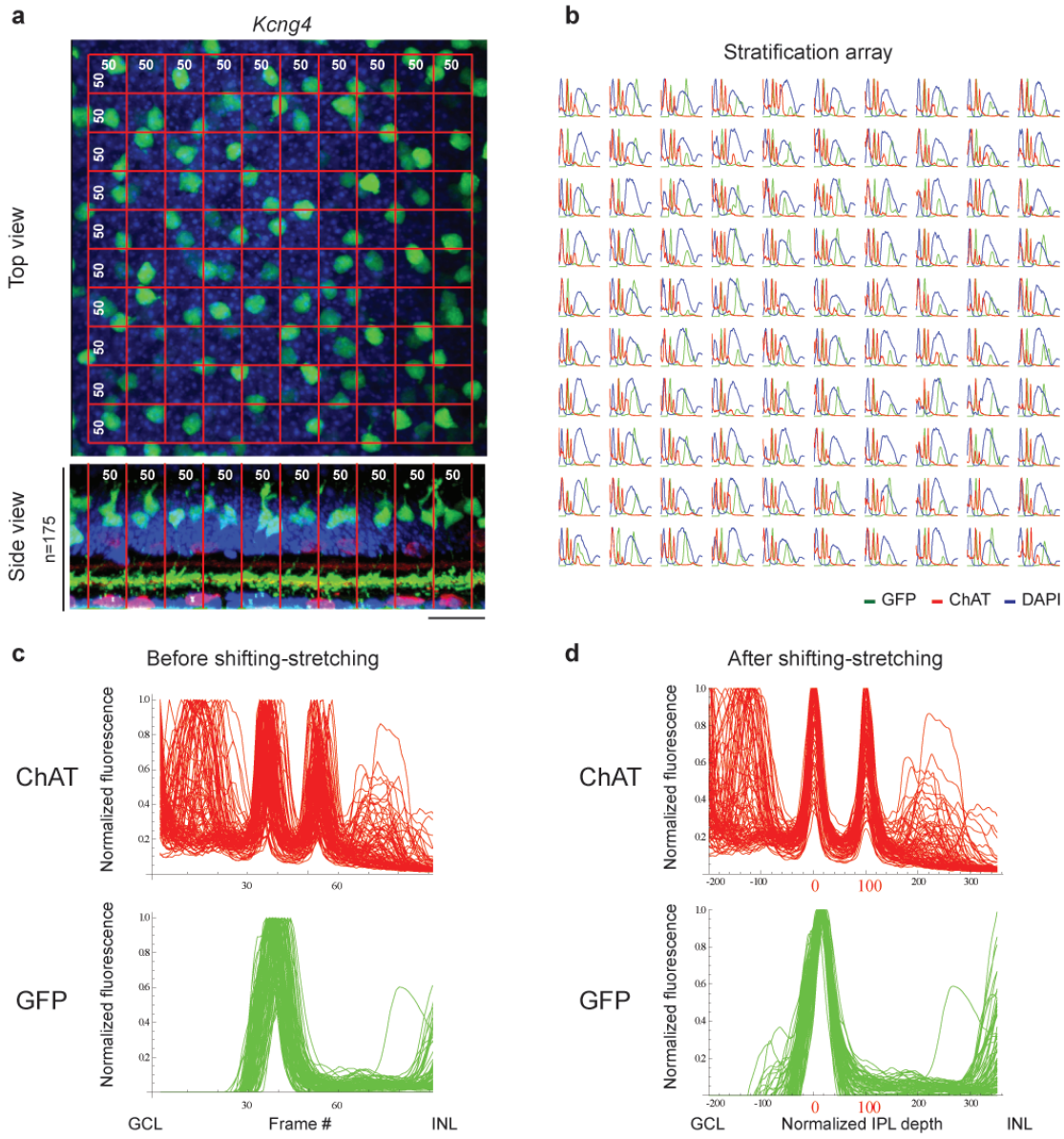

Supplementary Figure 15. Analysis of IPL stratification. **a**, Each 3D scan was divided into 10 x 10 smaller blocks (see Experimental Procedures). Top and side view of a scan from *Kcng4* is shown. "n" refers to the number of frames, each block is 50 x 50 pixel. **b**, Stratification in each block was calculated for GFP (green), ChAT (red) and DAPI (blue) by averaging intensity values in each frame. **c**, Each ChAT curve in b was shifted and stretched to position the location of the two ChAT peaks to 0 and 100 on the "x" axis. **d**, GFP curves were then also shifted and stretched using the shifted and stretched parameters of the ChAT curves. Scale bar, 20 µm.

"Connectivity score": In the inner retina two cells can only be synaptical-connected if they do have dendrites or axon terminals in the same stratum. This simple principle can be used to search for mouse lines ("candidates") in which the GFP labeled inner retinal cell types have the potential to be connected to a cell type of interest ("query"). The search was performed using a connectivity score which ranks the mouse lines

according to the number of commonly labeled strata in the candidate and query mice. We defined connectivity score as the number of commonly labeled strata divided by the number of all distinct strata in the query and candidate retinas. Formally the connectivity score is the dot product of the last 10 digits of the candidate and query binary stratification strings divided by the total number of distinct positions filled with “1” in the candidate and query strings. The first digit, which refers to GFP labeling in the OPL was not used for calculating the connectivity score. For example if the last 10 digits of the candidate string are 0101010000 and of the query string are 0000010000, the dot product is 1. The number of distinct positions with “1’ is 3. The connectivity score is then 1/3. If the connectivity score is 0, the cells labeled in the candidate and query, are not connected. If the connectivity score is 1, the candidate and query cells are either the same or have the same stratification pattern in the IPL.

Two-Photon Imaging and Patch Clamp recordings

The retinas were isolated under dim light in Ringer’s medium (in mM: 110 NaCl, 2.5 KCl, 1 $CaCl_2$, 1.6 $MgCl_2$, 10 D-glucose, 22 $NaHCO_3$, bubbled with 5% CO2/95% O2), mounted ganglion cell side up onto a filter paper (MF-membrane, Millipore) with a 2 x 2 mm hole and superfused with the same Ringer’s medium heated to 35–36°C for the duration of the experiment. For sections, the retina was mounted on a filter paper, ganglion cell side down, and sections were cut with a tissue chopper to a thickness of approx. 200 µm. A tuneable 800-1020 nm laser line from a Mai Tai HP two-photon laser (Spectra Physics) was attenuated by polarization optics and a Pockels cell (Conoptics, Model 302), and was scanned using mirrors (Cambridge Technologies) mounted on a modified Nikon upright microscope. The laser energy at the position of the retina was 5-20 mW. The GFP signal was detected with a Photo Multiplier Tube (Hamamatsu). The retina was stimulated with a DLP projector (V-332, PLUS Vision Corp, Japan) through the lamp port of the microscope. Whole-cell recordings were made using an Axon Multiclamp 700B amplifier (Molecular Devices). Patch electrodes were made from borosilicate glass (BF100-50-10, Sutter Instruments) pulled to 7 – 9 MΩ, and filled with (in mM): for the genetic address book either with: 5 CsCl, 113.7 CsMeSO4, 1 MgSO4, 7.8 x 10–3 CaCl2, 0.1 EGTA, 10 HEPES, 4 ATP-Na2, 0.5 GTP-Na3, 7.75 neurobiotin chloride (pH 7.2) or 7.75 CsCl, 110.3 CsCH3SO3, 1 MgSO4, 7.8 x 10–3 CaCl2, 0.5 BAPTA, 10 HEPES, 4 ATP-Na2, 0.5 GTP-Na3, 5 Qx314, 2.19 Lucifer yellow (pH 7.2). For the “molecular logic of cell types” part, the intracellular solution was: 130 KCl, 8 NaCl, 10 HEPES, 1 CaCl2, 5 EGTA, 4 MgATP; pH was adjusted to 7.3 with (KOH) and Lucifer yellow was added (1 mg/ml)[85]. Data was analyzed offline with Mathematica (Wolfram Research) and

Matlab (Mathworks). Currents were recorded by voltage clamping cells at -60 mV. Voltage was recorded by clamping the cell at 0 mA. All chemicals were obtained from Sigma, with the exception of ATP (Labforce) and neurobiotin (Vector Laboratories).

Dissociation of retina and fluorescence-activated cell sorting (FACS)

Mice were adult (average age: P66, youngest: P39, oldest: P243), animal sexes were randomly chosen. Biological triplicates of one genotype were always done in the morning at the same time and with maximum one hour delay between the first and the last sample. 40 µl Papain (Roche) was activated in 40 µl Cystein/EDTA mix (25 mM Cysteine (Sigma) + 5 mM EDTA (Amresco), pH around 6-7) and 320 µl 4-(2)-Hydroxythy(l)piperazine-1-ethansulfonic acid (HEPES, 100 mM, Fluka) and Hanks' balanced salt solution (HBSS, Sigma) mix for 15 minutes at 37°C. The retina was prepared in HBSS, then immediately added to the activated papain and incubated for 5 minutes at 37°C. For *PV*, the incubation was extended 2 minutes. The solution was spun down for 2.5 minutes at 1,600 rpm and the supernatant removed. 1 ml HBSS/ 2% heat-inactivated fetal calf serum (vol/vol) was added, spun down and the supernatant was removed. Then, 800 µl HBSS/ 2% fetal calf serum was added and gently triturated 10-15 times with a fire-polished Pasteur pipette until retinal tissue dissociated. The solution was filtered through a 70 µm cup filcons (BD) into a 5 ml polypropylene round-bottom Falcon tube (BD).
The sorts were done in MoFlo (Cytomation, Fort Collins, USA) with the bandpass-filter for GFP HQ515/30 and RFP HQ616/26. Gating was done with Summit Software V 4.3.01 Build 2449 after a couple of thousands events were recorded and the population of cell types of interest could be estimated. The first gate was set on the fluorescence population (**Fig. 16 a**-**b**). This gate was then back-gated on the total un-gated events to estimate the size (forward scatter) and the granularity (side scatter) of the fluorescence positive cells. Here, we have set our second gate to exclude cell debris. With the third gate on the pulse-width, we excluded any duplets or clumps. If the cell number was sufficient, we sorted our cells in single cell drop mode that allows us the greatest purity of the sort. For analyzing the number of dead cells, we added propidium iodide (PI, Sigma-Aldrich, 25 µg/ml in PBS) to our cell suspension.

After setting the gates, 200 fluorescence positive cells were sorted at RT into a low-binding tube (Eppendorf) containing 60 µl extraction buffer (TRI reagent, Sigma-Aldrich). The tube was shortly vortexed, quickly spun down, left to lyse at RT and stored at -80C until further processing.

RNA isolation, amplification and microarray profiling

All samples were obtained in biological triplicates per genotype for microarray gene expression profiling. Triplicates were processed separately (to even out the processing bias) in batches of maximum 12 samples (to lessen the extent of RNA degradation). Total RNA from samples containing 200 cells was isolated with the PicoPure RNA isolation kit (Arcturus) with the following modifications. The tubes were incubated at 42°C for 10 minutes and vortexed at low speed. Total RNA was treated with 10 units of DNase I (Qiagen) for 15 minutes to remove any remaining genomic DNA and eluted in 8 µl elution buffer. The RNA quality was assessed using RNA 6000 PicoChips with an Agilent 2100 Bioanalyzer. No traces of DNA were detected; degradation of the ribosomal RNA was absent. The rRNA represented 90–95% of total RNA and a ratio of 28S/18S equal to 1.9–2.2 was recorded indicating that the extractions met the criteria for downstream genetic analysis.

Total RNA from each sample was reverse transcribed using 4 µM T7-$(dT)_{24}$/T7-$(dN)_6$ primer mix (Affymetrix) and 150 units Superscript II reverse transcriptase (Invitrogen) in a volume of 10 µl. Synthesis of second-strand cDNA was performed by adding 4 mM dNTPs, 6 units DNA Polymerase I, and 0.4 units RNase H in a 20 µl reaction volume. cRNA was produced by *in vitro* transcription (IVT) with a T7 RNA polymerase at 37°C for 14 hours using the MEGAscript T7 kit (Ambion) as per manufacturer's instructions. For the second cycle, the first-strand cDNA was synthesized using 0.2 µg random primers from 9 µl of purified cRNA. The second-strand cDNA was produced using 10 µM T7-$(dN)_6$ primer and 40 units DNA polymerase at 16°C for two hours, after which 10 units T4 DNA polymerase (Invitrogen) were added and incubation continued for another 10 minutes. The cDNA was *in vitro* transcribed with a T7 RNA polymerase at 37°C for 16 hours. The single-strand cDNA was synthesized using 10 µg purified cRNA in the presence of 4 µg random primers, 0.2 M DTT, 12 mM dNTP + dUTP and 750 units Superscript II (Roche Diagnostics) in a total volume of 20 µl. The cRNA was hydrolyzed with 2 units RNase H at 37°C for 40 minutes. The sense cDNA was purified and eluted in 28 µl elution buffer. Amplified products were purified using the GeneChip cDNA Sample Cleanup Module (Affymetrix) applying a 6,000g centrifugation speed during the first two steps. To improve the recovery from the columns, water or elution buffer were spun into the matrix at 50g and then left to stand for 4 minutes prior to 16,000g centrifugation. Quantity and purity of the cRNA and cDNA produced during the first and second rounds were evaluated using the NanoDrop ND-1000 spectrophotometer (Nanodrop Technologies).

The cDNA was then fragmented by UDG (uracil DNA glycosylase) and APE 1 (apurinic/apyrimidic endonuclease 1) and biotin-labeled with TdT (terminal deoxynucleotidyl transferase) using the GeneChip WT Terminal labeling kit (Affymetrix). Hybridization was performed using 5 µg of biotinylated target, which was incubated with the GeneChip Gene 1.0 ST array (Affymetrix) at 45°C for 16 hours. Following hybridization, nonspecifically bound nucleotides were removed by washing, and detection of specifically bound target was performed using the GeneChip Hybridization, Wash and Stain kit, and the GeneChip Fluidics Station 450 (Affymetrix). The arrays were scanned using the GeneChip Scanner 3000 7G (Affymetrix) and CEL files acquired using the GeneChip Command Console Software (Affymetrix).

Data analysis

All data analysis was done with self-written scripts in R (version 2.11.1). After obtaining the CEL files for each gene array, all CEL files were normalized using the "rma" function in the bioconductor package "oligo". The resulting text file contained the normalized expression values for 35,556 probes in log2 scale. We removed the probes, where a gene entry had not been annotated yet, and we removed the duplicated annotated genes. The leftover 22,347 genes formed the *Raw Data* containing for each gene the values for the biological triplicate across all mouse lines (14 × 3). For each biological triplicate for a gene, we calculated the median (*Median Data*). The standard fold-change threshold was in all cases: log2 (1.75). One mouse line or a combination of different mouse lines of interest were defined as the selected combination (*sc*). The remaining non-selected mouse lines were defined as the non-selected combination (*n-sc*). All analysis was done comparing *sc* versus *n-sc*.
Removing columns: Due to the fact that the *Pdgfra* and *Chrna3* mouse lines are mixed with rod and cone photoreceptors, respectively, we removed for the cell type-specific analyzes the columns to unmask the specific genes.
Calculating fold-change: For each gene row in the *Median Data*, the minimum expression value of *sc* was subtracted from the maximum expression value of *n-sc*.
Calculating significance: We used the "Wilcoxon Rank Sum and Signed Rank Tests" (*wilcox.test*) function and calculated for each gene the difference between *sc* versus *n-sc* using the *RawData*.
Calculating highest-expressed genes for sc: We used three selection criteria: First, the expression value for *sc* must be higher than for *n-sc*. Second, a high fold-change difference between *sc* and *n-sc*, and third, the significance within the biological

triplicate should be high. Out of 22,347 genes a list of genes was generated for *sc*. We plotted the 25 highest expressed genes (*25-top*) in a heatmap using the function *heatmap.plus* with the colors of the *RColorBrewer* library. The expression values are normalized by subtracting from the *Median Data* the minimum value within the *Median Data* of the *25-top*, divided, by the maximum value within the *Median Data* of the *25-top,* subtracted by the minimum of the *Median Data*. The first 0.125 % of the normalized values were colored in dark. The fold-change and the significance values were color-coded and plotted next to the heatmap.
Hierarchical clustering: The *Median Data* or *Raw Data* were analysed with the *pvclust* function using the *mcquitty* cluster method and the *minkowski* distance measurement.
Calculating noisiness of Data: We summed the standard deviation for each gene that passes the threshold, and divided it by the mean of the gene across all cell types. *Calculating standard deviation* using the *sd* function.

Venn-Diagram: We used from the library (*limma*) the function *vennDiagram*. For all Venn-Diagram analysis, we removed *Pdgfra* that would overlap with the rod_{b2}. Furthermore, the lists for analysis contained only genes that passed in previous analysis the threshold.
Pairwise-Correlation plot: We used the *cor* function to compute the correlation using the Pearson correlation coefficient.

References

1. Masland, R.H. Neuronal cell types. *Curr Biol* **14**, R497-500 (2004).
2. Nelson, S.B., Sugino, K. & Hempel, C.M. The problem of neuronal cell types: a physiological genomics approach. *Trends Neurosci* **29**, 339-345 (2006).
3. Stevens, C.F. Neuronal diversity: too many cell types for comfort? *Curr Biol* **8**, R708-710 (1998).
4. Edlund, T. & Jessell, T.M. Progression from extrinsic to intrinsic signaling in cell fate specification: A view from the nervous system. *Cell* **96**, 211-224 (1999).
5. Livesey, F.J. & Cepko, C.L. Vertebrate neural cell-fate determination: Lessons from the retina. *Nat. Rev. Neurosci.* **2**, 109-118 (2001).
6. Famiglietti, E.V., Jr. 'Starburst' amacrine cells and cholinergic neurons: mirror-symmetric on and off amacrine cells of rabbit retina. *Brain Res* **261**, 138-144 (1983).
7. Gong, S.*, et al.* A gene expression atlas of the central nervous system based on bacterial artificial chromosomes. *Nature* **425**, 917-925 (2003).
8. Kim, D.S., Matsuda, T. & Cepko, C.L. A core paired-type and POU homeodomain-containing transcription factor program drives retinal bipolar cell gene expression. *J Neurosci* **28**, 7748-7764 (2008).
9. Kim, D.S.*, et al.* Identification of molecular markers of bipolar cells in the murine retina. *J Comp Neurol* **507**, 1795-1810 (2008).
10. Masland, R.H. The fundamental plan of the retina. *Nat Neurosci* **4**, 877-886 (2001).
11. Wassle, H. Parallel processing in the mammalian retina. *Nat Rev Neurosci* **5**, 747-757 (2004).
12. Dowling, J. *The Retina: An Approachable Part of the Brain* (Belknap Press, Cambridge, MA, 1987).
13. Roska, B. & Werblin, F. Vertical interactions across ten parallel, stacked representations in the mammalian retina. *Nature* **410**, 583-587 (2001).
14. DeVries, S.H. & Baylor, D.A. An alternative pathway for signal flow from rod photoreceptors to ganglion cells in mammalian retina. *Proc Natl Acad Sci U S A* **92**, 10658-10662 (1995).
15. Soucy, E., Wang, Y., Nirenberg, S., Nathans, J. & Meister, M. A novel signaling pathway from rod photoreceptors to ganglion cells in mammalian retina. *Neuron* **21**, 481-493 (1998).
16. MacNeil, M.A. & Masland, R.H. Extreme diversity among amacrine cells: implications for function. *Neuron* **20**, 971-982 (1998).
17. Haverkamp, S. & Wassle, H. Immunocytochemical analysis of the mouse retina. *J Comp Neurol* **424**, 1-23 (2000).
18. Manookin, M.B., Beaudoin, D.L., Ernst, Z.R., Flagel, L.J. & Demb, J.B. Disinhibition combines with excitation to extend the operating range of the OFF visual pathway in daylight. *J Neurosci* **28**, 4136-4150 (2008).
19. Carter-Dawson, L.D. & LaVail, M.M. Rods and cones in the mouse retina. I. Structural analysis using light and electron microscopy. *J Comp Neurol* **188**, 245-262 (1979).
20. Yoshida, K.*, et al.* A key role of starburst amacrine cells in originating retinal directional selectivity and optokinetic eye movement. *Neuron* **30**, 771-780 (2001).
21. Rice, D.S. & Curran, T. Disabled-1 is expressed in type AII amacrine cells in the mouse retina. *J Comp Neurol* **424**, 327-338 (2000).
22. Balse, E.*, et al.* Glycine receptors in a population of adult mammalian cones. *J Physiol* **571**, 391-401 (2006).
23. Huberman, A.D.*, et al.* Architecture and activity-mediated refinement of axonal projections from a mosaic of genetically identified retinal ganglion cells. *Neuron* **59**, 425-438 (2008).

24. Kim, I.J., Zhang, Y., Yamagata, M., Meister, M. & Sanes, J.R. Molecular identification of a retinal cell type that responds to upward motion. *Nature* **452**, 478-482 (2008).
25. Yonehara, K.*, et al.* Expression of SPIG1 reveals development of a retinal ganglion cell subtype projecting to the medial terminal nucleus in the mouse. *PLoS ONE* **3**, e1533 (2008).
26. Schmidt, T.M., Taniguchi, K. & Kofuji, P. Intrinsic and extrinsic light responses in melanopsin-expressing ganglion cells during mouse development. *J Neurophysiol* **100**, 371-384 (2008).
27. Jeon, C.J., Strettoi, E. & Masland, R.H. The major cell populations of the mouse retina. *J Neurosci* **18**, 8936-8946 (1998).
28. Fried, S.I., Munch, T.A. & Werblin, F.S. Mechanisms and circuitry underlying directional selectivity in the retina. *Nature* **420**, 411-414 (2002).
29. Morgan, J.L., Dhingra, A., Vardi, N. & Wong, R.O. Axons and dendrites originate from neuroepithelial-like processes of retinal bipolar cells. *Nat Neurosci* **9**, 85-92 (2006).
30. Hattar, S., Liao, H.W., Takao, M., Berson, D.M. & Yau, K.W. Melanopsin-containing retinal ganglion cells: architecture, projections, and intrinsic photosensitivity. *Science* **295**, 1065-1070 (2002).
31. McGuire, B.A., Stevens, J.K. & Sterling, P. Microcircuitry of beta ganglion cells in cat retina. *J Neurosci* **6**, 907-918 (1986).
32. Freed, M.A. & Sterling, P. The ON-alpha ganglion cell of the cat retina and its presynaptic cell types. *J Neurosci* **8**, 2303-2320 (1988).
33. Tomomura, M., Rice, D.S., Morgan, J.I. & Yuzaki, M. Purification of Purkinje cells by fluorescence-activated cell sorting from transgenic mice that express green fluorescent protein. *Eur J Neurosci* **14**, 57-63 (2001).
34. Rotolo, T., Smallwood, P.M., Williams, J. & Nathans, J. Genetically-directed, cell type-specific sparse labeling for the analysis of neuronal morphology. *PLoS ONE* **3**, e4099 (2008).
35. Walsh, M.K. & Quigley, H.A. In vivo time-lapse fluorescence imaging of individual retinal ganglion cells in mice. *J Neurosci Methods* **169**, 214-221 (2008).
36. Arlotta, P.*, et al.* Neuronal subtype-specific genes that control corticospinal motor neuron development in vivo. *Neuron* **45**, 207-221 (2005).
37. Trimarchi, J.M.*, et al.* Molecular heterogeneity of developing retinal ganglion and amacrine cells revealed through single cell gene expression profiling. *J Comp Neurol* **502**, 1047-1065 (2007).
38. Bertrand, N., Castro, D.S. & Guillemot, F. Proneural genes and the specification of neural cell types. *Nat. Rev. Neurosci.* **3**, 517-530 (2002).
39. Hirabayashi, Y. & Gotoh, Y. Epigenetic control of neural precursor cell fate during development. *Nat. Rev. Neurosci.* **11**, 377-388 (2010).
40. Esumi, S.*, et al.* Method for single-cell microarray analysis and application to gene-expression profiling of GABAergic neuron progenitors. *Neurosci. Res.* **60**, 439-451 (2008).
41. Levsky, J.M., Shenoy, S.M., Pezo, R.C. & Singer, R.H. Single-cell gene expression profiling. *Science* **297**, 836-840 (2002).
42. Trimarchi, J.M.*, et al.* Molecular heterogeneity of developing retinal ganglion and amacrine cells revealed through single cell gene expression profiling. *J. Comp. Neurol.* **502**, 1047-1065 (2007).
43. Sugino, K.*, et al.* Molecular taxonomy of major neuronal classes in the adult mouse forebrain. *Nat. Neurosci.* **9**, 99-107 (2006).
44. Siegert, S.*, et al.* Genetic address book for retinal cell types. *Nat. Neurosci.* **12**, 1197-U1130 (2009).
45. Brandon, C. & Criswell, M.H. DISPLACED STARBURST AMACRINE CELLS OF THE RABBIT RETINA CONTAIN THE 67-KDA ISOFORM, BUT NOT THE 65-

KDA ISOFORM, OF GLUTAMATE-DECARBOXYLASE. *Visual Neurosci.* **12**, 1053-1061 (1995).
46. Dedek, K.*, et al.* Localization of heterotypic gap junctions composed of connexin45 and connexin36 in the rod pathway of the mouse retina. *Eur. J. Neurosci.* **24**, 1675-1686 (2006).
47. Munch, T.A.*, et al.* Approach sensitivity in the retina processed by a multifunctional neural circuit. *Nat. Neurosci.* **12**, 1308-U1135 (2009).
48. Geisert, E.E.*, et al.* Gene expression in the mouse eye: an online resource for genetics using 103 strains of mice. *Mol. Vis.* **15**, 1730-1763 (2009).
49. Tu, Y., Stolovitzky, G. & Klein, U. Quantitative noise analysis for gene expression microarray experiments. *Proc. Natl. Acad. Sci. U. S. A.* **99**, 14031-14036 (2002).
50. Caputto, B.L. & Guido, M.E. Immediate early gene expression within the visual system: Light and circadian regulation in the retina and the suprachiasmatic nucleus. *Neurochem. Res.* **25**, 153-162 (2000).
51. Larhammar, D., Nordstrom, K. & Larsson, T.A. Evolution of vertebrate rod and cone phototransduction genes. *Philos. Trans. R. Soc. B-Biol. Sci.* **364**, 2867-2880 (2009).
52. Strissel, K.J.*, et al.* Recoverin undergoes light-dependent intracellular translocation in rod photoreceptors. *J. Biol. Chem.* **280**, 29250-29255 (2005).
53. Palczewski, K., Sokal, I. & Baehr, W. Guanylate cyclase-activating proteins: structure, function, and diversity. *Biochem. Biophys. Res. Commun.* **322**, 1123-1130 (2004).
54. Koike, C.*, et al.* TRPM1 is a component of the retinal ON bipolar cell transduction channel in the mGluR6 cascade. *Proc. Natl. Acad. Sci. U. S. A.* **107**, 332-337 (2010).
55. Kim, D.S., Matsuda, T. & Cepko, C.L. A core paired-type and POU homeodomain-containing transcription factor program drives retinal bipolar cell gene expression. *J. Neurosci.* **28**, 7748-7764 (2008).
56. Greferath, U., Grunert, U., Mohler, H. & Wassle, H. CHOLINERGIC AMACRINE CELLS OF THE RAT RETINA EXPRESS THE DELTA-SUBUNIT OF THE GABA(A)-RECEPTOR. *Neurosci. Lett.* **163**, 71-73 (1993).
57. Arvidsson, U., Riedl, M., Elde, R. & Meister, B. Vesicular acetylcholine transporter (VAChT) protein: A novel and unique marker for cholinergic neurons in the central and peripheral nervous systems. *J. Comp. Neurol.* **378**, 454-467 (1997).
58. Song, J.H., Song, H., Wensel, T.G., Sokolov, M. & Martemyanov, K.A. Localization and differential interaction of R7 RGS proteins with their membrane anchors R7BP and R9AP in neurons of vertebrate retina. *Mol. Cell. Neurosci.* **35**, 311-319 (2007).
59. Geyer, J.*, et al.* Cloning and molecular characterization of the orphan carrier protein Slc10a4: Expression in cholinergic neurons of the rat central nervous system. *Neuroscience* **152**, 990-1005 (2008).
60. Lucas, E.K.*, et al.* Parvalbumin Deficiency and GABAergic Dysfunction in Mice Lacking PGC-1 alpha. *J. Neurosci.* **30**, 7227-7235 (2010).
61. Kim, J.W. & Lemke, G. Hedgehog-regulated localization of Vax2 controls eye development. *Genes Dev.* **20**, 2833-2847 (2006).
62. Yamada, R., Mizutani-Koseki, Y., Koseki, H. & Takahashi, N. Requirement for Mab2112 during development of murine retina and ventral body wall. *Dev. Biol.* **274**, 295-307 (2004).
63. Inoue, T.*, et al.* Math3 and NeuroD regulate amacrine cell fate specification in the retina. *Development* **129**, 831-842 (2002).
64. Erlander, M.G., Tillakaratne, N.J.K., Feldblum, S., Patel, N. & Tobin, A.J. 2 GENES ENCODE DISTINCT GLUTAMATE DECARBOXYLASES. *Neuron* **7**, 91-100 (1991).

65. Morgans, C.W. Neurotransmitter release at ribbon synapses in the retina. *Immunol. Cell Biol.* **78**, 442-446 (2000).
66. Wycisk, K.A.*, et al.* Structural and functional abnormalities of retinal ribbon synapses due to Cacna2d4 mutation. *Invest. Ophthalmol. Vis. Sci.* **47**, 3523-3530 (2006).
67. Sherry, D.M., Wang, M.M., Bates, J. & Frishman, L.J. Expression of vesicular glutamate transporter 1 in the mouse retina reveals temporal ordering in development of rod vs. cone and ON vs. OFF circuits. *J. Comp. Neurol.* **465**, 480-498 (2003).
68. Nishida, A.*, et al.* Otx2 homeobox gene controls retinal photoreceptor cell fate and pineal gland development. *Nat. Neurosci.* **6**, 1255-1263 (2003).
69. Koike, C.*, et al.* Functional roles of Otx2 transcription factor in postnatal mouse retinal development. *Mol. Cell. Biol.* **27**, 8318-8329 (2007).
70. Ashery-Padan, R. & Gruss, P. Pax6 lights-up the way for eye development. *Curr. Opin. Cell Biol.* **13**, 706-714 (2001).
71. Reichman, S.*, et al.* The homeobox gene CHX10/VSX2 regulates RdCVF promoter activity in the inner retina. *Hum. Mol. Genet.* **19**, 250-261 (2010).
72. Furukawa, T., Kozak, C.A. & Cepko, C.L. rax, a novel paired-type homeobox gene, shows expression in the anterior neural fold and developing retina. *Proc. Natl. Acad. Sci. U. S. A.* **94**, 3088-3093 (1997).
73. Nelson, S.B., Sugino, K. & Hempel, C.M. The problem of neuronal cell types: a physiological genomics approach. *Trends Neurosci.* **29**, 339-345 (2006).
74. Imai, H.*, et al.* Molecular properties of rhodopsin and rod function. *J. Biol. Chem.* **282**, 6677-6684 (2007).
75. Chen, J.C., Rattner, A. & Nathans, J. The rod photoreceptor-specific nuclear receptor Nr2e3 represses transcription of multiple cone-specific genes. *J. Neurosci.* **25**, 118-129 (2005).
76. Cepko, C.L., Austin, C.P., Yang, X.J. & Alexiades, M. Cell fate determination in the vertebrate retina. *Proc. Natl. Acad. Sci. U. S. A.* **93**, 589-595 (1996).
77. Turner, D.L., Snyder, E.Y. & Cepko, C.L. LINEAGE-INDEPENDENT DETERMINATION OF CELL TYPE IN THE EMBRYONIC MOUSE RETINA. *Neuron* **4**, 833-845 (1990).
78. Swaroop, A., Kim, D. & Forrest, D. Transcriptional regulation of photoreceptor development and homeostasis in the mammalian retina. *Nat. Rev. Neurosci.* **11**, 563-576 (2010).
79. Weiss, J.*, et al.* Glycinergic input of small-field amacrine cells in the retinas of wildtype and glycine receptor deficient mice. *Mol. Cell. Neurosci.* **37**, 40-55 (2008).
80. Buck, L.B. The molecular architecture of odor and pheromone sensing in mammals. *Cell* **100**, 611-618 (2000).
81. Le, Y.Z.*, et al.* Mouse opsin promoter-directed Cre recombinase expression in transgenic mice. *Mol. Vis.* **12**, 389-398 (2006).
82. Le, Y.Z.*, et al.* Targeted expression of Cre recombinase to cone photoreceptors in transgenic mice. *Mol. Vis.* **10**, 1011-1018 (2004).
83. Luche, H., Weber, O., Rao, T.N., Blum, C. & Fehling, H.J. Faithful activation of an extra-bright red fluorescent protein in "knock-in" Cre-reporter mice ideally suited for lineage tracing studies. *European Journal of Immunology* **37**, 43-53 (2007).
84. Lagali, P.S.*, et al.* Light-activated channels targeted to ON bipolar cells restore visual function in retinal degeneration. *Nat Neurosci* **11**, 667-675 (2008).
85. Oltedal, L., Morkve, S.H., Veruki, M.L. & Hartveit, E. Patch-clamp investigations and compartmental modeling of rod bipolar axon terminals in an in vitro thin-slice preparation of the mammalian retina. *J. Neurophysiol.* **97**, 1171-1187 (2007).
86. Bhattacharya, S., Das, A., Mallya, K. & Ahmad, I. Maintenance of retinal stem cells by Abcg2 is regulated by notch signaling. *J. Cell Sci.* **120**, 2652-2662 (2007).

87. Zhao, S.H.*, et al.* Annexin A2 promotes choroidal neovascularization by increasing vascular endothelial growth factor expression in a rat model of argon laser coagulation-induced choroidal neovascularization. *Chin. Med. J.* **123**, 713-721 (2010).
88. Haire, S.E.*, et al.* Light-driven cone arrestin translocation in cones of postnatal guanylate cyclase-1 knockout mouse retina treated with AAV-GC1. *Invest. Ophthalmol. Vis. Sci.* **47**, 3745-3753 (2006).
89. Baudet, M.L.*, et al.* Growth hormone action in the developing neural retina: A proteomic analysis. *Proteomics* **8**, 389-401 (2008).
90. Bernstein, S.L., Koo, J.H., Slater, B.J., Guo, Y. & Margolis, F.L. Analysis of optic nerve stroke by retinal Bex expression. *Mol. Vis.* **12**, 147-155 (2006).
91. Haeseleer, F.*, et al.* Essential role of Ca2+-binding protein 4, a Ca(v)1.4 channel regulator, in photoreceptor synaptic function. *Nat. Neurosci.* **7**, 1079-1087 (2004).
92. Raven, M.A.*, et al.* Early afferent signaling in the outer plexiform layer regulates development of horizontal cell morphology. *J. Comp. Neurol.* **506**, 745-758 (2008).
93. Nakajima, Y., Moriyama, M., Hattori, M., Minato, N. & Nakanishi, S. Isolation of ON Bipolar Cell Genes via hrGFP-coupled Cell Enrichment Using the mGluR6 Promoter. *J. Biochem.* **145**, 811-818 (2009).
94. Couceyro, P.R., Koylu, E.O. & Kuhar, M.J. Further studies on the anatomical distribution of CART by in situ hybridization. *J. Chem. Neuroanat.* **12**, 229-241 (1997).
95. Francis, N. & Deneris, E.S. Retinal neuron activity of ETS domain-binding sites in a nicotinic acetylcholine receptor gene cluster enhancer. *J. Biol. Chem.* **277**, 6511-6519 (2002).
96. Moretti, M.*, et al.* Nicotinic acetylcholine receptor subtypes expression during rat retina development and their regulation by visual experience. *Mol. Pharmacol.* **66**, 85-96 (2004).
97. Geller, S.F.*, et al.* CLRN1 Is Nonessential in the Mouse Retina but Is Required for Cochlear Hair Cell Development. *PLoS Genet.* **5**, 18 (2009).
98. Kohl, S.*, et al.* Mutations in the CNGB3 gene encoding the beta-subunit of the cone photoreceptor cGMP-gated channel are responsible for achromatopsia (ACHM3) linked to chromosome 8q21. *Hum. Mol. Genet.* **9**, 2107-2116 (2000).
99. Pittler, S.J.*, et al.* Functional analysis of the rod photoreceptor cGMP phosphodiesterase alpha-subunit gene promoter - Nrl and Crx are required for full transcriptional activity. *J. Biol. Chem.* **279**, 19800-19807 (2004).
100. Blackburn, J., Tarttelin, E.E., Gregory-Evans, C.Y., Moosajee, M. & Gregory-Evans, K. Transcriptional regulation and expression of the dominant drusen gene FBLN3 (EFEMP1) in mammalian retina. *Invest. Ophthalmol. Vis. Sci.* **44**, 4613-4621 (2003).
101. Ekstrom, P. & Johansson, K. Differentiation of ganglion cells and amacrine cells in the rat retina: correlation with expression of HuC/D and GAP-43 proteins. *Dev. Brain Res.* **145**, 1-8 (2003).
102. Liu, R.Z.*, et al.* The fabp4 gene of zebrafish (Danio rerio) - genomic homology with the mammalian FABP4 and divergence from the zebrafish fabp3 in developmental expression. *Febs J.* **274**, 1621-1633 (2007).
103. Heglind, M.*, et al.* Lack of the central nervous system- and neural crest-expressed forkhead gene Foxs1 affects motor function and body weight. *Mol. Cell. Biol.* **25**, 5616-5625 (2005).
104. Self, J.*, et al.* Frmd7 expression in developing mouse brain. *Eye* **24**, 165-169 (2010).
105. Trifunovic, D.*, et al.* A high-resolution RNA expression atlas of retinitis pigmentosa genes in human and mouse retinas. *Invest. Ophthalmol. Vis. Sci.* **49**, 2330-2336 (2008).

106. Enz, R., Brandstatter, J.H., Wassle, H. & Bormann, J. Immunocytochemical localization of the GABA(c) receptor rho subunits in the mammalian retina. *J. Neurosci.* **16**, 4479-4490 (1996).
107. Corbo, J.C. & Cepko, C.L. A hybrid photoreceptor expressing both rod and cone genes in a mouse model of enhanced S-cone syndrome. *PLoS Genet.* **1**, 140-153 (2005).
108. Jomary, C.*, et al.* Expression patterns of neurturin and its receptor components in developing and degenerative mouse retina. *Invest. Ophthalmol. Vis. Sci.* **40**, 568-574 (1999).
109. Huang, L.Q.*, et al.* G protein subunit G gamma 13 is coexpressed with G alpha o, G beta 3, and G beta 4 in retinal ON bipolar cells. *J. Comp. Neurol.* **455**, 1-10 (2003).
110. Deng, W.T.*, et al.* Functional interchangeability of rod and cone transducin alpha-subunits. *Proc. Natl. Acad. Sci. U. S. A.* **106**, 17681-17686 (2009).
111. Rao, A., Dallman, R., Henderson, S. & Chen, C.K. G beta 5 is required for normal light responses and morphology of retinal ON-bipolar cells. *J. Neurosci.* **27**, 14199-14204 (2007).
112. McKillop, J.M.*, et al.* GASTRIN-RELEASING PEPTIDE (GRP) IMMUNOREACTIVITY IN THE RAT RETINA - A RADIOIMMUNOASSAY, IMMUNOHISTOCHEMICAL AND CHROMATOGRAPHIC STUDY. *Brain Res.* **447**, 239-245 (1988).
113. Nakazawa, T.*, et al.* Retinal G-substrate, potential downstream component of NO/cGMP/PKG pathway, is located in subtype of retinal ganglion cells and amacrine cells with protein phosphatases. *Mol. Brain Res.* **135**, 58-68 (2005).
114. Schoen, T.J.*, et al.* DIFFERENTIAL TEMPORAL AND SPATIAL EXPRESSION OF INSULIN-LIKE GROWTH-FACTOR BINDING PROTEIN-2 IN DEVELOPING CHICK OCULAR-TISSUES. *Invest. Ophthalmol. Vis. Sci.* **36**, 2652-2662 (1995).
115. Burren, C.P., Berka, J.L., Edmondson, S.R., Werther, G.A. & Batch, J.A. Localization of mRNAs for insulin-like growth factor-I (IGF-I), IGF-I receptor, and IGF binding proteins in rat eye. *Invest. Ophthalmol. Vis. Sci.* **37**, 1459-1468 (1996).
116. Chien, C.L. & Liem, R.K.H. The neuronal intermediate filament, alpha-internexin is transiently expressed in amacrine cells in the developing mouse retina. *Exp. Eye Res.* **61**, 749-756 (1995).
117. Polvani, S.*, et al.* Developmentally regulated expression of the mouse homologues of the potassium channel encoding genes m-erg1, m-erg2 and m-erg3. *Gene Expr. Patterns* **3**, 767-776 (2003).
118. Xiong, H., Xia, K., Li, B.S., Zhao, G.P. & Zhang, Z.H. KChIP1: a potential modulator to GABAergic system. *Acta Biochim. Biophys. Sin.* **41**, 295-300 (2009).
119. Song, X., Gurevich, E.V. & Gurevich, V.V. Cone arrestin binding to JNK3 and Mdm2: conformational preference and localization of interaction sites. *J. Neurochem.* **103**, 1053-1062 (2007).
120. Wu, M., Chen, D.F., Sasaoka, T. & Tonegawa, S. Neural tube defects and abnormal brain development in F52-deficient mice. *Proc. Natl. Acad. Sci. U. S. A.* **93**, 2110-2115 (1996).
121. Jung, B.P.*, et al.* Differential expression of methyl CpG-binding domain containing factor MBD3 in the developing and adult rat brain. *J. Neurobiol.* **55**, 220-232 (2003).
122. Hidaka, H. & Okazaki, K. NEUROCALCIN FAMILY - A NOVEL CALCIUM-BINDING PROTEIN ABUNDANT IN BOVINE CENTRAL-NERVOUS-SYSTEM. *Neurosci. Res.* **16**, 73-77 (1993).
123. Kim, C., Kuehn, M., Clark, A. & Kwon, Y. Gene expression profile of the adult human retinal ganglion cell layer. *Mol. Vis.* **12**, 1640-1648 (2006).

124. Hutsler, J.J. & Chalupa, L.M. DEVELOPMENT OF NEUROPEPTIDE-Y IMMUNOREACTIVE AMACRINE AND GANGLION-CELLS IN THE PRENATAL AND POSTNATAL CAT RETINA. *J. Comp. Neurol.* **361**, 152-164 (1995).
125. Inoue, M., Iida, A., Satoh, S., Kodama, T. & Watanabe, S. COUP-TFI and -TFII nuclear receptors are expressed in amacrine cells and play roles in regulating the differentiation of retinal progenitor cells. *Exp. Eye Res.* **90**, 49-56 (2010).
126. Ivanov, D., Dvoriantchikova, G., Nathanson, L., McKinnon, S.J. & Shestopalov, V.I. Microarray analysis of gene expression in adult retinal ganglion cells. *FEBS Lett.* **580**, 331-335 (2006).
127. Fujino, T., Wu, Z., Lin, W.C., Phillips, M.A. & Nedivi, E. cpg15 and cpg15-2 constitute a family of activity-regulated ligands expressed differentially in the nervous system to promote neurite growth and neuronal survival. *J. Comp. Neurol.* **507**, 1831-1845 (2008).
128. Chalmel, F.*, et al.* Rod-derived Cone Viability Factor-2 is a novel bifunctional-thioredoxin-like protein with therapeutic potential. *BMC Mol. Biol.* **8**, 12 (2007).
129. Nikonov, S.S., Kholodenko, R., Lem, J. & Pugh, E.N. Physiological features of the S- and M-cone photoreceptors of wild-type mice from single-cell recordings. *J. Gen. Physiol.* **127**, 359-374 (2006).
130. Applebury, M.L.*, et al.* Transient expression of thyroid hormone nuclear receptor TR beta 2 sets S opsin patterning during cone photoreceptor genesis. *Dev. Dyn.* **236**, 1203-1212 (2007).
131. Brandle, U., Guenther, E., Irrle, C. & Wheeler-Schilling, T.H. Gene expression of the P2X receptors in the rat retina. *Mol. Brain Res.* **59**, 269-272 (1998).
132. Schippert, R., Schaeffel, F. & Feldkaemper, M.P. Microarray analysis of retinal gene expression in Egr-1 knockout mice. *Mol. Vis.* **15**, 2720-2739 (2009).
133. Xu, Y.*, et al.* Retinal ON bipolar cells express a new PCP2 splice variant that accelerates the light response. *J. Neurosci.* **28**, 8873-8884 (2008).
134. Chang, B.*, et al.* A homologous genetic basis of the murine cpfl1 mutant and human achromatopsia linked to mutations in the PDE6C gene. *Proc. Natl. Acad. Sci. U. S. A.* **106**, 19581-19586 (2009).
135. Tsang, S.H.*, et al.* Removal of phosphorylation sites of gamma subunit of phosphodiesterase 6 alters rod light response. *J. Physiol.-London* **579**, 303-312 (2007).
136. Janisch, K.M.*, et al.* Light-dependent phosphorylation of the gamma subunit of cGMP-phophodiesterase (PDE6 gamma) at residue threonine 22 in intact photoreceptor neurons. *Biochem. Biophys. Res. Commun.* **390**, 1149-1153 (2009).
137. Hentges, S.T.*, et al.* GABA release from proopiomelanocortin neurons. *J. Neurosci.* **24**, 1578-1583 (2004).
138. Quina, L.A.*, et al.* Brn3a-expressing retinal ganglion cells project specifically to thalamocortical and collicular visual pathways. *J. Neurosci.* **25**, 11595-11604 (2005).
139. Snellman, J. & Nawy, S. Regulation of the retinal bipolar cell mGluR6 pathway by calcineurin. *J. Neurophysiol.* **88**, 1088-1096 (2002).
140. Roger, J.*, et al.* Involvement of Pleiotrophin in CNTF-mediated differentiation of the late retinal progenitor cells. *Dev. Biol.* **298**, 527-539 (2006).
141. Cueva, J.G.*, et al.* Vesicular gamma-aminobutyric acid transporter expression in amacrine and horizontal cells. *J. Comp. Neurol.* **445**, 227-237 (2002).
142. Parker, R.O., Fan, J., Nickerson, J.M., Liou, G.I. & Crouch, R.K. Normal Cone Function Requires the Interphotoreceptor Retinoid Binding Protein. *J. Neurosci.* **29**, 4616-4621 (2009).
143. Friedman, J.S.*, et al.* Premature truncation of a novel protein, RD3, exhibiting subnuclear localization is associated with retinal degeneration. *Am. J. Hum. Genet.* **79**, 1059-1070 (2006).
144. Chrispell, J.D.*, et al.* Rdh12 Activity and Effects on Retinoid Processing in the Murine Retina. *J. Biol. Chem.* **284**, 21468-21477 (2009).

145. Sato, H., Tomita, H., Nakazawa, T., Wakana, S. & Tamai, M. Deleted in polyposis 1-like 1 gene (Dp1l1): A novel gene richly expressed in retinal ganglion cells. *Invest. Ophthalmol. Vis. Sci.* **46**, 791-796 (2005).
146. Farkas, R.H., Qian, J., Goldberg, J.L., Quigley, H.A. & Zack, D.J. Gene expression profiling of purified rat retinal ganglion cells. *Invest. Ophthalmol. Vis. Sci.* **45**, 2503-2513 (2004).
147. Inoue-Mochita, M., Inoue, T., Epstein, D.L., Blumer, K.J. & Rao, P.V. RGS2-deficient mice exhibit decreased intraocular pressure and increased retinal ganglion cell survival. *Mol. Vis.* **15**, 495-504 (2009).
148. Lee, C.H.J., Della, N.G., Chew, C.E. & Zack, D.J. Rin, a neuron-specific and calmodulin-binding small G-protein, and Rit define a novel subfamily of Ras proteins. *J. Neurosci.* **16**, 6784-6794 (1996).
149. Clarke, G.*, et al.* Rom-1 is required for rod photoreceptor viability and the regulation of disk morphogenesis. *Nature Genet.* **25**, 67-73 (2000).
150. Yamashita, T.*, et al.* Essential and Synergistic Roles of RP1 and RP1L1 in Rod Photoreceptor Axoneme and Retinitis Pigmentosa. *J. Neurosci.* **29**, 9748-9760 (2009).
151. Won, J.Y.*, et al.* RPGRIP1 is essential for normal rod photoreceptor outer segment elaboration and morphogenesis. *Hum. Mol. Genet.* **18**, 4329-4339 (2009).
152. Wistow, G.*, et al.* Expressed sequence tag analysis of human retina for the NEIBank Project: Retbindin, an abundant, novel retinal cDNA and alternative splicing of other retina-preferred gene transcripts. *Mol. Vis.* **8**, 196-204 (2002).
153. Codega, P.*, et al.* Prolonged illumination up-regulates arrestin and two guanylate cyclase activating proteins: a novel mechanism for light adaptation. *J. Physiol.-London* **587**, 2457-2472 (2009).
154. Katoh, K.*, et al.* Blimp1 Suppresses Chx10 Expression in Differentiating Retinal Photoreceptor Precursors to Ensure Proper Photoreceptor Development. *J. Neurosci.* **30**, 6515-6526 (2010).
155. Wassle, H., Regus-Leidig, H. & Haverkamp, S. Expression of the vesicular glutamate transporter vGluT2 in a subset of cones of the mouse retina. *J. Comp. Neurol.* **496**, 544-555 (2006).
156. Gu, S.M., Roderick, H.L., Camacho, P. & Jiang, J.X. Characterization of an N-system amino acid transporter expressed in retina and its involvement in glutamine transport. *J. Biol. Chem.* **276**, 24137-24144 (2001).
157. Lee, E.J.*, et al.* AII amacrine cells in the distal inner nuclear layer of the mouse retina. *J. Comp. Neurol.* **494**, 651-662 (2006).
158. Aruga, J. Slitrk6 expression profile in the mouse embryo and its relationship to that of Nlrr3. *Gene Expr. Patterns* **3**, 727-733 (2003).
159. Soto, I.*, et al.* Retinal ganglion cells downregulate gene expression and lose their Axons within the optic nerve head in a mouse glaucoma model. *J. Neurosci.* **28**, 548-561 (2008).
160. Lin, Y.P., Ouchi, Y., Satoh, S. & Watanabe, S. Sox2 Plays a Role in the Induction of Amacrine and Muller Glial Cells in Mouse Retinal Progenitor Cells. *Invest. Ophthalmol. Vis. Sci.* **50**, 68-74 (2009).
161. Dietz, J.A.*, et al.* RgcsI, a dominant QTL that affects retinal ganglion cell death after optic nerve crush in mice. *BMC Neurosci.* **9**, 11 (2008).
162. Dal Monte, M., Petrucci, C., Cozzi, A., Allen, J.P. & Bagnoli, P. Somatostatin inhibits potassium-evoked glutamate release by activation of the sst(2) somatostatin receptor in the mouse retina. *Naunyn-Schmiedebergs Arch. Pharmacol.* **367**, 188-192 (2003).
163. Jansen, A., Hoepfner, M., Herzig, K.H., Riecken, E.O. & Scherubl, H. GABA(C) receptors in neuroendocrine gut cells: a new GABA-binding site in the gut. *Pflugers Arch.* **441**, 294-300 (2000).
164. Reh, T.A. & Levine, E.M. Multipotential stem cells and progenitors in the vertebrate retina. *J. Neurobiol.* **36**, 206-220 (1998).

165. Xi, Q.S., Pauer, G.J.T., Marmorstein, A.D., Crabb, J.W. & Hagstrom, S.A. Tubby-like protein 1 (TULP1) interacts with F-actin in photoreceptor cells. *Invest. Ophthalmol. Vis. Sci.* **46**, 4754-4761 (2005).
166. Haeseleer, F. Interaction and colocalization of CaBP4 and Unc119 (MRG4) in photoreceptors. *Invest. Ophthalmol. Vis. Sci.* **49**, 2366-2375 (2008).
167. Casini, G. & Brecha, N.C. VASOACTIVE INTESTINAL POLYPEPTIDE-CONTAINING CELLS IN THE RABBIT RETINA - IMMUNOHISTOCHEMICAL LOCALIZATION AND QUANTITATIVE-ANALYSIS. *J. Comp. Neurol.* **305**, 313-327 (1991).
168. Anderson, D.H., Johnson, L.V. & Hageman, G.S. VITRONECTIN RECEPTOR EXPRESSION AND DISTRIBUTION AT THE PHOTORECEPTOR-RETINAL PIGMENT EPITHELIAL INTERFACE. *J. Comp. Neurol.* **360**, 1-16 (1995).
169. Stohr, H.*, et al.* Cloning and characterization of WDR17, a novel WD repeat-containing gene on chromosome 4q34. *Biochim. Biophys. Acta-Gene Struct. Expression* **1579**, 18-25 (2002).
170. Horng, S.*, et al.* Differential Gene Expression in the Developing Lateral Geniculate Nucleus and Medial Geniculate Nucleus Reveals Novel Roles for Zic4 and Foxp2 in Visual and Auditory Pathway Development. *J. Neurosci.* **29**, 13672-13683 (2009).

References for individual genes

Gene	Reference	Gene	Reference
Abcg2	86	Fabp4	102
Anxa2	87	Foxs1	103
Arr3	88	Frmd7	104
Basp1	89	Fscn2	105
Bex1	90	Gabrd	56
Bex2	90	Gabrr1	106
Cabp1	91	Gabrr2	106
Cabp5	55	Gad1	64
Cacna1f	92	Gckr	107
Cacna2d3	93	Gfra2	108
Cacna2d4	66	Gjc1	46
Cartpt	94	Gnao1	109
Chrna3	95	Gnat2	110
Chrna6	96	Gnb1	51
Clrn1	97	Gnb5	111
Cnga1	51	Gng13	109
Cngb3	98	Grp	112
Crx	99	Gsbs	113
Efemp1	100	Guca1a	53
Elavl3	101	Igfbp2	114

Gene	Reference	Gene	Reference
Igfbp6	115	Rd3	143
Ina	116	Rdh12	144
Kcnh7	117	Reep6	145
Kcnip1	118	Resp18	146
Mab21l1	62	Rgs2	147
Mapk10	119	Rgs6	58
Marcksl	120	Rit2	148
Mbd3	121	Rom1	149
Ncald	122	Rp1h	150
Nefl	123	Rpgrip1	151
Neurod1	63	Rtbdn	152
Npy	124	Sag	153
Nr2e3	75	Scgn	154
Nr2f2	125	Slc10a4	59, 155
Nrn1	126	Slc17a6	155
Nrn1l	127	Slc17a7	155
Nxnl1	71	Slc18a3	57
Nxnl2	128	Slc32a1	141
Opn1mw	129	Slc38a1	156
Opn1sw	130	Slc6a9	157
Otx2	68, 69	Slitrk6	158
P2rx2	131	Sncg	159
Pax6	70	Sox2	160
Pcdhb9	132	Sparcl1	161
Pcp2	133	Sstr2	162
Pde6a	51	Stc1	163
Pde6b	51	Tcfap2b	37
Pde6c	134	Tgfb3	164
Pde6g	135	Trpm1	54
Pde6h	136	Tulp1	165
Pomc	137	Unc119	166
Pou4f1	138	Vax2	61
Ppargc1a	60	Vip	167
Ppp3ca	139	Vsx2	71
Prkca	17	Vtn	168
Ptn	140	Wdr17	169
Pvalb	141	Zic4	170
Rbp3	142		
Rcvrn	52		

Statement

For this work, I got following support:

Mice were produced at Rockefeller University by Nathaniel Heintz and Karina Del Punta. The web-based retina database was developed by Nick Didkovsky. Brigitte Gross Scherf helped in preparing the retina, doing the immunostaining and taking microscopy pictures. Botond Roska wrote the software for the stratification-depth analysis.

In the part of “Molecular logic of retinal cell types”, I got support by Hubertus Kohler for FACS. RNA amplification and hybridization on gene arrays were done by Erik Cabuy. The script for normalizing the gene arrays and to show the Pairwise-Correlation Plot was written by Michael B. Stadler. David Balya supported me in the first-phase of writing the R-scripts.

Sandra Siegert

Friedrich Miescher Institute for Biomedical Research
Maulbeerstrasse 66, 4058 Basel, Switzerland

• Phone: +41 61 69 78681 • E-Mail: sandra.siegert@fmi.ch

Education

07/2005 - present **Friedrich Miescher Institute for Biomedical Research**,
Basel, Switzerland
Ph.D. candidate, Division of Neuroscience, Neural Circuits Laboratories

10/2000 – 05/2005 **Johann Wolfgang Goethe-University**,
Frankfurt/Main, Germany
Studies in Biology,
main courses in neuroscience, biochemistry and microbiology
Diplom Biologin

Research Experience

07/2005 - present *Ph.D. candidate*, Laboratory of Botond Roska, MD, Ph.D.,
Friedrich Miescher Institute for Biomedical Research,
Basel, Switzerland
PhD thesis:
Molecular logic of cell types in the Mammalian retina

07/2004 – 05/2005 *Undergraduate,* Laboratory of PD Dr. Barbara Schnierle,
Georg-Speyer-Haus, Frankfurt/Main, Germany
Paul-Ehrlich Institute, Federal Agency for Sera and Vaccines,
Langen, Germany
Diploma thesis:
"Induction of an immune-response against HIV by
MLV/HIV pseudo-typed particles"

09/2003 – 01/2004 *Summer student*, Laboratory of PD Dr. Jörg Simon,
Johann Wolfgang Goethe-University, Frankfurt/Main,
Germany, Institute of Molecular Bio Sciences

Involved during the early stages of the publication by
Hartshorne RS *et al.*,
Molecular Microbiology (2007) 64(4), 1049-1060

Publications

2010 Busskamp V, Duebel J, Balya D, Fradot M, Viney TJ, **Siegert S**, Groner AC, Cabuy E, Forster V, Seeliger M, Biel M, Humphries P, Paques M, Mohand-Said S, Trono D, Deisseroth K, Sahel JA, Picaud S, Roska B
"Genetic reactivation of cone photoreceptors restores complex visual responses in *Retinitis pigmentosa*",
Science 2010 Jun; 329(5990): 413-7

2009 **Siegert S**, Gross Scherf B, Del Punta K, Didkovsky N, Heintz N, Roska B
"Genetic address book for retinal cell types"
Nat Neurosci. 2009 Sep; 12(9): 1197-204

2009 Münch TA, da Silveira RA, **Siegert S**, Viney TJ, Awatramani GB, Roska B
"Approach sensitivity in the retina processed by a multifunctional neuronal circuit"
Nat Neurosci. 2009 Oct; 12(10): 1308-16

2007 Viney TJ, Balint K, Hillier D, **Siegert S**, Boldogkoi Z, Enquist LW, Meister M, Cepko CL Roska B
"Local retinal circuits of melanopsin-containing ganglion cells identified by transsynaptic viral tracing"
Curr Biol. 2007 Jun 5; 17(11): 981-8

2006 **Siegert S**, Schnierle P, Schnierle BS
"Novel anti-viral therapy: Drugs that blocks HIV entry at different target sites"
Mini Rev Med Chem. 2006 May; 6(5): 557-62. Review

2005 **Siegert S**, Thaler S, Wagner R, Schnierle BS
"Assessment of HIV-1 entry inhibitors by MLV/HIV-1 pseudotyped vectors"
AIDS Res Ther. 2005 Sep 12, 2:7

Conferences and Meetings

10/2009 **Siegert S**, Balya D, Gross Scherf B, Cabuy E, Stadler MB, Roska B
Similarity of Gene Expression Pattern within and across Retinal Circuits
European Retina Meeting 2009, Oldenburg, Germany
Poster

06/2009 **Siegert S**, Gross Scherf B, Del Punta K, Didkovsky N, Heintz N, Roska B
Systematic Identification of Transgenic Mouse Lines Labeling a Selective Subpopulation of Retinal Cells
Gordon conference – Neural Circuits and Plasticity, Newport/RI, USA
Poster

05/2009 **Siegert S**, Gross Scherf B, Haverkamp S, Roska B
Genetic Dissection and Functional Investigation of Cellular Elements of the Rod Pathway

Roska B, Gross Scherf B, Del Punta K, Didkovsky N, Heintz N, **Siegert S**
Systematic Identification of Transgenic Mouse Lines Labeling Different Retinal Cell Types
ARVO (The Association for Research in Vision and Ophthalmology), Fort Lauderdale/FL, USA
Posters

08/2008 **Siegert S**, Gross Scherf B, Cabuy E, Gaidatzis D, Stadler MB, Oakley E, Del Punta K, Heintz N, Roska B
Development of Gene Expression, Physiology and Morphology of A17 Amacrine Cells
Gordon Conference – Visual System Development, Newport/RI, USA
Poster

07/2008 **Siegert S**, Gross Scherf B, Cabuy E, Stadler MB, Münch TA, Oakley E, DelPunta K, Heintz N, Roska B
Genetic Identification of a putative A17 Amacrine Cells in the Mouse Retina
FASEB - Retinal Neurobiology and Visual Processing, Snowmass/CO, USA
Poster

10/2007 **Siegert S**, Gross Scherf B, Gensat Team, Heintz N, Roska B
Selective Labeling of an Inner Plexiform Layer Stratum in a novel Transgenic Mouse Line
European Retina Meeting 2007, Frankfurt/Main, Germany
Poster

Courses

07/2006 "Advanced Techniques in Molecular Neuroscience"
Cold Spring Harbor Laboratory

Honors and Awards

10/2009 Best student poster award
European Retina Meeting 2009, Oldenburg, Germany

09/2009 Nature Neuroscience Cover of the September 2009, Volume 12, No.9 issue

Membership/Societies

2006 - present Schweizerische Gesellschaft für Zellbiologie,
Molekular-Biologie und Genetik (ZMG, member)

2007 - 2010 The Association for Research in Vision and Ophthalmology
(ARVO, student member)

Basel, July 20th, 2010

Sandra Siegert